International Journal of Science and Engineering Applications
Volume 7–Issue 09,254-259, 2018, ISSN:-2319–7560

Position Control of 3-DOF Articulated Robot Arm using PID Controller

War War Naing
Department of Mechatronic Engineering
Technological University
Thanlyin, Myanmar

Kyi Zar Aung
Department of Mechatronic Engineering
Technological University
Thanlyin , Myanmar

Aung Thike
Department of Mechatronic Engineering
Technological University
Thanlyin,Myanmar

Abstract: The purpose of this paper is to eliminate the manual control for pick and place system. The robot arm is designed with three joints, two links and three Dc motors. Arduino microcontroller is used to generate the required angular position of the robot joints. In this research, the link length of the robot arm is calculated to enable carrying the desire object weight. The position of the robot arm end effector is calculated with kinematic modeling method which include forward and inverse kinematic. Robotic tool box is used to task the position of the robot arm using forward and inverse kinematic. PID control method is used for accurate position of the end effector. In this research the gain of the PID controller is tuned by using the Ziegler-Nichol method. In this research, Output position of the robot arm are shown in MATLAB simulation. Forward and inverse kinematics result also are shown in MATLAB GUI.

Keywords: ARDUINO microcontroller, DC motors, Kinematic modeling, robot arm , PID controller, GUI

1. INTRODUCTION

An industrial manipulator is basically a mechanical arm operating under computer control, in other word a robot arm. Robots are modeled as rigid bodies (Links) and joints. The joints are assumed to induce either pure rotation or translation motion. These links and joints make up kinematic chains which form the basic structure of the equipment. In a production line like injection molding, stamping, assembly, packaging, etc. (i.e. point to point (PTP) application), or in specialized machine operations like welding, cutting, grinding, etc. (i.e. continuous path robots)[1].

Kinematics is the science of geometry in motion. It is restricted to a pure geometrical description of motion by means of position, orientation, and their time derivatives. The Denavit Hartenberg notation gives a standard methodology to write the kinematic equations of a manipulator. There are two important aspects in kinematic analysis of robots: the Forward Kinematics problem and the Inverse Kinematics problem. Forward kinematics refers to the use of the kinematic equations of a robot to compute the position of the end-effector from specified values for the joint parameters. Inverse kinematics refers to the use of the kinematics equations of a robot to determine the joint parameters that provide a desired position of the end-effector [2].

Robotic Arm controller is the challenging and demanding activity in industrial field as well as military and other applications. Robots are generally used to do unsafe, dangerous, highly repetitive, and unpleasant tasks which have many different functions such as material handling, assembly, arc welding, resistance welding, machines tool load and unload functions, painting, spraying, etc. A robotic arm is a Robotic Arm controller is the challenging and demanding activity in industrial field as well as military and other applications. A robotic arm is a robot manipulator, normally programmable with analogous functions to a human arm. Usually robots are set up for a task by the teach-and-repeat technique [3].

PID controller is a single loop controller which was introduced in 1940. PID controllers have been extensively used in industrial applications. The success of PID controllers is due to their simple structure and easiness of setting their parameters (Proportional - Integrative – Derivative[4].

This paper has three main contributions. Firstly, mechanical design of the robot arm is considered to pick up the desired object. Secondly, forward and inverse kinematic are described using the robotic tool box in MATLAB software. Finally, PID gain has been designed for the system using manual PID tuning by using Ziegler Nichol Method. This paper has been organized as follows, Section-II describes the mechanical design of 3_DOF(Degree of freedom) Articulated Robot Arm. Section-III calculates the kinematic modelling. Section-IV expresses tuning the PID gain for DC motor. Section V shows simulation results for 3-DOF Articulated robot arm with MATLAB/Simulink.

2. PROCESS FLOW CHART OF ROBOT ARM CONTROL

All In this research, the design parameters of the robot arm are considered. And then, the position of the end effector is calculated with kinematic modeling method in PC. To get the actual position of the robot joint angle, PID controller is used. In this paper, Kinematic modeling is an essential role in design and robot arm control. Robot arm kinematics deals with the analytical study of geometry motion of robot arm from fixed reference of coordinate system as a function of time without regard to movements that causes the motion.

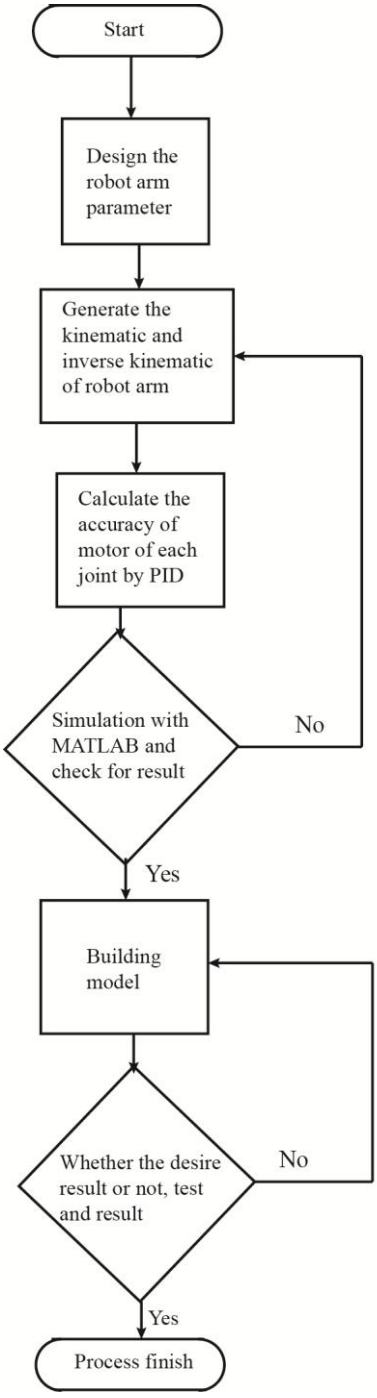

Figure 1. Flow chart of the robot arm system

3. DESIGN OF 3-DOF ARTICULATED ROBOT ARM

All in this research, the design of the system is shown in fig.1. In this design, there are two conveyors and robot arm. Conveyor 2 carries the objects and conveyor 1 carries the packages. Robot arm performs picking and placing the objects. The design of robot arm is 3-DOF articulated robot arm and consist of three joints. Joint 1 is base. Joint 2 and joint 3 are elbow and shoulder respectively.

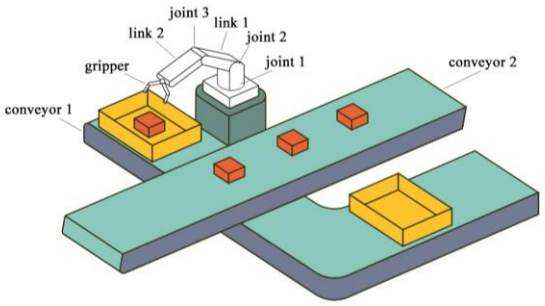

Figure 2. Design of the system

Table 1 shows the motor specifications for each motor in robot arm. In this table 70:1 means the gear ratio of output shaft and inner rotor. Three motors are different in weight because require torques are differed. Motor cap means that it is mounted on the shaft. Table 2 shows the material specification for 3-DOF articulated robot.

Table 1. Motor specifications of each joint

Type	Weight	Torque
70:1 Metal gear motor	225g	14kg-cm
75:1 Metal gear motor	104g	17kg-cm
19:1 Metal gear motor	215g	6.04kg-cm
Motor cap	6.8g	----------

Table 2. Material specification

Material	Density	L_1	L_2	Width	Thickness
Acrylic	0.00118 (kg/cm^3)	16 (cm)	15 (cm)	3 (cm)	1 (cm)

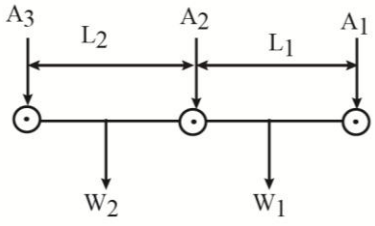

Figure 3. Free body diagram of the robot arm

T_2=0.48036N-m

T_1=1.2633N-m

3.1 Calculate the Kinematic Modelling

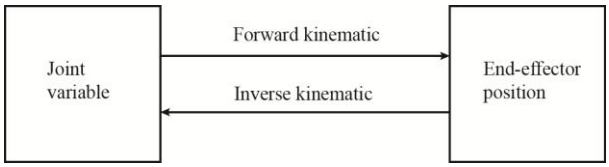

Figure 4. Kinematic block diagram of robot arm.

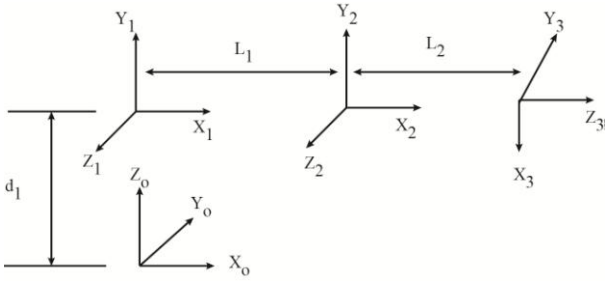

Figure 5. Kinematic Frame of 3-DOF robot arm

Table 3. D-H Parameters for robot arm

I	a_i	d_i	α_i	θ_i
1	0	5	90	θ_1
2	13	0	0	θ_2
3	9	0	0	θ_3

Transformation matrix for robot arm

$$ {}^{i-1}_{i}T = \begin{bmatrix} c\alpha_i & -c\alpha_i s\theta_i & s\alpha_i s\theta_i & a_i c\theta_i \\ s\theta_i & c\alpha_i c\theta_i & -s\alpha_i s\theta_i & a_i s\theta_i \\ 0 & c\alpha_i & c\alpha_i & d_i \\ 0 & 0 & 0 & 1 \end{bmatrix} $$

3.2 Forward Kinematics Analysis

Forward kinematics usually refers to home position of geometric link parameters and used to find the position and orientation of end effectors. For the research work, 3-DOF robotic arm was selected. It is a vertical articulated robot, with three revolute joints. It has a stationary base, shoulder and elbow. Fig. 1 is a simple block diagram which indicates the relationship between direct and inverse kinematics problem. Fig.3 indicates robots arm links and the coordinate frame assignment.

$$P_x = L_2 C\theta_2 C\theta_1 C\theta_3 - L_2 C\theta_1 S\theta_3 S\theta_2 + L_1 C\theta_1 C\theta_2 \quad (1)$$

$$P_y = L_2 C\theta_2 S\theta_1 C\theta_3 - L_2 S\theta_2 S\theta_1 S\theta_3 + L_1 S\theta_1 C\theta_2 \quad (2)$$

$$P_z = -L_2 S\theta_2 C\theta_3 - L_2 S\theta_3 C\theta_2 - L_1 S\theta_2 + d_1 \quad (3)$$

Where, $S\theta = \sin\theta$ and $C\theta = \cos\theta$

3.3 Inverse Kinematics Analysis

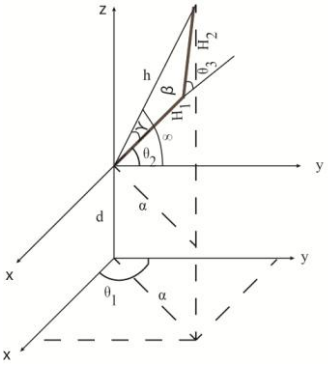

Figure 6. Isometric view of the robot arm

Inverse kinematics usually refers to position and orientation of end effectors. It helps to find joint variables to achieve correct position of source location part .The orientation can be calculated with the given position into one homogeneous transformation matrix (T) that describes the orientation and position of the end effector, and then the inverse kinematics is applied to determine each joint angle. Three are three solution approaches; analytical, numerical and semi analytical [11].In this paper, analytical method is used.

$$\theta_1 = \tan^{-1}\frac{y}{x} \quad (4)$$

$$\theta_3 = 180 - \beta \quad (5)$$

$$\theta_2 = \tan^{-1}\frac{z}{a} - \sin^{-1}\frac{H_2.\sin\beta}{h} \quad (6)$$

4. TUNING THE PID GAIN FOR DC MOTOR

In the system, power supply of robot arm control system is used the 12V DC supply for all DC motors and arduino microcontroller.

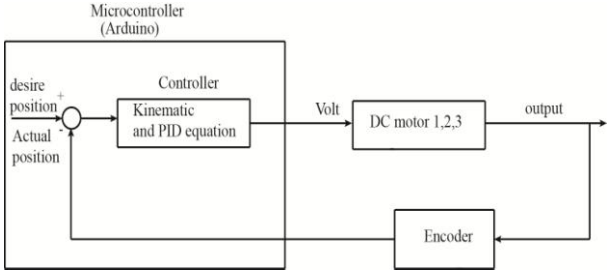

Figure 7. Control block diagram of robot arm control

In this system, DC Motors have six wires. Red colour is motor power (connect to one motor terminal). Black colour is also motor power (connects to the other motor terminal). Green colour is encoder GND. Blue colour is encoder Vcc (3.5-20V). Yellow colour is encoderA output and White colour is encoderB output. Most DC motors run at the highest RPM (revolutions per minute) when the required power is supplied. The speed of DC motors is controlled by using pulse width modulation (PWM), a technique of rapidly pulsing the power on and off. The percentage of time spent cycling the on/off ratio determines the speed of the motor. Each pulse is so rapid

that the motor appears to be continuously spinning with no stuttering.

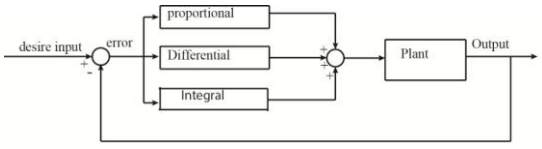

Figure 8. Block diagram of PID Controller

PID is a classic way of automatic control theory and the general trial control mode. Position can be controlled by PID controller. A PID controller supplies a control signal that has a component proportional to the tracking error of a system, a component proportional to the accumulation of this error over time and a component proportional to the time rate of change of this error. This module will cover these different components and some of their different combinations that can be used for control purposes. In engineering applications, the controllers appear in many different forms: as a stand-alone controller, as part of hierarchical, distributed control systems, which was built into embedded components. A proportional–integral– derivative controller (PID controller) is widely used in industrial control systems. It is a generic feedback control loop mechanism and used as feedback controller. PID loop defines how much energy is to be fed to the motor at any instant during a move. This is based on where the motor is and where it was expected to be. There are four parts in the equation and this determines the load in which three main components are referred to as the P, I, D and the minor friction component is referred to as K.

P determines the reaction to current error, I determines reaction to the sum of recently appeared errors, and D determines reaction according to the rate off error changing. The sum of all three parts contribute the control mechanism such as speed control of a motor in which P value depends upon current error, I also depends on the accumulation of previous error and D predicts future error based on the current rate of change.

Table 4. Manual P,I and D Parameters tuning

Gain	Rise time	Overshoot	Settling time	Steady state error	Stability
Increasing Kp	Decrease	Increase	Small Increase	Decrease	Degrade
Increasing Ki	Small Decrease	Increase	Increase	Large Decrease	Degrade
Increasing Kd	Small Decrease	Decrease	Decrease	Minor Change	Improve

$$U_p(t) = K_p.e(t) \quad (7)$$

$$U_I(t) = K_I \int_0^t e(t)dt \quad (8)$$

$$U_D(t) = K_D \frac{d}{dt}.e(t) \quad (9)$$

$$U(t) = K_p.e(t) + K_I \int_0^t e(t)dt + K_D \frac{d}{dt}e(t) \quad (10)$$

Table 5. Ziegler-Nichols tuning rule based on critical gain K_{cr} and critical period P_{cr} (second method).

Type of controller	K_P	T_i	T_d
P	$0.5K_{cr}$	∞	0
PI	$0.45K_{cr}$	$1/1.2P_{cr}$	0
PID	$0.6K_{cr}$	$0.5P_{cr}$	$0.125P_{cr}$

$$G_c(s) = K_p(1 + \frac{1}{T_i s} + T_d s) \quad (11)$$

5. GRAPHICAL USER INTERFACE (GUI)

Graphical User Interface development environment offers a set of tools in order to generate graphical user interface (GUI) [11].They greatly facilitate the operation of designing and building GUIs. A GUI example has been prepared for 3 DOF Robot including the forward kinematics. GUI is given in the following figures. Push buttons, sliders, axes etc. can be added on it. Additions are being visible on the m. file simultaneously as a function .Robotics Toolbox is embedded in to GUI. The results are compared with the expressions obtained in the analytical solution. It is proved that same results are obtained by the robotic toolbox and the analytical solution.

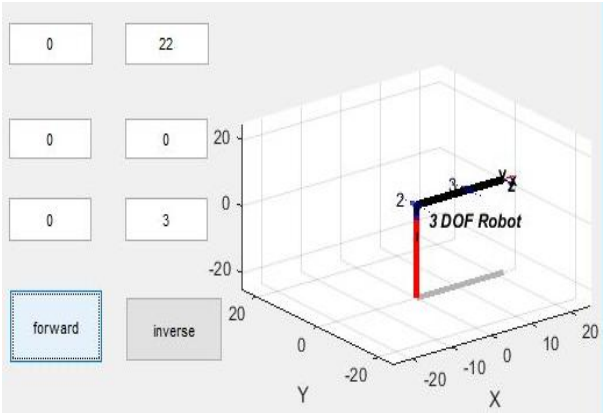

Figure 9. GUI window for robot arm

Figure 9. Shows the designed simulation program by MATLAB/GUIDE to create serial link robot (Link 1-3) and

control the joint angles(q_1, q_2, q_3). DH parameters can directly be changed .Figure 9 shows the home position of the robot and the path generated with the given coordinates, respectively.

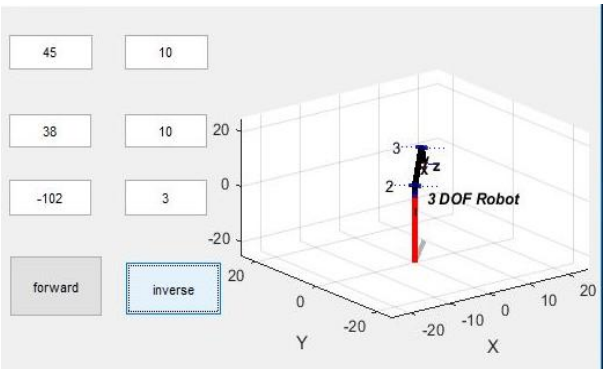

Figure 10. The robot arm position when x=10, y=10and z=3

6. EXPERIMENTAL TEST AND RESULTS

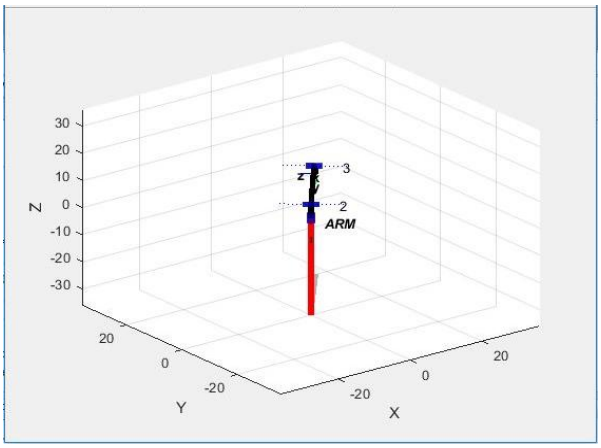

Figure 11. The robot arm position when θ1=55°, θ2=25° and θ3=66°

The transformation matric is following.

0.4924	– 0.4132	– 0.7660	17.0504
0.4924	– 0.4132	0.6428	20.3199
– 0.6428	– 0.7660	0.0000	0.8305
0	0	0	1.0000

Therefore, from the matric, the position of end effector is X=17.0504 cm, Y=20.3199 cm and Z=0.8305.

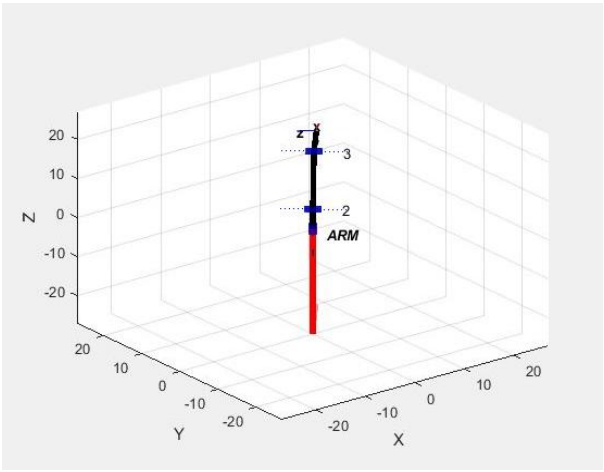

Figure 10. The robot arm position when θ1=50°, θ2=-75° and θ3=70°

The transformation matric is following

0.6428	0.0000	– 0.7660	8.6431
0.7660	0.0000	0.6428	10.3004
0	–1.0000	0.0000	17.2160
0	0	0	1.0000

Therefore, from the matric, the position of end effector is X=8.6431 cm, Y=10.3004 cm and Z=17.2160.

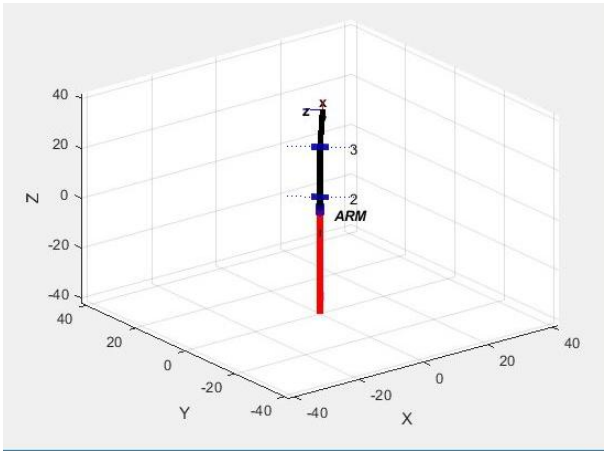

Figure 11. The robot arm position when θ1=50°, θ2=-75° and θ3=70°

The transformation matric is following

0.6040	0.2198	– 0.7660	10.2684
0.7198	0.2620	0.6428	12.2374
0.3420	–0.9397	0.0000	30.8143
0	0	0	1.0000

Therefore, from the matric, the position of end effector is X=10.2684 cm, Y=12.2374 cm and Z=30.8143.

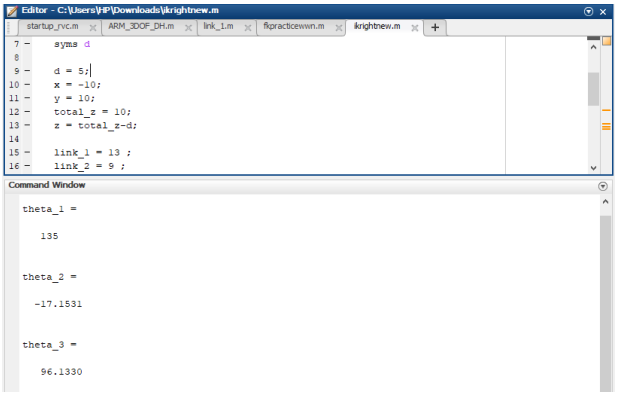

Figure 12. The robot arm position with inverse kinematic

From Fig.12, when the robot arm position is X=-10, Y=10 and Z=10, the joint angles are θ1=135°, θ2=-17.1531° and θ3=96.1330°

The following results are tuning the PID gain for each DC gear motor.

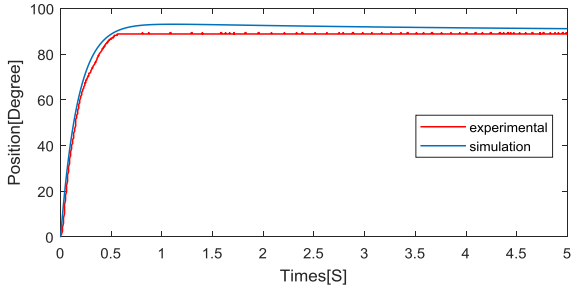

Figure 13. The combinatin of simulation and experimental for 19:1 metal gear motor with the gain is Kp=1.14, Ki=0.2923, Kd=0.185 with desire angle is 90°.

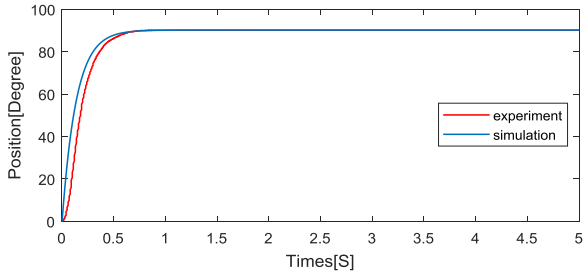

Figure 14. The combinatin of simulation and experimental for 70:1 metal gear motor with the gain is Kp=4.14, Ki=0.075, Kd=0.056 with desire angle is 90°.

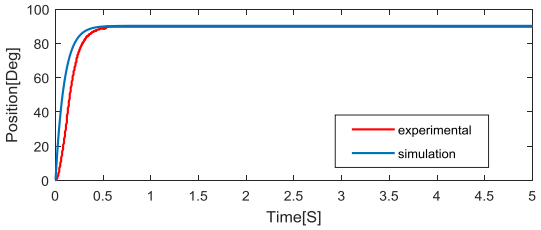

Figure 15. 75:1 metal gear motor with the gain is Kp=5.28, Ki=0.144, Kd=0.4818 with desire angle is 90°.

7. DISCUSSION AND CONCLUSION

This paper has been researched the position control for 3 DOF articulated robot arm. The link length and weight of the robot arm are considered by using required parameters. The forward and inverse kinematic are calculated by using D-H parameters and analytical method. And then, PID controller is used to get the actual position of robot arm. PID gains are tuned by using Ziegler Nichol method. Finally, the results are shown in MATLAB Simulink software..

8. ACKNOWLEDGMENTS

The author is very thankful to Dr.Theingi, Rector of Technological University Thanlyin, for her encouragement, invaluable permission and her kind support in carrying out this paper work. The author is deeply grateful to all the teachers from Department of Mechatronic Engineering, Technological University(Thanlyin), for their support, encouragement and invaluable guidance in preparation of this research. The author would like to express their thanks to all persons who have given support during the preparation period of this research work.

9. REFERENCES

[1] Umar Abubakar, Wang Zhongmin and Gao Ying.2014.”Kinematic Analysis and Simulation of a 6-DOF Industrial Manipulator”. International Journal of science and Research(IJSR), volume 3.

[2] Daniel Constantin, Marin Lupoae, Catalin Baciu and Dan-Ilie Buliga,2013,ISBN: 978-1-61804-288-0.

[3] Asnor Juraiza Ishak, Azura Che Soh and Mohamad Asmi Ashaari.2013.”Positin Control of Arm Mechanism Using PID Controller”vol.47 No2, Journal of Theoretical Applied Information Technology.

[4] N.G. ADAR and R.Kozan,2016. “Comparsion between Real Time PID and 2-DOF PID Controller for 6-DOF Robot Arm”. Vol130,No 1,Special issue of the 2nd International Conference on Computational and Experimental Science and Engineering(ICCESEN)

[5] J.Lin and Z.-Z Huang,2006, “Tuning the PID Parameters for Robot Manipulators With Compliant Bases By Using Grey Theory”, Proceeding of the 2006 IEEE International Conference on Control Applications Munich, Germany.

[6] Vivek Deshpande and P M George, “ Kinematic Modelling and Analysis of 5 DOF Robotic Arm” vol 4,No 2, International Journal of Robotics Research and Development(IJRRD) ISSN(P): 2250-1592;ISSN(E):2278-9421.

[7] Suyash Shrivastava and Eklavya Gupta,2017,”Forward Kinematics of Articulated Robotic Arm”vol.6 No8. International Journal of Research and Scientific Innovation(IJRSI).

[8] Ms. Vaijayanti B. and PG. 2017.” Robotic Arm Control Using Pid Controller and Inverse Kinematics” vol5,No 2. International Journal of Engineering Development and Research.

[9] Mehment Erkan Kutuk, Memik Taylan DAS and Lale Canan Dulger. 2017,” Forward and Inverse Kinematics Analysis of Denso Robot” Proceedings of the International Symposium of Mechanism and Machine Science.

[10] H.Ferdinando, H.Wicaksono and R.Wibowo, 2017," The Implementation of PID Controller in the Pick and Place Robot".Proceeding of the International Symposium of Mechanism and Machine Science.

[11] S.Kucuk and H.Bingul, 2016. "The Inverse Kinematic Solution of Industrial robot manipulators" IEEE conference on Mechatronics, pages 274-279.

International Journal of Science and Engineering Applications
Volume 7–Issue 09,260-264, 2018, ISSN:-2319–7560

Implementation of Fingerprint based Student Attendance System with Notification by GSM Module

Zin Nwe Soe
Department of Electronic Engineering
Technological University
Thanlyin, Myanmar

Dr. Aye Mya Win
Department of Electronic Engineering
Technological University
Thanlyin, Myanmar

Daw Thae Hsu Thoung
Department of Electronic Engineering
Technological University
Thanlyin, Myanmar

Abstract: Attendance and academic success are directly related in educational institutions. The continual absence of students in lecture, practical and tutorial is one of the major problems of decadence in the performance of academic. The authorized person needs to prohibit truancy for solving the problem. In existing system, the attendance is recorded by calling of the students' name, signing on paper, using smart card and so on. These methods are easy to fake and to give proxy for the absence student. For solving inconvenience, fingerprint based attendance system with notification to guardian is proposed. The attendance is recorded using fingerprint module and stored it to the database via SD card. This system can calculate the percentage of attendance record monthly and store the attendance record in database for one year or more. In this system, attendance is recorded two times for one day and then it will also send alert message using GSM module if the attendance of students don't have eight times for one week. By sending the alert message to the respective individuals every week, necessary actions can be done early. It can also reduce the cost of SMS charge and also have more attention for guardians. The main components of this system are Fingerprint module, Microcontroller, GSM module and SD card with SD card module. This system has been developed using Arduino IDE, Eclipse and MySQL Server.

Keywords: fingerprint module, GSM module, microcontroller, Eclipse, MySQL Server

1. INTRODUCTION

Attendance system is important role for any organization such as office, companies, schools, universities and so on. In conventional attendance system, the teachers either call the name or identity number of the students or allow the students to sign on paper. It is not convenient to track the attendance for the increase number of students. So, it can have the problems such as proxy attendance and time consuming. The traditional system can also have the difficulty for manipulating the stationery materials of the attendance record and posting the attendance report to guardians. Biometrics authentication is used for taking attendance of students. The most common used of biometrics authentication methods are fingerprint, facial, iris, voice authentication and so on. In this system, fingerprint authentication method is used to record attendance because it is easy to use, more accuracy and cost effective. The attendance management system is also involved alerting system to perform together with guardians and the authorized person for the students to attend the class regularly. The main purpose of this research work is to make the attendance management system more efficient, secure, portable, easy to use and less time consuming.

2. LITERATURE REVIEW

A number of existing works focus on the application of various methods and principles to effectively monitor the attendance of students. Design and development of smart student management system was proposed. The system consists of two parts, one is fingerprint based student attendance system and another one is notice board [3]. A wireless attendance system using Zigbee technology that authenticates using fingerprints of an individual. The system is mentioned with transmitter and receiver. The transmitter comprises controller, fingerprint module section, LCD, keypad and PC is the receiver. The system takes attendance records with fingerprint module and updates the database attendance records of students via Zigbee module [8]. RFID based student attendance system with notification to parents was designed. This paper presents a design of an automatic attendance system for both students and professor with parents notification sent via GSM [11].

3. SYSTEM DESCRIPTION

The block diagram of the system is shown in Figure 1.

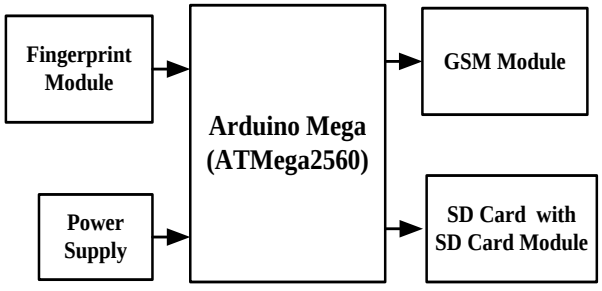

(a)

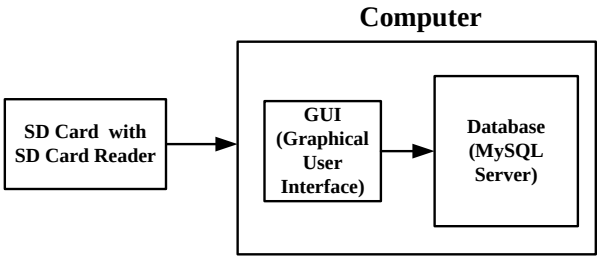

(b)

Figure 1. Block Diagram of the System

This system consists two parts. One part of the system is taking attendance using fingerprints of students and storing data to SD card with text file and sending message after extracting absence from SD card. Another one is storing the attendance via SD card and calculating the percentage of attendance.

3.1 System Schematic Diagram

The schematic diagram is depicted in Figure 2. The circuit diagram illustrates interfacing Arduino Mega (ATmega 2560) with GSM module (SIM900A), fingerprint module, SD card module and two LEDs. It allows from 7volts to 12volts for the power. TX (transmit) and RX (receive) of SIM900A is connected with 2 and 3 pins of Arduino Mega. Pin 10 and 11 are used to connect with transmit and receive pins of fingerprint module. The pins of SD card module are connected with 50, 51, 52 and 53 pins of Arduino Mega. The black color of the wire is defined for the ground (GND) and the red color of the wire is defined for the voltage (V_{CC}). Two LEDs are used for showing the processing time of fingerprint. These are connected with 6 and 7 pins of the Arduino Mega.

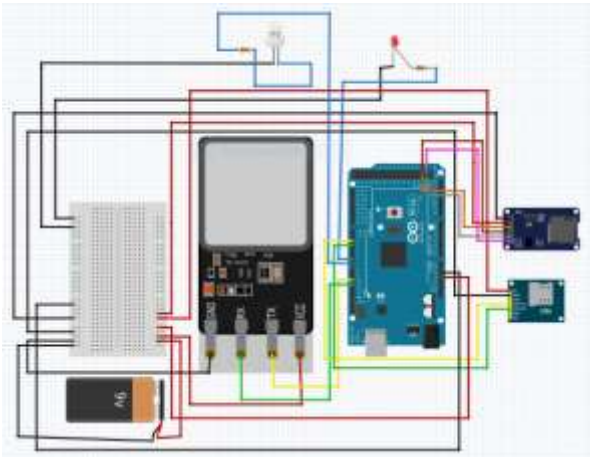

Figure 2. Schematic Diagram of the System

4. HARDWARE AND SOFTWARE DESCRIPTION

To reduce the complexity of the design process, simple algorithms, low cost and commercially available devices have been used to implement the system.

4.1 Fingerprint Reader

Fingerprint authentication is used for the student attendance system. It consists of two parts. One is enrollment and another one authentication. During enrollment, the fingerprint of the student is captured using fingerprint reader and the unique features are extracted and stored in the database as the template with the student ID. In the processing of authentication, the fingerprint of student is captured again and compared with the extracted features already existing in the database for determining match or mismatch. In this system, Biovo-C3 fingerprint identification integrated reader is used to capture fingerprints as shown in Figure 3. Fingerprint module mainly has three types of fingerprint sensors like optical fingerprint sensor, ultrasonic fingerprint sensor and capacitive fingerprint sensor. The sensor type of Biovo-C3 fingerprint reader is high-definition optical sensor. This reader can store 200 fingerprints. It has 256 bytes for fingerprint extraction template size and 512 bytes fingerprint match template size. This reader is integrated image collecting and algorithm chip together with a tiny configuration of 18.5mm × 14.6mm.

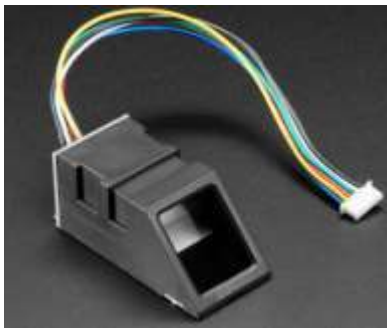

Figure 3. Biovo-C3 Fingerprint Reader

4.2GSM SIM 900A Modem

A GSM SIM 900A modem is used to send alert messages to guardians as shown in Figure 4. A GSM modem is a specialized type of modem which accepts a SIM card, and operates over a subscription to a mobile operator, just like a mobile phone. From the mobile operator perspective, a GSM modem looks just like a mobile phone. While these GSM modems are most frequently used to provide mobile internet connectivity, many of them can also be used for sending and receiving SMS (short message service) and MMS (multimedia messaging service) messages. SIM900 is designed with a very powerful single-chip processor integrating AMR926EJ-S core. The SIM900A is a complete Quad-band GSM/GPRS solution in a SMT module which can be embedded in the customer applications. Featuring an industry-standard interface, the SIM900 delivers GSM/GPRS 850/900/1800/1900MHz performance for voice, SMS, Data, and Fax in a small form factor and with low power consumption. With a tiny configuration of 24mm x 24mm x 3 mm, SIM900 can fit almost all the space requirements in M2M application, especially for slim and compact demand of design. AT commands are instructions used to control a modem. AT is the abbreviation of Attention. Every command line starts with “AT” or “at”. That’s why modem commands are called AT commands. Many of the commands are called AT commands that are used to control dial-up modems such as ATD (Dial), ATA (Answer), ATH (Hook control) and

ATO (Return to online data state). These commands are also supported by GSM/GPRS modems and mobile phones. The SMS-related commands are AT+CMGS (Send SMS message), AT+CMSS (Send SMS message from storage), AT+CMGL (List SMS messages) and AT+CMGR (Read SMS messages).

Figure 4. GSM (SIM 900A) Modem

4.3Arduino Mega (ATmega 2560)

Arduino is a software company, project, and user community that designs and manufactures computer open-source hardware, open-source software and microcontroller-based kits for building digital devices and interactive objects that can sense and control physical devices. These systems provide sets of digital and analog I/O pins that can interface to the various expansion boards and other circuits. The boards feature serial communication interfaces, including Universal Serial Bus (USB) on some models, for loading programs from personal computers. For programming the microcontrollers, the Arduino project provides an integrated development environment (IDE) based on Arduino programming language which is controlled by a set of C/C++ functions. The Arduino Mega is a microcontroller board based on the ATmega2560. It has 54 digital input/output pins (of which 14 can be used as PWM outputs), 16 analog inputs, 4 UARTs (hardware serial ports), a 16 MHz crystal oscillator, a USB connection, a power jack, an ICSP header, and a reset button. The board can operate on an external supply of 6 to 20 volts. If supplied with less than 7V, however, the 5V pin may supply less than five volts and the board may be unstable. If using more than 12V, the voltage regulator may overheat and damage the board. The recommended range is 7 to 12 volts. The Arduino Mega (ATmega2560) is shown Figure 5.

Figure 5. Arduino Mega (ATmega2560)

4.4 SD Card Module

The SD card module is a sample solution for transferring data to and from a standard SD card. It used to store the attendance and transfer to database of PC in this system. The pin out is directly compatible with Arduino, but can also be used with other microcontrollers. It allows to add the mass storage. The module has SPI interface which is compatible with any SD card and it use 5v or 3.3v power supply which is compatible with Arduino mega. The communication between the microcontroller and SD card uses SPI, which takes place on digital pins 50, 51, 52 for the Arduino Mega. Additionally, another pin must be used to select the SD card. SS pin of SD card module is connected with pin 53 on the Arduino Mega. The size of module is 20×28mm.This module is shown in Figure 6.

Figure 6. SD Card Module

4.5 Software Description

To complete this system, Eclipse, MySQL server and phpMyAdmin are used. Eclipse is an integrated development environment (IDE) used in computer programming. Eclipse is written mostly in Java and its primary use for developing Java applications, but it may also be used to develop applications in other programming languages. Java is used to develop this system. MySQL is a relational database management system (RDBMS) based on SQL (Structured Query Language) and phpMyAdmin is a web-based interface to a MySQL server. It can be created new databases import table using phpMyAdmin.

5. TESTS AND RESULTS

The working diagram of the system is shown in Figure 7. In the system, the students are not allowed to take the attendance if the teacher does not reach in the class because the fingerprint of teacher is set as a password to secure for the students. After taking attendance, the teacher or authorized person must take SD card to store attendance in the database of PC. GSM module will also send alert message to guardians' mobile phone for the students don't enough the percentage of attendance weekly. The alert message of guardians' mobile is shown in Figure 8.

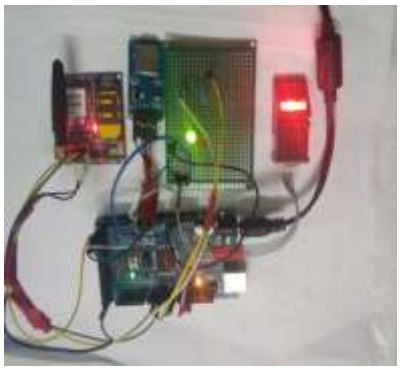

Figure 7. The Working Diagram of the System

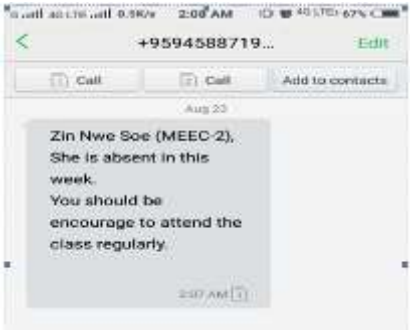

Figure 8. Alert Message Display in Guardians' Mobile

In the system, the data of the students from SD card are copied in the database with the date. It can store data for long time. This system can also calculate the percentage of students with no time consuming. If the data are not need, the authorized person can edit the database from phpMyAdmin. The table in database of fingerprint attendance system is shown in Figure 9. The calculating of the attendance percentage is shown in Figure 10. The editing to database using phpMyAdmin is shown in Figure 11.

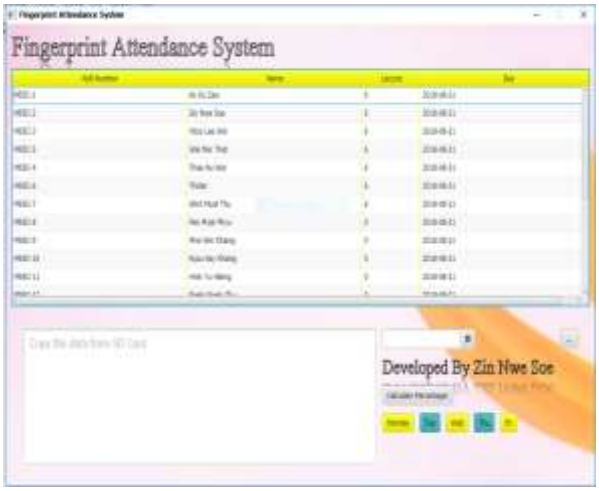

Figure 9. Table of Fingerprint Attendance System

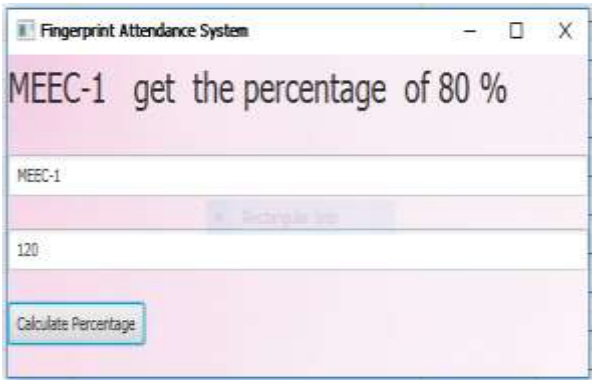

Figure 10. Calculating the Percentage of Student Attendance

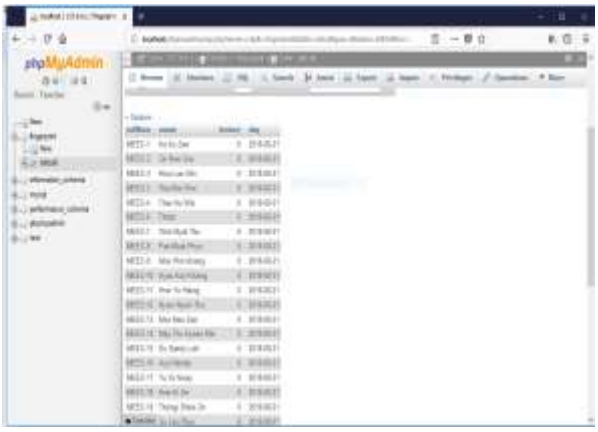

Figure 11. Editing the database of Attendance System

6. CONCLUSION

Attendance system could not only speed up the process taking attendance but also reduce the error rate and produce faster verification process of authenticating student attendance. This system calculates the attendance of students and sends alert message for the absence students to relevant guardians' mobile phone. This system can also store the data of students for long time.

7. ACKNOWLEDGEMENTS

Firstly, the author would like to acknowledge Dr. Thein Gi, Rector of Technological University (Thanlyin), for her kind permission to carry out this research work. The authors would like to thank many colleagues from digital image processing research group of Department of Electronic Engineering of Technological University (Thanlyin). The author particularly wishes to acknowledge all the teachers from Department of Electronic Engineering, Technological University (Thanlyin), for their support, encouragement and invaluable guidance in preparation of this research. The authors would like to express their thanks to all persons who have given support during the preparation period of this research work.

7. REFERENCES

[1] Dhiman Kumar Sarker, Nafize Ishtiaque Hossain, Insan Arafat Jamil. 2016 "Design and Implementation of Smart Attendance Management System Using Multiple Step Authentication", International Workshop on Computational Intelligence(IWCI), 12-13.

[2] Mr. Sopan D.Borale, Ms. Poonam G.Chaudhari, Ms. Vaijanti B.Patil, Ms. Apurva D.Shingne, Prof.G.N.Dhoot. 2016. "Fingerprint Based Attendance Management System with SMS Alert to Parents", International Journal Research in Advent Technology (IJRAT) (E-ISSN: 2321-9637) Special Issue National Conference "CONVERGENCE 2016".

[3] Rakib-UI Hasan, Md. Akibul Azam, Md. Riifat Rahman, Abdulian-AL Mamum, Md. Saniat Rahman Zishan. 2017. "Design and Development of Smart Student management System ", International Journal of Modern Education Research, ISSN: 2375-3781.

[4] Karthik Krishnamurthi, S.Irudaya Mary, B.N. Sumalatha, Adler Pereira. 2015. "Fingerprint Based Attendance System", International Journal of Advanced Research in Computer and Communication Engineering, Vol.4, Issue 3.

[5] Nur Izzti Zainal, Khairul Azami Sidek, Teddy Surya Gunawan, Hasmah Mansor, Mira Kartiwi. 2014. "Design and Development of Portable Classroom Attendance System Based on Arduino and Fingerprint Biometric", Information and Communication Technology for the Muslim World (ICT4M), 5th International Conference.

[6] Hitesh Walia, Neelu Jain. 2016. "Fingerprint Based Attendance System Using LabVIEW and GSM", International Journal of Innovative Research in Science, Enginering and Technology, Vol.5, Issue 7.

[7] Ravishankar Yadav, Sumita Nainan. 2014. "Design Based Student Attendance System with Notification to Parents Using GSM", International Journal of Engineering Research & Technology (IJERT), ISSN:2278-0181, Vol.3, Issue 2.

[8] Akshay v. Bhoyar, Shruti A. Borgave, A.S Bhandare. 2014. "Wireless Fingerprint Based Attendance System Using Zigbee Technology", International Journal of Innovative Resarch In Technology, ISSN: 2349-6002,Volume 1, Issue 11.

[9] Vishal Suryawnshi, Kiran Puri, Prashant Devkar, Dr.K.S Tiwari. 2017 "Attendance Monitoring System Automation Using Fingerprint Module", International Journal of Electrical, Electronics and Computer Systems (IJEECS), ISSN(Online) 2347-2820, Volume-5, Issue-1.

[10] Shweta K Nandya, Baswaraj Gadgey, Veeresh Pujari. 2017. "RFID and Fingerprint Based Smart Attendance System", International Journal for Research in Applied Science & Engineering Technology (IJRASET), Volume 5, Issue VI, ISSN: 2321-9653.

[11] Ravishankar Yadav, Sumita Nainan.2014. "Design of RFID Based Student Attendance System with Notification to Parents Using GSM", International journal of Engineering Research & Technology (IJERT) ,ISSN:2278-0181, Vol.3 Issue 2.

International Journal of Science and Engineering Applications
Volume 7–Issue 09,265-273, 2018, ISSN:-2319–7560

Exploratory Geochemical Studies to Determine the Mineralization Zones Around the Zarshuran Gold Mine

Saeed Heidarlaki
Shahrood University of Technology
Shahrood, Iran

Mansour Ziaii *
Shahrood University of Technology
Shahrood, Iran

Peyman Afzal
Islamic Azad University
Tehran, Iran

Mehdi Ziaei
Shahrood University of Technology
Shahrood, Iran

Abstract: The study area is located in the northern part of Takab, West Azarbaijan Province, northwest of Iran. Since geochemical explorations, especially the drainage sediments, play a very important role in finding promising areas and providing conditions for more detailed exploration. Detection and separation of geochemical anomalies from the field is one of the most important and fundamental issues in geochemical exploration. In this study, using the classical statistcs methods, anomalous values were determined. Other methods used in this study is the concentration-area (C-A) fractal method. This method is a very successful method for separating anomalies from the field due to simultaneous consideration of the frequency and spatial variations of geochemical data. Multivariate statistical analysis including principal component analysis (PCA) was used to obtain anomaly values related to determine the anomaly values. Favorable results for the methods used for this region was presented.

Keywords: PCA; C-A Fractal; Geostatistics; Gold Mineralization; Zarshuran

1. INTRODUCTION

The statistics are a vast array of maths that study ways to collect, summarize, and conclude data. This science applies to a wide range of academic sciences from physics and social sciences to anthropology, as well as business, government, and industry. Statistics is the science and practice of human development through the use of experimental data. Statistics are based on the theory of statistics, which is a branch of applied mathematics. In statistical theory, random events and uncertainty are modeled by probability theory. In this science, studying and judging on various subjects is done on the basis of a society and judgment about a particular person is not at all questionable [1] [2].

The geostatistics is the most important statistical theory based on the field concept of the place, is the theory of regional variables. The regional variable is defined as any environment property whose numerical values are distributed in one, two, or three-dimensional sampling space. The spatial variations of a regional variable have two structural and random components. One of the main goals of spatial statistics is to provide an appropriate model for describing the regional variable by taking into account the structural and random variability components. This section of spatial statistics is called geostatistics [3] [2].

Separation of anomalies from the background is one of the most important and key steps in geochemical exploration. There are several ways to identify and separate anomalous areas from the field [4]. Separation of geochemical anomalies from background has always been a major concern of exploration geochemistry[5]. The search for methods that can make this analysis quantitative and objective aims not only at the reduction of subjectiveness but also at providing an automatic routine in exploration, assisting the interpretation and production of geochemical maps [6].

Geochemical explorations are the basis for the mineral processing studies. Therefore, in exploration, the economy and the processing capabilities should always be easy and cost-effective [7]. In determining the zones of alteration and mineralization in the area, remote sensing methods help a lot, in addition to giving us a large view of the mineralization process in the region. Therefore, if remote sensing and geochemical studies are combined, mineralization can be accurately determined [8] [9].

2. Methodology and Dataset

2.1. Geolocation and Sampling

The Zarshuran mineral zone is located in West Azarbaijan province of Iran and on geological sheet of Takht-e-Soleyman (on sclae 1:100,000). The Takht-e-Soleyman sheet covers parts of Zanjan, West Azarbaijan and East Azarbaijan provinces. The Takht-e-Soleyman sheet is part of the 1: 250000 geological map of the Takab rectangle between the eastern longitude 47° 00' and 47° 30' and the north latitude 36° 30' 'to 37° 00' . The quadrilateral coordinates of the studied area are presented in Table 1. Due to its location in the Takab metallurgical province and the location of the Alborz-Azarbaijan, Iran Central and Sanandaj-Sirjan construction zones, this area has a lot of mineralization diversity. The most important mineralization in this area is the lead and zinc mineralization (Anguran, Alam Kandy and Arpachai) and gold mineralization (Zarshuran, Aghdare and Tozlar). The study area of this project is located between Zanjan and East Azarbaijan provinces around the Zarshuran gold mine. Geolocation of study area in Iran map is shown in figure 1.

Table 1. Geographical coordinates of study area

Geographical Coordinates		points
Latitude (Y)	Longitude (X)	
36° 40' 49"	47° 08' 00"	**A**
36° 44' 06"	47° 08' 00"	**B**
36° 44' 06"	47° 12' 03"	**C**
36° 40' 49"	47° 12' 03"	**D**

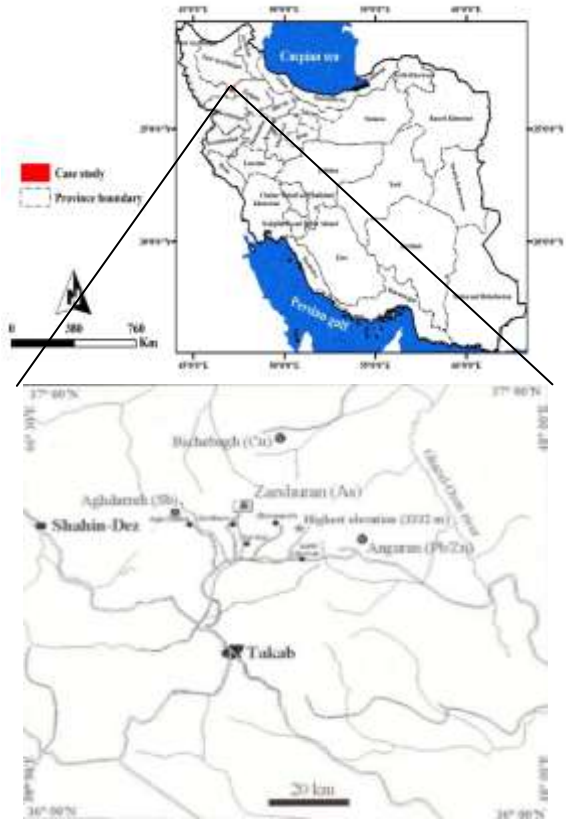

Figure 1. Geolocation of study area in Iran map

In the study area, 72 geochemical samples were taken from the drainage sediments. The position map of the 72 drainage sediments samples taken from the study area is shown in Figure 2.

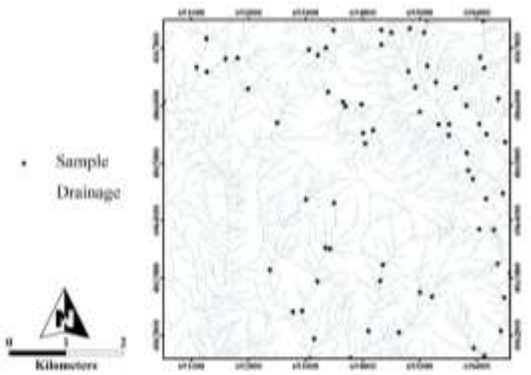

Figure 2. Position of drainage sediments samples taken from the study area.

2.2. Correlation Analysis

Correlation is used to test relationships between quantitative variables or categorical variables. In other words, it's a measure of how things are related. The study of how variables are correlated is called correlation analysis [10]. Correlations are useful because if you can find out what relationship variables have, you can make predictions about future behavior [11]**.** Correlation analysis in geochemical data is very important. One of the valuable results of the investigation of the correlation between chemical elements is the identification of the mineralization and geochemical behavior of the region [12] [2].

2.3. Hierarchical Clustering

In data mining and statistics, hierarchical clustering (also called hierarchical cluster analysis or HCA) is a method of cluster analysis which seeks to build a hierarchy of clusters. Strategies for hierarchical clustering generally fall into two types [13]:

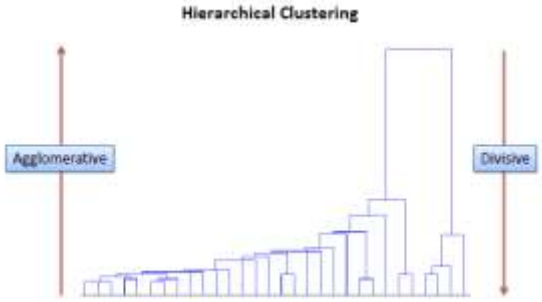

Figure 3. hierarchical clustering strategies

- **Agglomerative Method**:

  This is a "bottom up" approach: each observation starts in its own cluster, and pairs of clusters are merged as one moves up the hierarchy.

- **Divisive Method**:

  This is a "top down" approach: all observations start in one cluster, and splits are performed recursively as one moves down the hierarchy (see figure 3).

2.6. Principal Components Analysis (PCA)

Principal component analysis (PCA) is a statistical procedure that uses an orthogonal transformation to convert a set of observations of possibly correlated variables into a set of values of linearly uncorrelated variables called principal components. Principal Component Analysis (PCA) is the general name for a technique which uses sophisticated underlying mathematical principles to transforms a number of possibly correlated variables into a smaller number of variables called principal components. The origins of PCA lie in multivariate data analysis, however, it has a wide range of other applications, as we will show in due course. PCA has

been called, 'one of the most important results from applied linear algebra and perhaps its most common use is as the first step in trying to analyse large data sets. Some of the other common applications include; de-noising signals, blind source separation, and data compression [14] [15].
In general terms, PCA uses a vector space transform to reduce the dimensionality of large data sets. Using mathematical projection, the original data set, which may have involved many variables, can often be interpreted in just a few variables (the principal components). It is therefore often the case that an examination of the reduced dimension data set will allow the the user to spot trends, patterns and outliers in the data, far more easily than would have been possible without performing the principal component analysis. The aim of this essay is to explain the theoretical side of PCA, and to provide examples of its application. We will begin with a non-rigorous motivational example from multivariate data analysis in which we will attempt to extract some meaning from a 17 dimensional data set. After this motivational example, we shall discuss the PCA technique in terms of its linear algebra fundamentals. This will lead us to a method for implementing PCA for real-world data, and we will see that there is a close connection between PCA and the singular value decomposition (SVD) from numerical linear algebra. We will then look at two further examples of PCA in practice; Image Compression and Blind Source Separation [16] [17].

2.4. Concentration-Area (C-A) Fractal

Ever since Mandelbrot (1974, 1972) introduced the concept offractals in the last century [18], fractal or multi-fractal analysis hasquickly developed into an important branch of non-linear scienceand has had significant impacts in many areas of natural sciencesto characterize self-similar or self-affine measures [19]. The C-A method serves to illustrate the relationship between theobtained results and the geological, geochemical and mineralogicalinformation. Its most useful features are the easy implementa-tion and the ability to compute quantitative anomalous thresholds. Cheng et al. (1994) proposed an element concentration–area (C–A) model, which may be used to define the geochemical backgroundand anomalies. The model has the general form of Eq. following [20] [21]:

$$(\rho \le v) \propto \rho^{-a_1}; \quad A(\rho \le v) \propto \rho^{-a_2}$$

Where $A(\rho)$ denotes the area with concentration values greaterthan the contour value ρ ; v represents the threshold; and a1and a2are characteristic exponents. Using the fractal theory, Cheng et al.(1994) derived similar power–law relationships and equations inextended form. The two approaches which were used to calculate $A(\rho)$ by Cheng et al. (1994) were (1) the $A(\rho)$ is the area enclosedby contour level q on a geochemical contour map resulting frominterpolation of the original data using a weighted moving aver-age method, and (2) $A(\rho)$ are the values obtained by box-countingof the original elemental concentration values. By box-counting,one superimposes a grid with cells on the study region. The area $A(\rho)$ for a given q is equal to the number of cells multiplied by thecell area with concentration values greater than ρ . Average concen-tration values are used for those boxes containing more than onesample. Area ρ concentration $[A(\rho)]$ with element concentrationsgreater than ρ usually shows a power–law relation [22] [23]. The breaks betweenstraight-line segments on this plot and the corresponding values of _ have been used as cut-offs to separate geochemical values intodifferent components, representing different causal factors, suchas lithological differences and geochemical processes. Factors suchas mineralizing events, surface geochemical element concentra-tions, and surface weathering are of considerable importance [24]. The multi-fractal theory may be interpreted as a theo-retical framework that explains the power–law relations betweenareas enclosing concentrations below a given value and the actualconcentrations.

3. Results and Discussion

3.1. Correlation Analysis

In Table 2, the correlation coefficients of elements are derived from the Spearman method. Therefore, in this project, the basis for interpreting the relations between different elements is Spearman's nonparametric correlation test. According to the two-variable Spearman test, the following results can be presented:

- Pearson correlation coefficient between 0.230 and -0.230 and Spearman between 0.231 and -0.231 at 95% confidence level are invalid and meaningless. This value is at the confidence level of 99% for Pearson correlation coefficients and Spearman between 0.300 and -0.300.
- Au with As, Cd, Sb and Zn correlations show a significant and moderate to high correlation.
- Ag only has a significant and moderate correlation with Zn.
- As, Cd, Cu, S, Sb and Zn have a positive and significant correlation with each other and can therefore be considered as a tracer or associated with mineralization.
- There is a positive and significant correlation between elements such as Al, Ba, Be, Ca, Ce, Cu, K, La, Li, Mo, Na, P, Pb, Sr, Th, Ti, U, Y, Yb and Zr. There is a medium to large. This correlation is undoubtedly influenced by the surrounding stones.
- There is a significant correlation between Au, Cr, Co, Fe, Mg, Mn, Ni, Sb and Zn. The group also describes the chemistry of the rocky outcrops of the region, which are considered to be mafic as compared to the elements of the preceding clause.

Table 2. Calculation of correlation coefficients of elements using Pearson method for normalized geochemical data

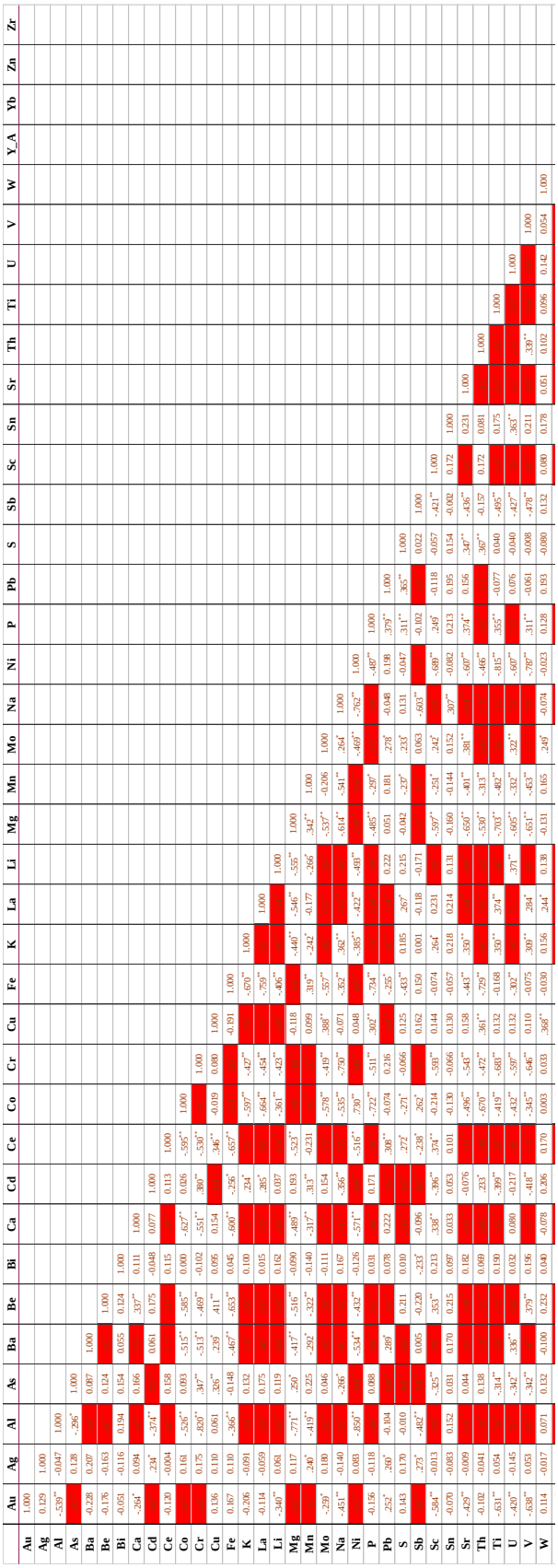

3.2. Hierarchical Clustering

Figure 4 shows the Hierarchical Clustering chart for cluster analysis of normal data. According to this diagram, the following results can be obtained :

- The resulting chart has two main clusters. Each of these clusters is divided into two sub-clusters.
- The lower cluster is not explicitly exploratory, and due to the correlation of elements of this cluster, it is anticipated that these elements are related to the chemistry of surface rocks in the region.
- The upper cluster itself is divided into two sub-branches or branches, each of which in turn has smaller subdivisions. Meanwhile, confirmation of the correlation between the elements Ag, As, Au, Cd, Cu, Mn, Pb, S, Sb and Zn is the most important finding of this graph.
- The three Bi, Sn, and W elements form a sub branch of the upper branch. These elements are notable in this exploratory area. However, the combination of these elements with elements of Ag, As, Au, Cd, Cu, Mn, Pb, S, Sb and Zn elements can be of great importance from the genetic point of view.
- Another major branch of the upper branch is the Co, Cr, Fe, Mg and Ni elements. The existence of such a correlation was also detectable in a bivariate test. Therefore, it can be used in genetic topics.
- Finally, according to the analyzes carried out at the earlier stages among all the elements, 14 important elements were detected that included Au, Ag, As, Cd, Co, Cr, Cu, Mn, Mo, Ni, Pb, Sb , W and Zn and were selected by main component analysis method (PCA).

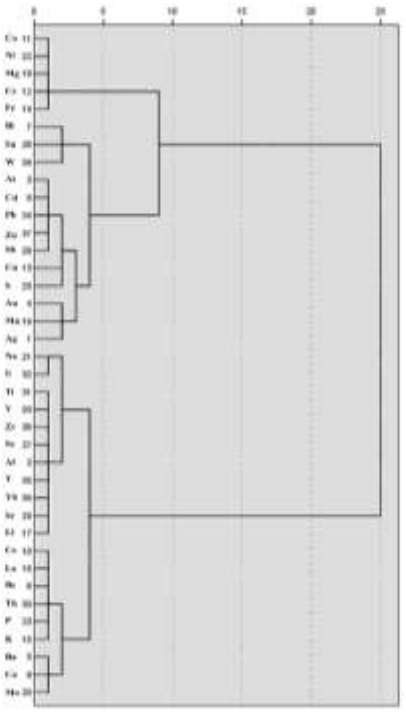

Figure 4. Logarithmic Dendrogram for Ward Method.

3.3. Principal Components Analysis (PCA)

According to the Scree Plot chart (Figure 5), there are 14 total factors, of which only 3 first factors have been selected due to special values above 1 as effective factors.

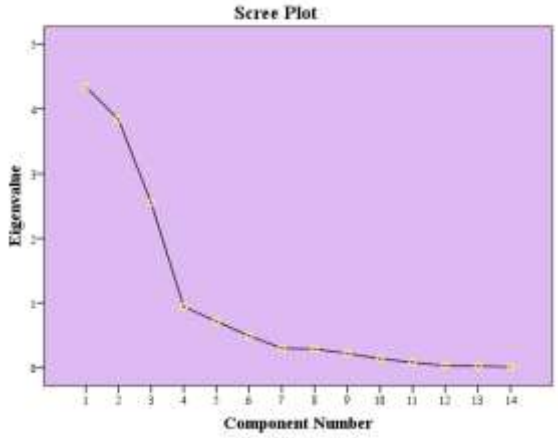

Figure 5. Scree plot derived from the results of the factor analysis of the 14 selected normal elements.

The PCA results are characterized by three main components. According to Table 3, all three main components have special values greater than 1. The value of the variance for each component indicates the degree of variability of the data in that particular component.

Table 3. The results of the main components analysis (PCA) for the 14 selected elements.

Elements	PC1	PC2	PC3
Au	0.450	0.094	**0.524**
Ag	0.052	0.016	**0.533**
As	0.149	-0.091	**0.820**
Cd	0.000	**0.819**	**0.475**
Co	**0.960**	-0.162	0.049
Cr	**0.944**	0.098	0.175
Cu	-0.157	**0.505**	**0.521**
Mn	0.181	**0.923**	0.007
Mo	-0.723	0.317	0.367
Ni	**0.958**	0.175	0.110
Pb	-0.103	0.316	**0.754**
Sb	-0.037	**0.550**	**0.642**
W	-0.104	**0.955**	-0.212
Zn	0.188	-0.532	**0.776**
Var.	26.03	25.43	25.25

3.4. Distribution of elements concentration

At this stage, the values of the 8 selected elements of importance identified in the previous sections were used to represent the distribution of various elements in the study area. They were interpolated using the IDW method (weighted by inverted distance) in the Arc GIS 10.2 environment.

To map geochemical information in the software environment, an appropriate size is chosen for the size of the pixels for interpolation . In this step, in order to find the appropriate size for the size of the pixels for interpolation, according to Hengl [25] the following formula is used:

$$x = \sqrt{\frac{A}{n}} \times 0.05$$

In this formula, x is the appropriate cell size, A is the area of the study area in m^2, and n is the number of samples taken from the range. Here, A = 6 * 6 and n = 72, which after reaching the formula above is x = 0.03 m^2, after which all interpolations made with cell size will be 0.03 square meters.

Subsequently, using the inverse distance weighing method (IDW), 8 elements including Ag, As, Au, Cd, Cu, Pb, Sb and Zn were continuously interpolated and the distribution maps of the geochemical anomalies related to these elements in figure 6 to 13 are visible. According to the studies carried out in the previous section, according to the main components analysis method, based on the points allocated to each of the samples under the third component (PC3), the final map of the geochemical anomaly is also drawn (Figure 4- 14).

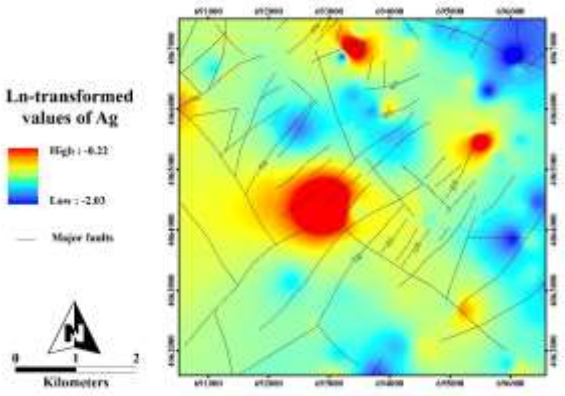

Figure 6. Distribution map of geochemical anomalies for Ag element.

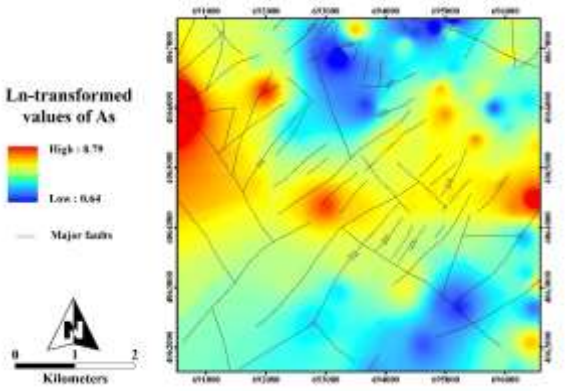

Figure 7. Distribution map of geochemical anomalies for As element.

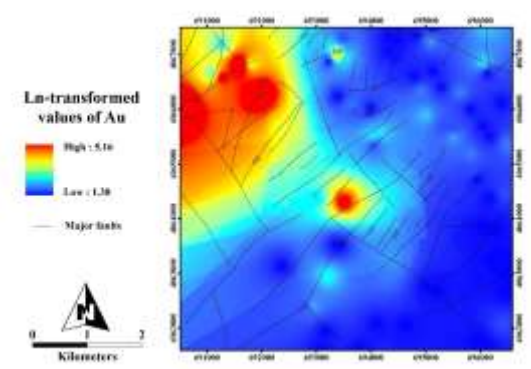

Figure 8. Distribution map of geochemical anomalies for Au element.

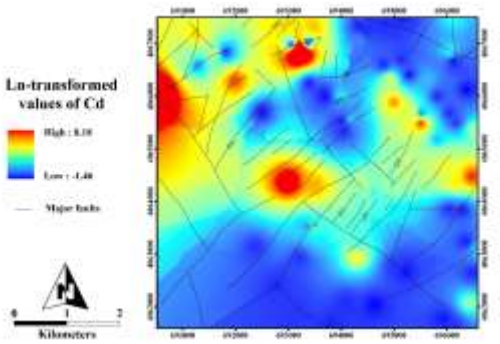

Figure 9. Distribution map of geochemical anomalies for Cd element.

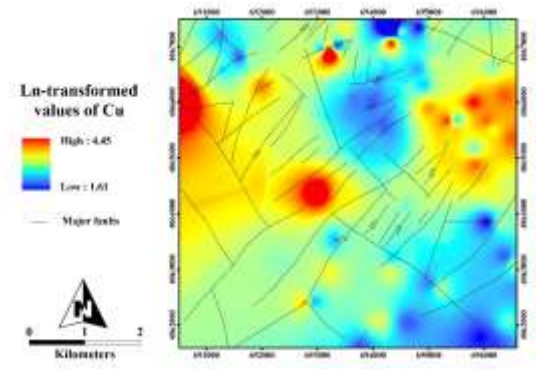

Figure 10. Distribution map of geochemical anomalies for Cu element.

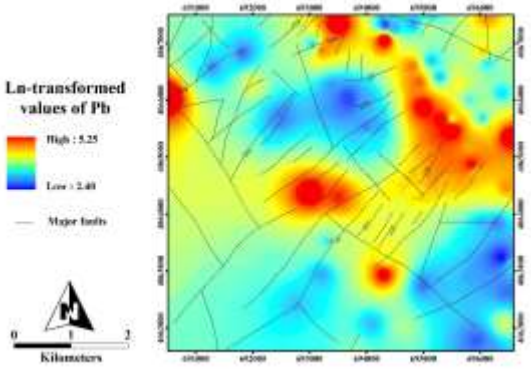

Figure 11. Distribution map of geochemical anomalies for Pb element.

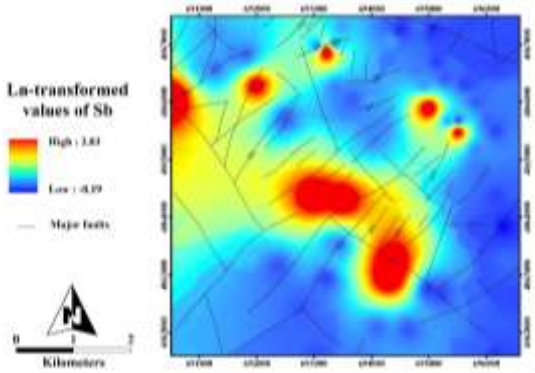

Figure 12. Distribution map of geochemical anomalies for Sb element.

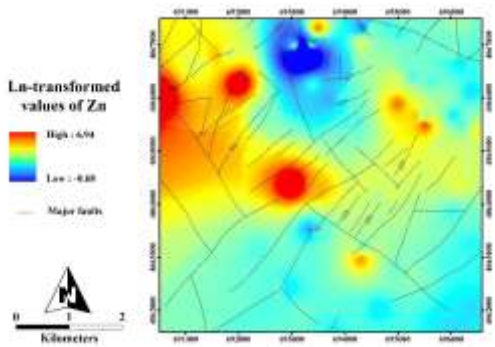

Figure 13. Distribution map of geochemical anomalies for Zn element.

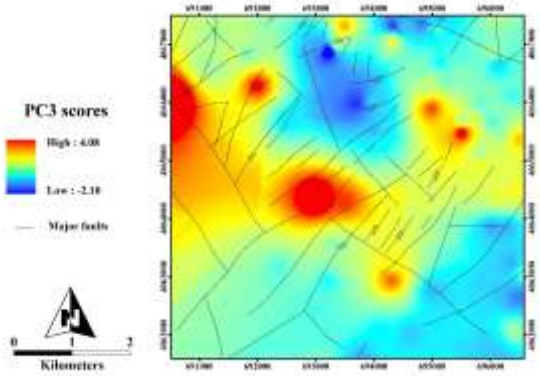

Figure 14. Distribution Map of Geochemical Anomalies for the Scores derived from the Third Component Analysis of Principal Components.

3.5. Estimated threshold

Firstly, eight elements were selected first for single-element geochemical data fractal modeling. For the fractal modeling by concentration-area method, the distribution of the 8 elements of the above mentioned elements, as described in the previous sections, was first normalized using logarithmic transformation, then ArcGIS 10.2 software was interpolated using the IDW method and mapped. Then, using the initial maps, the cumulative area of the pixels was calculated for definite grades, and the graphs plotted against the area were plotted in full logarithm. In order to determine the different

communities, direct lines were fitted on the points of the diagram based on the least squares law, and on the basis of which the thresholds and the number of different geochemical communities were determined.

It should be noted that the number of thresholds from the number of geochemical communities is always one unit less. In Figure 15, the Fractal Characteristics of the Gradient-Area Fractures for the 8 elements, As, Au, Cd, Cu, Pb, Sb and Zn are shown with the threshold lines.

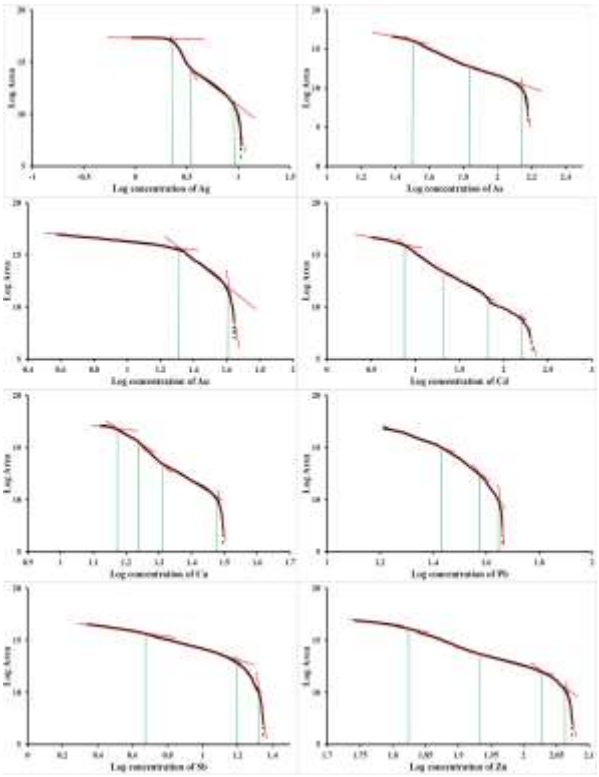

Figure 15. full-logarithmic graphs of concentration-area for the elements

After plotting full-logarithmic graphs for the elements studied and determining the thresholds and different geochemical communities, using the thresholds obtained from the diagram, from the existing data set, the value of the equivalent of each threshold limit (Table 4) and the final anomaly map classified using a full-gravity fractal method.

Figure 16 illustrates anomaly maps classified for the eight elements using the full-size fractal method. As is clear from the figure, geochemical communities are distinguished for different elements and can be used for more detailed studies on the region and for the discovery of new anomalies and for finding promising areas.

3.6. C-A fractal modeling of the values of PCA Values

The PC3 privileges were logged into Arc GIS 10.2 software and were internalized by the IDW method. Then all logarithmic graphs of values were plotted against the area occupied by those values (Figure 17). According to the entire logarithmic diagram of the concentration-area, four geochemical societies are identified and segregated based on the lines fitted on the chart based on the least squares method. These societies are composed of fields, low anomalies, moderate anomalies and strong anomalies, respectively.

Then, the estimated thresholds were entered into the software and the final map of the geochemical anomaly modeling for gold mineralization in Zarshuran range was obtained by the concentration-area fractal method, which provided low, medium and strong anomaly values for exploration and investigation More precise in the studied area can be used. The community with a moderate anomaly in identifying promising areas can be a good exploratory guide, and communities with strong anomaly values can also be used in more detailed exploration areas (Figure 18).

Table 4. The thresholds obtained for each selected element

Element	Population	Thresholds (ppm)	
Ag	1	0.13	0.20
	2	0.20	0.27
	3	0.27	0.66
	4	0.66	0.80
As	1	1.90	107.13
	2	107.13	578.36
	3	578.36	4713.75
	4	4713.75	6576.82
Au (ppb)	1	4	40.2
	2	40.2	146.7
	3	146.7	174.9
Cd	1	0.23	1.45
	2	1.45	5.66
	3	5.66	71.80
	4	71.80	951.71
	5	951.71	3588.23
Cu	1	5	24.96
	2	24.96	31.15
	3	31.15	41.54
	4	41.54	78.90
	5	78.90	85.97
Pb	1	11.03	66.24
	2	66.24	128.35
	3	128.35	178.26
	4	178.26	191.89
Sb	1	0.82	2.61
	2	2.61	10.02
	3	10.02	15.39
Zn	1	0.50	178.34
	2	178.34	373.96
	3	373.96	750.97
	4	750.97	946.29
	5	964.29	1038.28

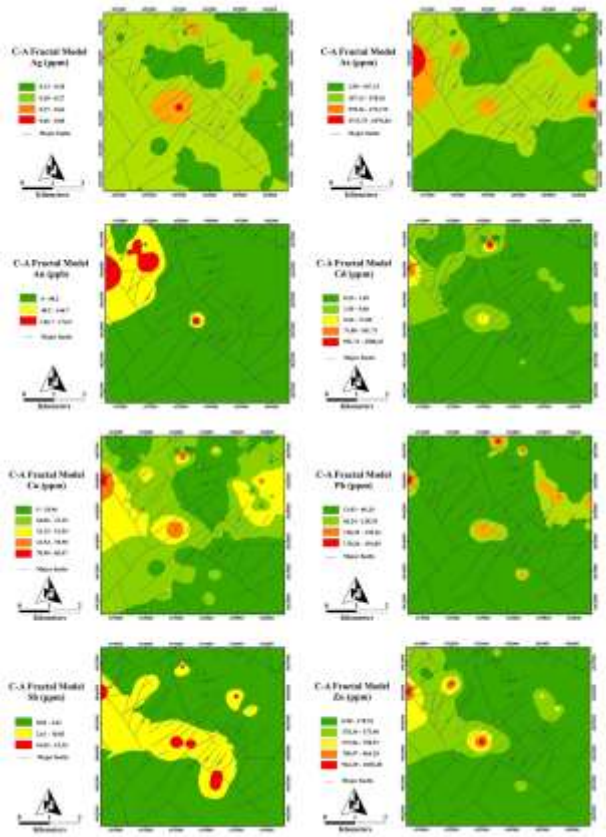

Figure 16. Distribution maps of geochemical communities using concentration-area fractal method for elements.

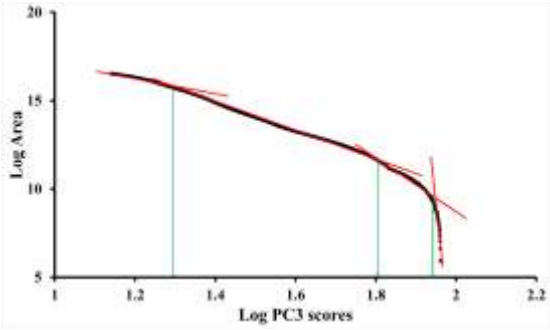

Figure 17: Full-logarithmic plot of concentration-area fractals for values obtained from PC3.

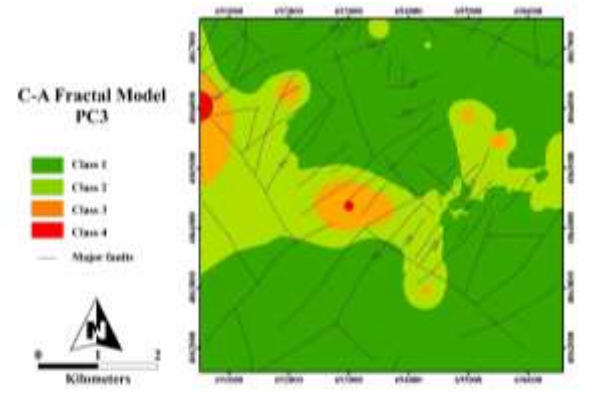

Figure 18. Final map of distribution of geochemical communities for PC3 values using concentration-area fractal method.

4. Conclusion

- To study the potential of gold mineralization in the Zarshuran area, field separation from anomalies such as fractal-geometric methods including concentration-area was used to separate the anomalous areas from the field and identify the geochemical promising areas.

- In this study, all 38 elements were first studied as monovalent and each geochemical pattern was detected. Then, based on the two-variable analysis of geochemical elements, using the coefficients of correlation and principal components analysis, the main values of the third component, as well as the 8 elements including Ag, As, Au, Cd, Cu, Pb, Sb and Zn, which are most related to mineral The gold mining of the Zarshuran range was selected and used to identify and isolate geochemical patterns.

- In the next step, 8 elements of the method based on the concentration-area fractal geometry were used to separate the anomal area from the background. Based on full logarithmic diagrams, concentration-area fractal method, 4 enrichment steps for Ag, As and Pb elements, 5 enrichment steps for Cu and Cd elements, 3 enrichment steps for Au and Sb elements were obtained. As in the geochemical anomaly maps derived from full-gravity fractal methods, the elements in the central, northeastern and northwest of the Zarshuran range have high-level anomalies.

- In the next step, by using the principal component analysis method, in the form of a multi-element geochemical map for the identification of gold mineralization, they are combined and for separating the anomaly of the communities from the field for continuous quantities obtained from the method of analysis of the main components of the concentration fractal method -The area was used.

- Based on the full logarithmic graphs of the concentration-area fractal method, 4 different geochemical societies including background, weak anomalies, modal anomalies and strong anomalies were obtained, which shows the high resolution of these methods for identifying areas with potential potential for exploration in this area.

References :

[1] Dodge, Y. (2006). *The Oxford dictionary of statistical terms*: Oxford University Press on Demand.
[2] Alahgholi, S., Shirazy, A., & Shirazi, A. (2018). Geostatistical Studies and Anomalous Elements Detection, Bardaskan Area, IRAN. *Open Journal of Geology, 8*(07), 697.
[3] Webster, R., & Oliver, M. A. (2007). *Geostatistics for environmental scientists*: John Wiley & Sons.
[4] Shirazi, A., Hezarkhani, A., Shirazy, A., & Shahrood, I. (2018). Exploration Geochemistry Data-Application for Cu Anomaly Separation Based On Classical and Modern Statistical Methods in South Khorasan, Iran. *International Journal of Science and Engineering Applications, 7*, 39-44.
[5] Shirazi, A., Shirazy, A., Saki, S., & Hezarkhani, A. (2018). Geostatistics Studies and Geochemical Modeling Based on Core Data, Sheytoor Iron Deposit, Iran. *Journal of Geological Resource and Engineering, 6*, 124-133.
[6] de Mulder, E. F., Cheng, Q., Agterberg, F., & Goncalves, M. (2016). New and game-changing developments in geochemical exploration. *Episodes, 39*(1), 70-71.
[7] Khakmardan, S., Shirazi, A., Shirazy, A., & Hosseingholi, H. (2018). Copper Oxide Ore Leaching Ability and Cementation Behavior, Mesgaran Deposit in IRAN. *Open Journal of Geology, 8*(09), 841.
[8] Shirazi, A., Hezarkhani, A., Shirazy, A., & Shahrood, I. (2018). Remote Sensing Studies for Mapping of Iron Oxide Regions, South of Kerman, IRAN. *International Journal of Science and Engineering Applications, 7*(4), 45-51.
[9] Shirazi, A., Shirazy, A., & Karami, J. (2018). Remote Sensing to Identify Copper Alterations and Promising Regions, Sarbishe, South Khorasan, Iran. *International Journal of Geology and Earth Sciences, 4*(2), 36-52.
[10] Chatfield, C. (2018). *Introduction to multivariate analysis*: Routledge.
[11] Mertler, C. A., & Reinhart, R. V. (2016). *Advanced and multivariate statistical methods: Practical application and interpretation*: Taylor & Francis.
[12] Rollinson, H. R. (2014). *Using geochemical data: evaluation, presentation, interpretation*: Routledge.
[13] Rokach, L., & Maimon, O. (2005). Clustering methods *Data mining and knowledge discovery handbook* (pp. 321-352): Springer.
[14] Manuel, R., Brito, M. d. G., Chichorro, M., & Rosa, C. (2017). Remote Sensing for Mineral Exploration in Central Portugal. *Minerals, 7*(10), 184.
[15] Wang, G., Du, W., & Carranza, E. J. M. (2017). Remote sensing and GIS prospectivity mapping for magmatic-hydrothermal base-and precious-metal deposits in the Honghai district, China. *Journal of African Earth Sciences, 128*, 97-115.
[16] Richardson, M. (2009). Principal component analysis. *URL: http://people. maths. ox. ac. uk/richardsonm/SignalProcPCA. pdf (last access: 3.5. 2013). Aleš Hladnik Dr., Ass. Prof., Chair of Information and Graphic Arts Technology, Faculty of Natural Sciences and Engineering, University of Ljubljana, Slovenia ales. hladnik@ ntf. uni-lj. si, 6*, 16.
[17] Jolliffe, I. (2011). Principal component analysis *International encyclopedia of statistical science* (pp. 1094-1096): Springer.
[18] Mandelbrot, B. B. (1974). Intermittent turbulence in self-similar cascades: divergence of high moments and dimension of the carrier. *Journal of Fluid Mechanics, 62*(2), 331-358.
[19] Davis, A., Lovejoy, S., & Schertzer, D. (1991). Radiative transfer in multifractal clouds *Non-Linear Variability in Geophysics* (pp. 303-318): Springer.
[20] Mohammadi, N. M., Hezarkhani, A., & Saljooghi, B. S. (2016). Separation of a geochemical anomaly from background by fractal and U-statistic methods, a case study: Khooni district, Central Iran. *Chemie der Erde-Geochemistry, 76*(4), 491-499.
[21] Cheng, Q., Agterberg, F., & Ballantyne, S. (1994). The separation of geochemical anomalies from background by fractal methods. *Journal of Geochemical Exploration, 51*(2), 109-130.
[22] Pazand, K., Hezarkhani, A., Ataei, M., & Ghanbari, Y. (2011). Application of multifractal modeling technique in systematic geochemical stream sediment survey to identify copper anomalies: a case study from Ahar, Azarbaijan, Northwest Iran. *Chemie der Erde-Geochemistry, 71*(4), 397-402.
[23] Afzal, P., Harati, H., Alghalandis, Y. F., & Yasrebi, A. B. (2013). Application of spectrum–area fractal model to identify of geochemical anomalies based on soil data in Kahang porphyry-type Cu deposit, Iran. *Chemie der Erde-Geochemistry, 73*(4), 533-543.
[24] Lima, A., De Vivo, B., Cicchella, D., Cortini, M., & Albanese, S. (2003). Multifractal IDW interpolation and fractal filtering method in environmental studies: an application on regional stream sediments of (Italy), Campania region. *Applied Geochemistry, 18*(12), 1853-1865.
[25] Hengl, T. (2006). Finding the right pixel size. *Computers & geosciences, 32*(9), 1283-1298.

International Journal of Science and Engineering Applications
Volume 7–Issue 09,274-279, 2018, ISSN:-2319–7560

Exploratory Remote Sensing Studies to Determine the Mineralization Zones around the Zarshuran Gold Mine

Adel Shirazy
Shahrood University of Technology
Shahrood, Iran

Aref Shirazi
AmirKabir University of Technology
Tehran, Iran

Saeed Heidarlaki
Shahrood University of Technology
Shahrood, Iran

Mansour Ziaii *
Shahrood University of Technology
Shahrood, Iran

Abstract: Zarshuran gold mine is located in Takab city and West Azarbaijan province. Due to the importance of remote sensing in the identification of mineralization and alterations in mineral areas, remote sensing studies were carried out around the gold mine. The purpose of these studies was to identify mineralization zones around the mine area. In this study, due to the suitability of Aster Images to identify copper alterations various methods of remote sensing such as false color combinations (FCC) and spectral angle mapper (SAM) for mapping altrations and promising regions were used. Finally, areas with mineralization and alteration were presented as maps.

Keywords: Remote Sensing; FCC; SAM; Aster; Gold

1. INTRODUCTION

We Remote sensing is the acquisition of information about an object or phenomenon without making physical contact with the object and thus in contrast to on-site observation. Remote sensing is used in numerous fields, including geography, land surveying and most Earth Science disciplines (for example, hydrology, ecology, oceanography, glaciology, geology); it also has military, intelligence, commercial, economic, planning, and humanitarian applications [1] [2].

In current usage, the term "remote sensing" generally refers to the use of satellite- or aircraft-based sensor technologies to detect and classify objects on Earth, including on the surface and in the atmosphere and oceans, based on propagated signals (e.g. electromagnetic radiation). It may be split into "active" remote sensing (i.e., when a signal is emitted by a satellite or aircraft and its reflection by the object is detected by the sensor) and "passive" remote sensing (i.e., when the reflection of sunlight is detected by the sensor) [3] [4] [5].

Remote sensing is one of the methods that can be used to separate surface anomalies from the field by detecting alterations and target minerals. In the early stages of regional exploration, it is possible to identify mineralization and alteration by using the classic and modern statistical methods on the geochemical data in the study region [6] [7]. The combination of remote sensing results and geochemical statistical studies can provide more reliable results [8]. Also, initial exploratory studies include economic studies and mineral processing in the region. Statistical and geochemical studies are the basis of these studies [9].

All material on each page should fit within a rectangle of 18 x 23.5 cm (7" x 9.25"), centered on the page, beginning 2.54 cm (1") from the top of the page and ending with 2.54 cm (1") from the bottom. The right and left margins should be 1.9 cm (.75”). The text should be in two 8.45 cm (3.33") columns with a .83 cm (.33") gutter[10].

2. METHODOLOGY AND DATASET

2.1 Geolocation of Study Area

The Zarshuran mineral zone is located in West Azarbaijan province of Iran and on geological sheet of Takht-e-Soleyman (on sclae 1:100,000). The Takht-e-Soleyman sheet covers parts of Zanjan, West Azarbaijan and East Azarbaijan provinces. The Takht-e-Soleyman sheet is part of the 1: 250000 geological map of the Takab rectangle between the eastern longitude 47° 00' and 47° 30' and the north latitude 36° 30' 'to 37° 00' . The quadrilateral coordinates of the studied area are presented in Table 1. Due to its location in the Takab metallurgical province and the location of the Alborz-Azarbaijan, Iran Central and Sanandaj-Sirjan construction zones, this area has a lot of mineralization diversity. The most important mineralization in this area is the lead and zinc mineralization (Anguran, Alam Kandy and Arpachai) and gold mineralization (Zarshuran, Aghdare and Tozlar). The study area of this project is located between Zanjan and East Azarbaijan provinces around the Zarshuran gold mine. Geolocation of study area in Iran map is shown in figure 1.

Table 1. Geographical coordinates of study area

Geographical Coordinates		points
Latitude (Y)	Longitude (X)	
36° 40' 49"	47° 08' 00"	A
36° 44' 06"	47° 08' 00"	B
36° 44' 06"	47° 12' 03"	C
36° 40' 49"	47° 12' 03"	D

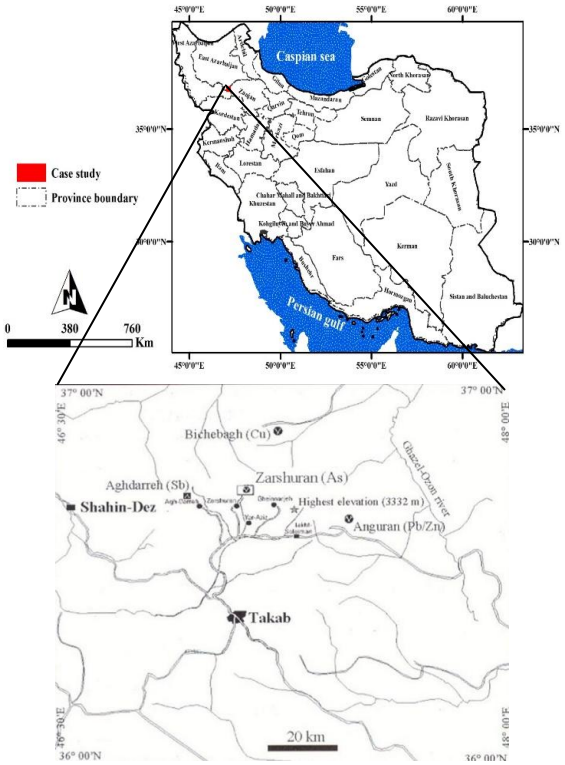

Figure 1. Geolocation of study area in Iran map

2.2. Satellite Remote Sensing Data

In this study, the image of the ASTER Satellite Sensor was used. ASTER *(*Advanced Spaceborne Thermal Emission and Reflection Radiometer) is a high resolution imaging instrument that is flying on the Terra satellite [11]. *ASTER* will obtain detailed maps of land surface temperature, emissivity, reflectance and elevation of the Earth.

ASTER has three sensors to measure and record the reflected and emitted Electromagnetic Radiation (EMR). They are working in different wavelength regions the Visible and Near Infrared (VNIR) between 0.52 and 0.86 μm, Short Wave Infrared (SWIR) between 1.6 and 2.43 μm, and Thermal Infrared (TIR) between 8.125 and 11.65 μm. ASTER data consists of 14 spectral bands 3 VNIR, 6 SWIR, and 5 TIR with 15, 30, and 90 m spatial resolution, espectively [12]. The VNIR, SWIR and TIR wavelength regions provide complementary data for lithological mapping [13].

Geometric corrections were made using the satellite ETM^+ satellite image on the study area image. In order to ensure the results, IAR Reflectance radiometric corrections were applied to the region image and the results for applying different types of processes were introduced into ENVI software[5; 14].

Please use a 9-point Times Roman font, or other Roman font with serifs, as close as possible in appearance to Times Roman in which these guidelines have been set. The goal is to have a 9-point text, as you see here. Please use sans-serif or non-proportional fonts only for special purposes, such as distinguishing source code text. If Times Roman is not available, try the font named Computer Modern Roman. On a Macintosh, use the font named Times. Right margins should be justified, not ragged [10].

2.3. False Color Combinations Method

The importance of displaying the color combination of images in remote sensing can be considered due to their effectiveness in visual interpretation of various effects. One of the effective methods for identifying and separating various geological units is the false color combination (FCC) method [15].

The false color combination is a combination of three different bands combined in red, green, and blue (RGB) colors. If the combined bands of red, green, and blue wavelengths are the visible spectrum of electromagnetic spectrum, the resulting image will be a true color combination. If a different combination of red, green and blue bands or other bands of the electromagnetic spectrum is used, a false color image will be obtained that is not similar to the surface of the earth and its colors [16].

In making false color combinations it is better to use bands that have less correlation. Since the interaction of different wavelengths of electromagnetic energy is different in dealing with rock units, the sensitivity of the human eye to minor changes in color is much greater than its sensitivity to changes in black and white images. Choosing the best band combination depends on the target [17].

Three images can be combined to make the images visible for viewing in three blue, green, and red wavelengths (original RGB color combinations). In this study, this combination has been used to display several images in a single image and simultaneously display different information from a single point [18].

Calculation of the optimum index factor amount (OIF) is required to obtain the best false color combination (OIF of the higher color combinative with more information). The formula below shows the OIF calculation method [19].

$$OIF = \frac{\sum_{k=1}^{3} S_k}{\sum_{j=1}^{3} r_j} \qquad (1)$$

In formula 1 : S_k is the standard deviation of the k band, r_j is the two-band correlation coefficient of the three-band combination [20]. Sometimes visually, the false color combinations containing major information are determined by the variety of colors [5; 21] [10].

2.4. Spectral Angle Mapper (SAM) Method

Spectral angle mapping (SAM) method is an image classification method by calculating the similarity between the image spectrum and a reference spectrum (e.g., spectral libraries) [22]. The algorithm of this method calculates the similarity between two spectra by the spectral angle between

them [23]. In fact, by transforming the spectra into a vector in a space in the number of dimensions of the bands, the angle between the two vectors is calculated (See figure 2) [24] .

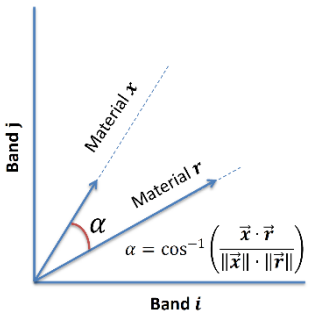

Figure. 2 Example of SAM classification in case of 2 spectral bands. Scalar product between unknown material x and library sample r [24].

In this method, the direction is important for calculating vectors, not length. Therefore, other factors are not considered in this method. In fact, the more the angle (between 0 and 1) is less, the more accurate it will be. If the value is 0, the whole image is identified as the desired phenomenon. To compare a pixel, the desired pixel spectrum is plotted from the examined area with the same pixel spectrum in the laboratory (library) on two bands in a coordinate axis. Then the points are connected to the coordinate center, and the angle between the two lines is used as the pixel identification angle. If the n bands are used to identify the phenomenon concerned, the following formula is used to obtain an angle[5] [25] [10].

$$\alpha = \mathrm{Cos}^{-1}\left[\frac{\sum_{i=1}^{nb} x_i r_i}{(\sum_{i=1}^{nb} x_i^{\,2})^{\frac{1}{2}}(\sum_{i=1}^{nb} r_i^{\,2})^{\frac{1}{2}}}\right] \qquad (3)$$

In formula 3 : nb is the number of bands. unknown material x and library sample r.

3. RESULTS AND DISCUSSION

3.1. False Color Combinations Method

One of the methods used to identify hydrothermal alterations in esters is the use of false color combinations. Al-OH bonded minerals such as kaolinite, muscovite and montmorillonite and ilite, index minerals (phylic and argillic alteration zones) have maximum reflection in the band of 4 SWIR regions. Also, minerals containing Mg-OH such as chlorite and epidote, which are the propylitic altration zone index, have a high reflection in the ASTER spectral band of the spectral range of the SWIR. Therefore, the false color combination (FCC) 4-6-8 of the SWIR region will show the red and pink red and red and pink red argillic zones and the proplyitic alteration zones in green [26]. In the study area, phylic and argillic alterations are seen in red to pink, while the alteration stones related to propylitic alteration are green in the vicinity of the argillic-phyllic alterations (Figure 3).

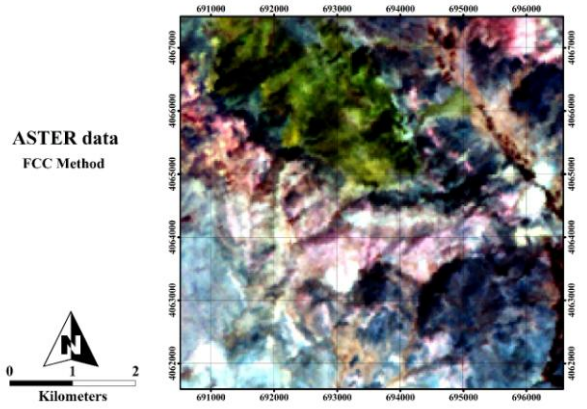

Figure 3. False color combination 4-6-8 (RGB). Phylic alteration and argillic are seen in red to pink and propylitic alterations are green.

Most deposits and minerals are closely related to geological structures, lithological units, tectonics and faults in the region. Using satellite imagery, lithological units and geological structures of the region can be identified and differentiated, which would help to identify the mineralogy and ultimately explore the deposits in them. One of the best ways to identify these structures is the use of ETM + images. The use of these images provides a good idea to identify the structure of tectonics and geological structures and rock units in the area. For the detection and separation of stone units in ETM + images, the color combination of the band 5 in the red channel and the band 3 in the green channel and the band 1 in the blue channel is the best color combination[27]. In this research, ETM + band 5, 3 and 1 were used to distinguish rock units and identify lines such as faults in the region.

The false color combination of 5-3-1 was used to display the image. As shown in Figure 4, the stone units are well separated. In Figure 5, the main faults in the area are well identified. By matching the image from the color combination 5-3-1 with the geologic map of the area, the accuracy of the results obtained from the processing of ETM + images is confirmed for the identification and separation of rock units and lineaments in the region.

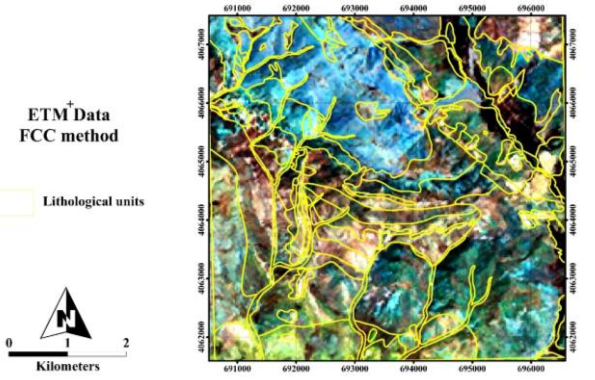

Figure 4. Map of the division of linguistic units of the study area using the false color combination of the 5-3-1 band of the ETM + sensor.

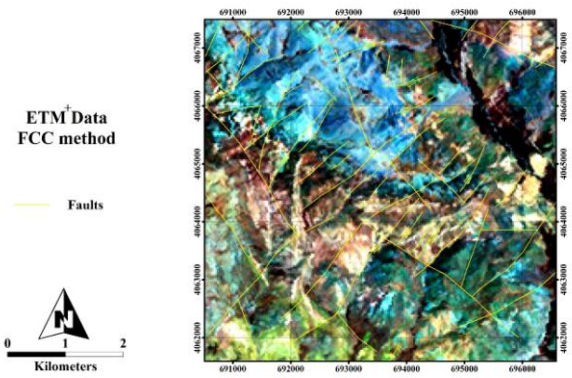

Figure 5. Identification map of the lines (faults) of the study area using the false color combination of the 5-3-1 band of the ETM+ sensor.

3.2. Spectral Angle Mapper (SAM) Method

Spectral analysis of ASTER images can be a very useful tool for identifying various types of alterations such as argillic, advanced argillic, sericitic, propylitic, silicification and iron oxides. In practice, the ability of this tool depends on a large number of factors, including:

- Presence of vegetation: vegetation strongly influences spectral properties of alteration areas.
- Effect of surface coating system: Small systems such as mesothermal veins and mild sulfide systems are often smaller than the spatial resolution of ASTER images.
- Host rock: Spectral analysis in volcanic systems is a very useful tool, so that in these rocks the alteration areas are in contrast to the surrounding rocks and can be distinguished. In these systems, even very tight target areas can be identified.

The main advantage of this method, among the methods of satellite data classification, is the ease and speed of mapping based on the spectral similarity between the spectrum of the problem and the reference spectrum. As you can see in Figure 6, various minerals, which indicate hydrothermal alterations and iron oxide and silica alterations are identified separately.

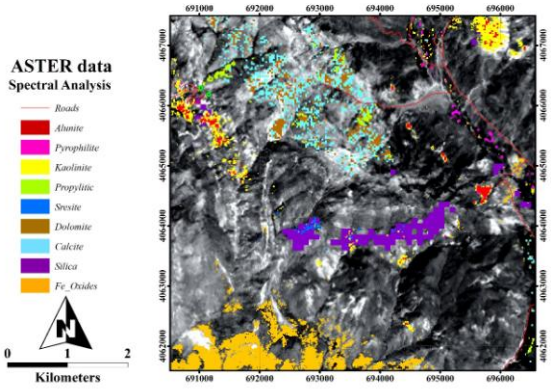

Figure 6. Map of alterations in the study area using the SAM method

4. CONCLUSION

- Considering the importance of remote sensing in identifying mineralization and alterations in mineral areas, this study was carried out in the studied area under the name of Zarshuran in the north of Takab in West Azarbaijan province in northwest.
- In these studies, after corrections made on satellite images, methods such as false color combination, band ratio and spectral analysis method have been used.
- The result of these surveys is the identification of alterations and mineralization of the region, as presented in Figures 3 to 6. The results indicate that there are several promising regions, most of them in the west and northwest of the region. The results of this research can be used to promote the mineral exploration project around the Zarshuran mine.

REFERENCES :

[1] Schott, J. R. (2007). *Remote sensing: the image chain approach*: Oxford University Press on Demand.

[2] Guo, H., Huang, Q., Li, X., Sun, Z., & Zhang, Y. (2013). Spatiotemporal analysis of urban environment based on the vegetation–impervious surface–soil model. *Journal of Applied Remote Sensing, 8*(1), 084597.

[3] Zhang, X., Pazner, M., & Duke, N. (2007). Lithologic and mineral information extraction for gold exploration using ASTER data in the south Chocolate Mountains (California). *ISPRS Journal of Photogrammetry and Remote Sensing, 62*(4), 271-282.

[4] Robert, A. S. (2007). Remote sensing: Models and methods for image processing. *By Elsevier Inc. All rights reserved*, p300-304.

[5] Shirazi, A., Hezarkhani, A., Shirazy, A., & Shahrood, I. (2018). Remote Sensing Studies for Mapping of Iron Oxide Regions, South of Kerman, IRAN. *International Journal of Science and Engineering Applications, 7*(4), 45-51.

[6] Shirazi, A., Hezarkhani, A., Shirazy, A., & Shahrood, I. (2018). Exploration Geochemistry Data-Application for Cu Anomaly Separation Based On Classical and Modern Statistical Methods in South Khorasan, Iran. *International Journal of Science and Engineering Applications, 7*, 39-44.

[7] Shirazi, A., Shirazy, A., Saki, S., & Hezarkhani, A. (2018). Geostatistics Studies and Geochemical Modeling Based on Core Data, Sheytoor Iron Deposit, Iran. *Journal of Geological Resource and Engineering, 6*, 124-133.

[8] Alahgholi, S., Shirazy, A., & Shirazi, A. (2018). Geostatistical Studies and Anomalous Elements Detection, Bardaskan Area, IRAN. *Open Journal of Geology, 8*(07), 697.

[9] Khakmardan, S., Shirazi, A., Shirazy, A., & Hosseingholi, H. (2018). Copper Oxide Ore Leaching Ability and Cementation Behavior, Mesgaran Deposit in IRAN. *Open Journal of Geology, 8*(09), 841.

[10] Shirazi, A., Shirazy, A., & Karami, J. (2018). Remote Sensing to Identify Copper Alterations and Promising Regions, Sarbishe, South Khorasan, Iran. *International Journal of Geology and Earth Sciences, 4*(2), 36-52.

[11] Arivazhagan, S., & Anbazhagan, S. (2017). ASTER Data Analyses for Lithological Discrimination of Sittampundi Anorthositic Complex, Southern India.

[12] Obata, K., Tsuchida, S., Yamamoto, H., & Thome, K. (2017). Cross-Calibration between ASTER and MODIS Visible to Near-Infrared Bands for Improvement of ASTER Radiometric Calibration. *Sensors, 17*(8), 1793.

[13] Amer, R., Kusky, T., & Ghulam, A. (2010). Lithological mapping in the Central Eastern Desert of Egypt using ASTER data. *Journal of African Earth Sciences, 56*(2-3), 75-82.

[14] Padró, J.-C., Pons, X., Aragonés, D., Díaz-Delgado, R., García, D., Bustamante, J., . . . Cristóbal, J. (2017). Radiometric Correction of Simultaneously Acquired Landsat-7/Landsat-8 and Sentinel-2A Imagery Using Pseudoinvariant Areas (PIA): Contributing to the Landsat Time Series Legacy. *Remote Sensing, 9*(12), 1319.

[15] Abdelaziz, R., El-Rahman, Y. A., & Wilhelm, S. (2018). Landsat-8 data for chromite prospecting in the Logar Massif, Afghanistan. *Heliyon, 4*(2), e00542.

[16] Masoumi, F., Eslamkish, T., Honarmand, M., & Abkar, A. A. (2017). A Comparative Study of Landsat-7 and Landsat-8 Data Using Image Processing Methods for Hydrothermal Alteration Mapping. *Resource Geology, 67*(1), 72-88.

[17] Yao, K., Pradhan, B., & Idrees, M. O. (2017). Identification of rocks and their quartz content in gua musang goldfield using advanced spaceborne thermal emission and reflection radiometer imagery. *Journal of Sensors, 2017*.

[18] Hereher, M. E., & Abdullah, S. E. (2017). Lithologic mapping of Aja granitic batholiths, Ha'il, Saudi Arabia, using remote sensing. *Arabian Journal of Geosciences, 10*(14), 313.

[19] Razmi, M., Asgari, H. M., Sohrab, A. D., Nazemosadat, S. M. J., & Khazaei, S. H. (2017). Monitoring oscillations coastline of Dayyer city during the El Niño and La Niño using OIF utility index.

[20] Abbaszadeh, M. (2010). Mapping hydrothermal alterations using ASTER images in Parkam area, Kerman. *GEOSCIENCES, 78*.

[21] Hooshyari, N. (2005). *Separation of alteration zones in relation to possible mineralization of gold and copper Zofre area using satellite data ASTER.* (BSc), Isfahan University of Technology.

[22] Asadzadeh, S., & de Souza Filho, C. R. (2016). A review on spectral processing methods for geological remote sensing. *International journal of applied earth observation and geoinformation, 47*, 69-90.

[23] Hasan, E., Fagin, T., El Alfy, Z., & Hong, Y. (2016). Spectral Angle Mapper and aeromagnetic data integration for gold-associated alteration zone mapping: a case study for the Central Eastern Desert Egypt. *International Journal of Remote Sensing, 37*(8), 1762-1776.

[24] Markovskiy, N. (2014). Drop-in Acceleration of GNU Octave.

[25] Esmaeeli, M., Tabaee, M., & Asadiharooni, H. (2012). *Remote Sensing Study (ASTER & TM) and Geology of Southwest Meyme Iron Ore Deposit, IRAN*. Paper presented at the 31st Symposium of Geosciences, Tehran, IRAN.

[26] Alimohammadi, M., Alirezaei, S., & Kontak, D. J. (2015). Application of ASTER data for exploration of porphyry copper deposits: A case study of Daraloo–Sarmeshk area, southern part of the Kerman copper belt, Iran. *Ore Geology Reviews, 70*, 290-304.

[27] Sadeghi, B., Khalajmasoumi, M., Afzal, P., Moarefvand, P., Yasrebi, A. B., Wetherelt, A., . . . Ziazarifi, A. (2013). Using ETM+ and ASTER sensors to identify iron occurrences in the Esfordi 1: 100,000 mapping sheet of Central Iran. *Journal of African Earth Sciences, 85*, 103-114.

International Journal of Science and Engineering Applications
Volume 7–Issue 09,280-283, 2018, ISSN:-2319–7560

Design of Distillation Column for Liquid Fuel from Waste Tire

Zarni Htay
Department of Chemical Engineering, Mandalay Technological University, Myanmar

Moe Moe Kyaw
Department Chemical Engineering , West Yangon Technological University, Myanmar

Tint Tint Kywe
Department of Chemical Engineering, Mandalay Technological University, Myanmar

***Abstract*— In this study, tire chips (without steel cords) obtained from waste tire were used as raw material to prepare valuable products; liquid fuel, char and gas. Two-stage reaction system was used in this experiment. Three types of catalyst pellets (volcanic ash, dolomite and Mabisan clay) were prepared by activation in furnace about 3 hours and temperature range from 800˚C to 850˚C.These catalyst were analyzed by using X-ray Diffraction (XRD) and gravimetric analysis method. There were four experiments in this study. The final product, liquid fuel was measured its density, viscosity, kinematic viscosity and refractive index. The experiments were carried out at temperatures between 210 - 400 ˚C with and without using any catalyst. Yield percent of liquid fuels were 50.12%, 51.34%, 48.54% and 44.65% for using Mabisan clay, volcanic ash, dolomite and without catalyst respectively.Moreover,yield percent of char and gas fuel of the experiment was obtained 40% and 10 % respectively.**

***Keywords*—waste tire, catalyst pellets, liquid fuel, XRD, gravimetric analysis method**

I. INTRODUCTION

Around the world, there are initiatives to replace gasoline and diesel fuel due to the impact of fossil fuel crisis, hike in oil price and stringent emission norms. Millions of dollars are being invested in the search for alternative fuels. On the other hand, the disposal of waste tyres from automotive vehicles is becoming more and more complex [1]. As a result of rapidly growing number of car owners, among others, also the production of used tires increases. Most of the used tires accumulates in landfills, they are bulky and do not degrade. Currently, it is preferable to reduce filling the landfills and focus on recycling methods, the use of tires as a valuable source of energy and chemical substances. The pyrolysis is one of the conventional methods, however in the field of processing of used tires is a relatively new technology. This is the decomposition of organic material at high temperatures in an inert atmosphere (or vacuum). The pyrolysis of waste tires represents an alternative environmentally-friendly processing and at the same time enables you to gain useful products [2].

Pyrolysis is the chemical conversion or breakdown of organic compounds by heating in the total or partial absence of oxygen. Energy recovery from pyrolytic gas , the valuable liquid products and char are obtained, which may become commercial products after additional processing [3]. Another solution of removing tires from the waste stream is incineration. A serious consequence of burning tires is that it may release toxic chemical compounds such as dioxin, furans, and aromatic hydrocarbons into the atmosphere. The final products from the open combustion of waste tires are ash, particulates, tar, and exhaust gases, which are blamed for several physical health problems such as eye irritation and respiratory problems. The high levels of pollution generated from open tire burning are unacceptable to the public [4]. The aim of the present research work was to study the fuel oil derived from the waste tires .

In Myanmar, liquid fuel from the waste tire is potentially increased as a National project. In this study , the tire chips (without steel cords) from waste truck tire was used as a raw material to prepare valuable products such as liquid fuel ,char and gas.

II. MATERIALS AND METHODS

A. Raw Materials

Tire chips (bulk density = 0.87g/cm^3, thickness = 0.9 cm, average volume = 1.4 cm^3) were obtained from waste tire of truck cars. These were purchased from local market. Different natural catalysts (Mabisan clay Mhawbe township, Yangon division, volcanic ash from Popa region, Mandalay division and dolomite from Kyaukse, Mandalay division) were used to pyrolyse the waste tire.

B. Preparation of Tire Chips from the Waste Truck Car Tire

Tire chips were obtained from waste truck car tire. But it is impossible to pyrolyse the whole tire in the thermal reactor. Firstly, steel cords were removed from waste tire. And then, waste tire were washed and cleaning to remove dust and sand. Moreover, these were dried in the oven at 60˚C for two hour. Finally, waste tire was chipped into cylinder shape with 1.4 cm^3 in volume. The moisture content, bulk density and ash content of truck car tire were initially determined. Tire chips from waste tire are as shown in Fig 1.

Fig. 1 Tire chips from waste tire

C. Preparation of Natural Catalyst Pellets

In this study, three types of catalyst were used. These were Mabisan clay, dolomite and volcanic ash. The catalyst powder was moulded to make required shape. Prior to use, all the natural catalysts were crushed and sieved. Particle sizes having (< 495µm) were used and pelletised by moulding. And then, these catalysts were activated by heating at the temperature range from 800˚C to 850˚C for 3 hours. The catalyst pellets (a) Mabisan clay, (b) dolomite and (c)volcanic ash are as shown in Fig 2. The chemical compositions such as SiO_2, Al_2O_3, $CaCO_3$ and Fe_2O_3 contents of all catalyst samples were determined by using the gravimetric analysis method at the Department of Technology Promotion and Coordination Metallurgical Research and Development Centre in Ela.

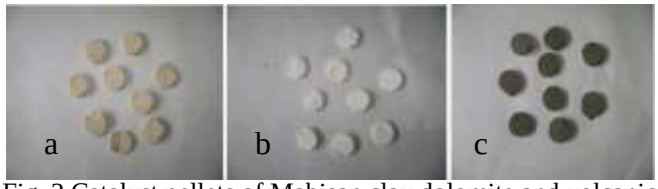

Fig. 2 Catalyst pellets of Mabisan clay dolomite and volcanic ash

D. Preparation of Crude Liquid Fuel from Waste Tire

The two-stage reactor for waste tire cracking was set-up as shown in Fig 6. The weight ratio of raw material and catalyst was 10:1 ratio. To do catalytic cracking, 200 g of waste tire chips were loaded into the reactor and 20 g of each natural catalyst was placed in the catalytic bed. The thermal reactor was heated to 250˚C with the heating rate of 5˚C min^{-1} and then to reach the final setting temperature 400˚C by using the heating rate of 2˚C per minute. The thermal reactor was purged with nitrogen gas throughout the process. The catalytic bed was heated to 300˚C. The organic vapours thermally cracked from waste tire chips were passed through the catalytic bed for catalytic cracking. After that, the vapour were condensed as liquid fuel in the 1st and 2nd condenser. The yield percent of liquid fuel from the condenser were determined. And then, density, refractive index and kinematic viscosity of product liquid fuel were determined.

III. RESULTS AND DISCUSSION

The result of characteristics of waste tire are shown in Table1. After activating by heating at the temperature range from 800˚C to 850˚C for 3 hours, the natural catalyst pellets were analyzed by using XRD at the Department of Technology Promotion and Coordination Metallurgical Research and Development Centre in Ela. The XRD patterns of natural catalysts are shown in Fig 3, 4 and 5. Chemical compositions of natural catalysts are shown in Table 2. Table 3 illustrates the densities, refractive indices and kinematic viscosities of product liquid fuels obtained from the process by using with and without catalysts. The colour of product liquid fuels obtained by using catalysts and without catalyst were nearly the same in greenish brown colour. According to Table 3 and 4, the yield (%) and colour of liquid fuel depend on the usage with and without catalyst. It was found that the yield (%) of product liquid fuels using catalysts were higher than the yield (%)of product liquid fuel using without catalysts. Among them, the highest yield of liquid fuel can be obtained using volcanic ash catalyst . The odour of liquid fuel without using catalyst was worse than using catalysts. According to the literature, during the pyrolysis process, 33-38 wt. % of pyrolytic char occur, 38 -55 wt. % of pyrolytic oil and 10-30 wt. % of gases[2]. According to Table 4, the result of yield percent of liquid fuel from the two-stage reaction system were found to be nearly 50%. And then, liquid fuel from the pyrolysis of waste tire will be the qualified product. And then, the yield (%) of char was found to be high carbon content. Therefore, it could be suggested that activated carbon should be produced from this high carbon content.

TABLE 1
CHARACTERISTICS OF RAW MATERIAL

Parameter	Unit	Value
Total moisture	%wt	1.2
Bulk density	g/cm^3	0.87
Ash content	%wt	5.50

TABLE 2
CHEMICAL COMPOSITIONS OF NATURAL CATALYST

Components	Mabisan clay	Volcanic ash	Dolomite
SiO_2(%)	58.9	45.87	20.12
Al_2O_3(%)	27.8	17.6	3.23
Fe_2O_3(%)	1.34	10.12	5.12
$CaCO_3$(%)	-	0.054	51.67

TABLE 3
COMPARISON OF QUALITATIVE ANALYSIS OVER PRODUCT CRUDE LIQUID FUEL

Catalyst	Density (g/cm^3)	Refra-ctive index	Kinematic viscosity (mm^2/s)	Colour	Odour
Mabisan clay	0.807	1.498	3.57	Greenish brown	Like diesel
Volcanic ash	0.805	1.487	3.32	Greenish brown	Like diesel
Dolomite	0.87	1.497	3.71	Greenish brown	Like diesel
Without catalyst	0.88	1.496	4.54	Brown	Strong

TABLE 4
COMPARISON OF PRODUCT YIELD BY USING NATURAL CATALYSTS
Reaction temperature: 210 – 400 ˚C
Reaction time : 3.5 hours

Catalyst	Liquid fuel yield (%)	Char yield (%)	Gas yield (%)
Mabisan clay	50.12	42.12	6.12
Volcanic ash	51.34	40.43	6.01
Dolomite	48.54	41.54	6.45
Without catalyst	44.65	39.78	8.12

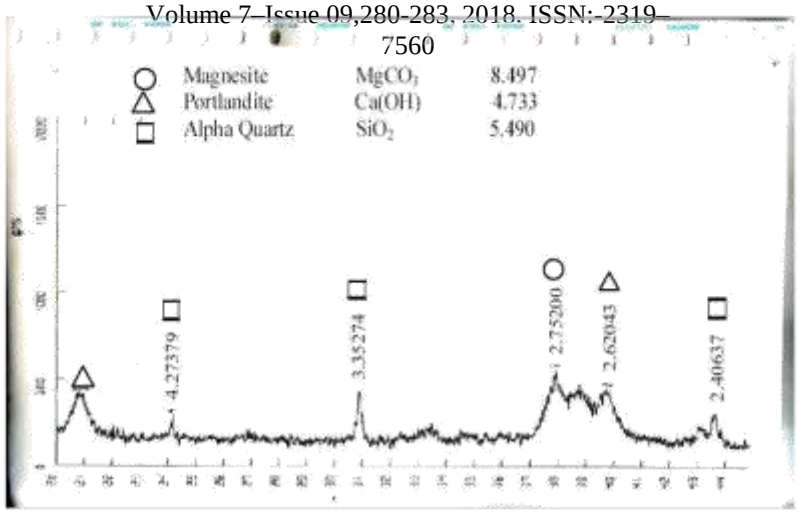

Fig. 3 XRD pattern of dolomite after activating

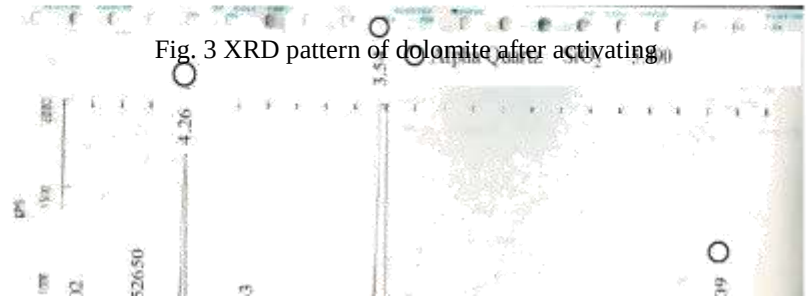

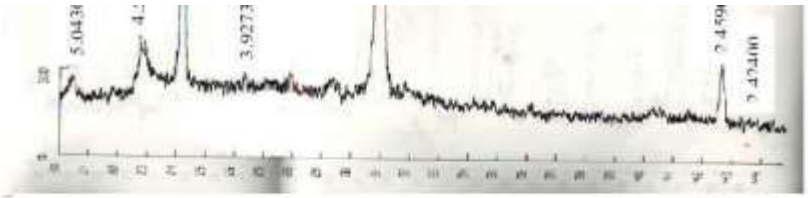

Fig. 4 XRD pattern of Mabisan clay after activating

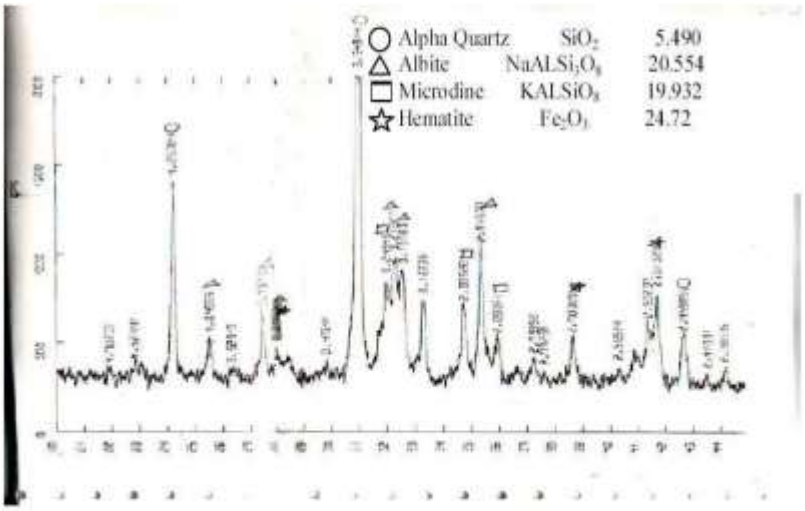

Fig. 5 XRD pattern of volcanic ash after activating

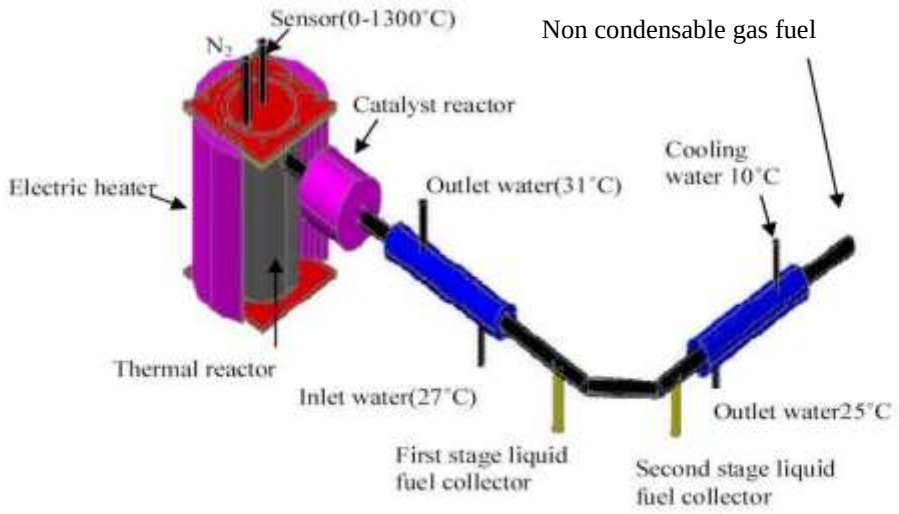

Fig. 6 Schematic representation of the two-stage reaction system[5]

IV. CONCLUSION

In this study, the liquid fuel from waste tire pyrolysis experiment can be given crude oil. Therefore, the crude oil should be needed to distillate for the pure fuel properties. The pyrolysis results showed that the waste tire degradation takes place at temperature from (210˚C-400˚C). Upon reaching the final pyrolysis temperature about 50yield% of liquid fuel, 40 yield% of char and, 10 yield% of non condensable gas fuel were obtained. Oil obtained by pyrolysis can be used directly as a fuel or admixture to the products of petrochemical industry. Gases can also be used as a fuel. Char can be used either as a smokeless fuel, carbon black or activated carbon, or can be gasified to obtain gaseous fuels. Moreover, this research can be beneficial for environmental control and can also support to solve the shortage problems of fossil fuels at the near future.

ACKNOWLEDGMENT

The authors would like to express their profound gratitude to U Zaw Lay win and Dr.April Nwayy Nwayy Htett, Department of Chemical Engineering, Yangon Technological University(YTU), for valuable instructions throughout the whole period of research work.

REFERENCES

[1] Adéla ČÍŽKOVÁ, *Comparison of yield of tire pyrolysis Laboratory and pilot scales*, Czech Republic (2009)
[2] A.M. Fernández, *Pyrolysis of tire wastes*, Apartado 73,3 3080, Oviedo, Spain (2008)
[3] S.Murugan, *The use of tire pyrolysis oil in diesel engines*, Chennai, India Anna University (2005)
[4] S. Murugan, *A comparative study on the performance emission and combustion studies of a DI diesel engine using distilled tire pyrolysis oil-dieselblends*, Anna Univ ersity, Chennai, India (2008)
[5] Myat Taw Htet, *Performance Investigation of Naturally Occurring Catalysts on Cracking of High Density polyethylene (HDPE) waste*, Department of Chemical Engineering YTU(2010)

International Journal of Science and Engineering Applications
Volume 7–Issue 09,284-286, 2018, ISSN:-2319–7560

A Review of Using Green Technology in Civil Engineering

Mohammed Noori Hussein Alhashimi
Department of Civil Engineering
Iraq University College
Basra, Iraq

Abstract: Due to the evolution of life in the last century and the continuing development to the present time, in addition to the increase in the presence of factories and laboratories and modern means of transport and increase the requirements of living such as housing and work and the resources of consumption of food, water and energy. All these things led to a large pollution in the environment in which we live. And the increase in the consumption of fuel and energy will lead to an increase in the proportion of harmful substances that will be put in the environment as a result of the consumables we use in our daily lives. Hence, there is an urgent need to preserve the environment and to detoxify harmful substances and human waste. The term green technology refers to the use of healthy resources and clean energy sources that do not contain harmful residues when used. One of the areas in which green technology is involved is the engineering fields, especially structural engineering, so that waste recycling and its use for construction purposes can be achieved in addition to building environmentally friendly facilities. This paper presents a review of the use of green technology in the fields of civil engineering.

Keywords: Green Technology, Green Building, Waste Recycling Materials

1. INTRODUCTION

Green technology is an environmentally friendly technology that prevents pollution that harms human health and living organisms. This technology provides energy sources and alternative resources to sources and resources that cause damage to the environment. The world has large natural resources that can be used to produce green technology. Some of these resources have been fully depleted and others are still available. For instance - family unit batteries and hardware frequently contain unsafe synthetic concoctions that can dirty the groundwater after transfer, debasing our dirt and water with synthetics that can't be expelled from the drinking water supply and the nourishment crops developed on defiled soil. The dangers to human wellbeing are incredible. In this way, the need of great importance is that each financial specialist should think green. They should realize that green innovations and clean advances are great business. These are quickly developing markets with developing benefits. From the view purpose of purchasers, they ought to likewise realize that purchasing green developments can diminish their vitality charge and that green creations are regularly more secure and more advantageous items [1]. Green technology covers an expansive territory of generation and utilization advancements. The appropriation and utilization of green advances includes the utilization of ecological advances for checking and appraisal, contamination counteractive action and control, and remediation and rebuilding. Checking and evaluation innovations are utilized to gauge and track the state of the earth, including the arrival of common or anthropogenic materials of a hurtful sort. Aversion innovations maintain a strategic distance from the generation of earth dangerous substances or adjust human exercises in ways that limit harm to nature; it includes item substitution or the update of a whole creation process as opposed to utilizing new bits of gear. Control innovation renders unsafe substances innocuous before they enter the earth. Remediation and reclamation advancements exemplify techniques intended to enhance the state of biological systems, debased through normally instigated or anthropogenic impacts [1].

2. GREEN TECHNOLOGY IN BUILDINGS

Civil engineering projects can have noteworthy site-particular and combined effects on our environmental and social frameworks if not accurately arranged, outlined and executed[2]. In the region of manageability, there is an earnest

need to apply advances and techniques that convey better and more reasonable execution in a way that is financially savvy. Feasible, versatile and mitigative ways to deal with environmental change, in the outline of framework are subsequently critical directing components [3]. Moderately couple of planners have so far investigated the transformative capability of environmental outline and have liked to stay unopinionated and unconcerned with the distributional effects of plan as they influence the wellbeing of people and biological communities [4]. Infrastructure components, for example, streets, water, sewage and stormwater can result in loss of basic biological systems and biodiversity. There is a need to make an eco-delicate framework configuration rating framework that empowers and advances the utilization of "gentler" outline arrangements. The rating of green structures assesses the ecological effects of structures however with little accentuations on the natural execution of structural building foundation. The proposed examine utilizes the idea of the green rating of green structures and makes a choice toolbox that evaluates the ecological effects of framework plan choices on advancement. By using enhanced earth benevolent looking for outline arrangements, this investigation intends to present ecologically well-disposed plan choices before the framework plan endorsement process [2].

3. APPLICATION OF GREEN TECHNOLOGY IN CONSTRUCTION

3.1 Green technology for Low cost housing

The construct of building houses or housing units requires a lot of money and this is because of the high prices of construction materials clearly. So it became difficult to provide housing units for millions of people at the time of rising prices, it was necessary to find an alternative to the construction materials to make this alternative is low cost and available. The procedure needs to choose based on nearby climatic condition and on the accessibility of neighborhood normal building materials/assets. There is a dire need to grow new building materials and advancements for minimal effort lodging in provincial territories. This requires the utilization of fitting and savvy building materials and advances in the development of abiding units. The utilization of bamboo as a fortifying material after reasonable treatment with economically accessible material like black-top is one of the answer for minimal effort lodging. The fundamental issue with utilizing bamboo as fortification instead of steel is that it ingests water what's more, swells and later on when it dries it lessens to its typical measure and from now on decreasing the quality of the bond between bamboo and concrete. Treatment of bamboo with some waterproof covering makes bamboo less powerless to dampness. In this manner irrelevant swelling and shrinkage of bamboo happens amid the relieving time of concrete [5].

3.2 Blended Cement

These are cements containing a high volume of one or more complementary cementing materials (CCM), such as coal fly ash, granulated slag, silica fume and reactive rice-husk ash. A large volume of CO2 is directly emitted during the cement manufacturing process (0.9 tonnes/tonne of clinker). Reduction in the quantity of clinker by substituting
with CCM results in lesser CO2 emissions [5].

3.3 Green technology for Road, Parking and Residential Construction

low volume streets can be made penetrable so rain water goes into the asphalts and afterward gradually trickles into the ground water. This will likewise wipe out sprinkle of water when an auto moves amid light rains. Most fitting sort of asphalt is precast solid asphalt. For low volume streets, the sub base furthermore, base layers must be open reviewed granular layer which have great porousness. Treatment with concrete or bitumen can improve the quality of the granular layers for substantial movement [5].

3.4 Buildings with low Carbon Pollution

Disclosure of normal inorganic covers like pozzolanic materials brought about lime-pozzolanic (LP) cement and this made ready for the development of Portland cement in 1824. Portland cement also, steel acquired progressive changes the development hones since early piece of twentieth century. Later on plastics furthermore, plastic items entered the development business. As we moved far from zero vitality materials to more present day materials for the development exercises, it wound up fast approaching to spend more vitality and normal assets. These cutting edge materials are vitality escalated and are pulled over long separations previously being utilized for development. With regards to carbon discharge decrease and the issue of a dangerous atmospheric devation, there is a need to focus on utilization of present day building materials with reference to (I) vitality power of materials, (ii) characteristic assets what's more, crude

materials devoured, (iii) reusing and safe transfer what's more, (iv) effect on condition. Aimless utilization of common assets and vitality concentrated process for the building materials won't prompt supportable choices [5].

4. ADVANTAGES AND DISADVANTAGES OF GREEN TECHNOLOGY

1. Does not discharge anything negative into climate
2. Convey monetary benefits to specific zones
3. Need less maintenance
4. It is sustainable which means will never run out
5. Moderate the effects of a worldwide temperature alteration by diminishing CO2 outflows

The upside of utilizing environmentally friendly power vitality sources is that it must be spotless in this manner there is no release or harm into the earth or air. Furthermore, it is additionally replenishable rather than oil. What's more, efficient power vitality offices are troublesome on the wallet to assemble, it requests a lesser measure of upkeep in this manner it needs to spend some enormous money to work it. In addition, this may likewise make financial favorable circumstances to some specific regions and even create tourism industry. Indeed, even while these appear to be phenomenal, there are a rare sorts of people who accept there exists benefits to utilize such innovation. Setting up these offices moreover needs a lot of land so we may need to cut on farmland which clarifies what many are stressed over if more breeze generators must be set up. A second negative perspective is the reality huge numbers of the efficient power vitality sources can't generally be introduced in particular places of the earth [6][7]. Green procedures and innovation alludes to trying endeavours to enhance vitality effectiveness or decrease the contamination delivered by your home, business and general living propensities. The principle reason for this sort of procedures and innovation is to lessen the potential negative effect that vitality utilization and contamination can have on nature. While ecologically agreeable living is a positive perfect, there are a few conceivable weaknesses of Green procedures and innovation, for example, high executing costs, absence of data, no known elective compound or crude material sources of info, no known elective process innovation, vulnerability about execution effects, and absence of HR and aptitudes [7][8].

5. CONCLUSION

Green buildings can be constructed in simple and cost-effective ways, in addition to the availability of the materials needed for their construction. Green buildings and eco-friendly buildings are more economical than the traditional lines that arise from the use of traditional materials. The conservation process is the result of recycling and use of waste for construction purposes.

6. REFERENCES

[1] Soni, G. D. (2015). "Advantages of green technology." International Journal of Research **3**(9).

[2] Saroop, S. and D. Allopi (2012). Establishing a Green Rating System on Civil Engineering Infrastructure Projects. Abstracts of the 31st Southern African Transport Conference (SATC 2012), Citeseer.

[3] FIDIC, 2009. FIDIC State of the World Infrastructure Report 2009.

[4] Van Wyk, L. 2009. EcoBuilding: Towards an Appropriate Architectonic Expression, In *Green Building Handbook for South Africa* [online]. [Accessed 13 April 2011]. http://researchspace.csir.co.za/dspace/bitstream/10204/3262/1/vanWyk1_2009.pdf

[5] Verma.I , Sohoni P and Verma.N . " application of Green Technology in Infrastructure" INTERNATIONAL JOURNAL OF SCIENTIFIC RESEARCH. Volume : 2 Issue : 2 Feb 2013.

[6] Sanjukta Banerjee et al. "Advantages of green technology" Recent Research in Science and Technology 2014, 6(1): 97-100.

[7] A. Iravani, I. Birjand, and M. Zohoori, "Advantages and disadvantages of green technology; goals, challenges and strengths," *Int. J. Sci. Eng. Appl*, vol. 6, p. e284, 2017.

[8] (Recent Research in Science and Technology 2014, 6(1): 97-100 ISSN: 2076-5061 Available Online: http://recent-science.com).

International Journal of Science and Engineering Applications
Volume 7–Issue 09,287-290, 2018, ISSN:-2319–7560

Client Server Based Security Management System

Dr. May Paing Paing Zaw
Technological University (Thanlyin)
Yangon, Myanmar

Abstract: Nowadays, Network Management System (NMS) is a vital role and some key components of NMS include network device discovery, network device monitoring, network performance analysis and so many benefits. This paper aims to present a security management system for a own LAN based Client Server Network to control the security of a network using Java Programming Language. This system can provide the security feature for the user account setting and user management and proxy server feature. And all of the history of the security such as user account and proxy server history are kept in the java standard serializable file. So the user can view anytime the history of the security and proxy server.

Keywords: security management; TCP/IP based client server system; local area network

1. INTRODUCTION

A network management system is used to design, organize, analyze and administer computer and telecommunication networks, in order to maintain a desired level of service at all times. Network management software is designed to provide automated support for some or all of the network management functions. Network management software systems are used to perform some of the functions of monitors and analyzers, identify errors, run diagnostic tests, monitor entire an network, compile statistics, and prepare real-time management reports. The ISO network management model's five functional areas: such as configuration management, fault management, performance management, security management, accounting management and etc. Among them, security management is more important than others. Because it is very essential and useful in any fields[3,4].

2. METHODOLOGY

In general terms, LAN (Local Area Network) refers to a group of computers interconnected into a network so that they are able to communicate, exchange information and share resources (e.g. printers, application programs, database etc). A Local Area Network (LAN) is the result of connecting a number of computers or other IP devices together in a localized geographic area – for example in one room, building or several buildings. LANs are typically connected to each other via cable and more recently via radio waves. In an office building for example, workstations and personal computers (PCs) are commonly connected to each other with a Local Area Network. This allows an employees' equipment to communicate - send and receive files, share access to the files or data on another workstation even share applications [1].

TCP/IP (Transmission Control Protocol/Internet Protocol) is the basic communication language or protocol of the Internet. It can also be used as a communications protocol in a private network (either an intranet or an extranet). TCP/IP is a two-layer program. The higher layer, Transmission Control Protocol, manages the assembling of a message or file into smaller packets that are transmitted over the Internet and received by a TCP layer that reassembles the packets into the original message. The lower layer, Internet Protocol, handles the address part of each packet so that it gets to the right destination. Each gateway computer on the network checks this address to see where to forward the message. TCP/IP uses the client/server model of communication in which a computer user (a client) request and is provided a service (such as sending a Web page) by another computer (a server) in the network [2].

In this system, If a user logon to server, server checks client's username, password and decide which client should permit or not. Server identifies the user which connects the server and shows correspondence date in event viewer.

3. CLIENT SERVER SYSTEM

3.1 Client/Server Paradigm

The Client/Server paradigm has become a dominant one for the Internet. In this model, the clients are programs running on remote machines that communicate with a program called the server that runs at a single site and responds to requests from many clients. The server provides the clients with, say, Web pages or database information. Much of the World Wide Web is built on the client/server paradigm. The clients are Web browsers run by many millions of individual users, and the servers are the many Web hosting systems running at the many host sites on the Web [6].

A single server at a single host can support many hundreds or thousands or more of clients from around the world. Large systems that serve hundreds of thousands of clients balance the server load over multiple machines in an arrangement called "server farms." With Java you can build client/server systems with sockets or with RMI (Remote Method Invocation). In a socket based client/server system, a server listens to a particular port for client applications sending requests for connections. A Server Socket class is provided in Java that allows for a server to monitor and answer such requests for connections. The client sends the request for a connection by creating a socket with the host name and port for that server as discussed in the previous section.

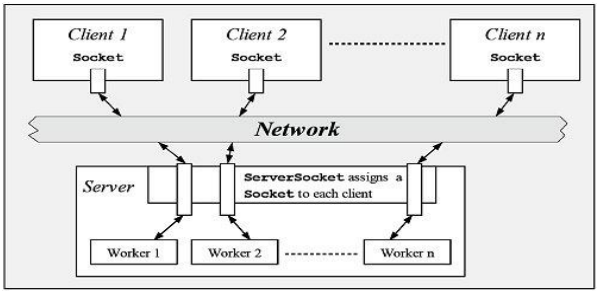

Figure 1 The basic aspects of a socket based client/server system

The above figure shows a diagram illustrating the basics of a socket-based client/server system. The Server Socket instance listens for a client to connect to the particular port. When a client request arrives, the Server Socket object sets up a Socket instance for the connection and then spins off a new thread to interact with the client via that socket. Many clients can therefore be served since each client has an independent thread dedicated to it [5].

3.1.1 Class Server Socket (TCP Server Connections)

A ServerSocket is a mechanism by which a server can accept connections from clients across a network. The server will open the ServerSocket and wait or listen for connections from clients. The ServerSocket class creates a Socket for each client connection. The server then handles the connections in the normal manner with Input and Output streams.

3.1.2 Class Client Socket (TCP Client Connections)

A Socket is a Java representation of a TCP network connection. In order to communicate with a remote host the Java client must first create a Socket, which will establish the TCP connection. In doing so a host name and port number must be specified. There must be a server actively listening on the specified port or the connection will fail with IOException. These constructors allow the Socket connection to be established.

3.2 Security Management System Design

In this system, the system will check all of the user which will connect from the clients and if this user is valid user of the system, the server will allow to enter the server and if invalid user will connect the system can not accept and resend to the client that the user is invalid and all of these messages are kept in the database file. Moreover in this system, there is the user management function to disable or enable the user account. If the disable user will connect from client to server, this system will send the message to the client that the client is connecting the server with the disable user. And this message will save to the data file with the detail time. So the system can view the message of the security that which client is connected to the server with which user at when. And moreover, this system can provide the proxy server feature. So this system can save the track of the proxy server message in the data file.

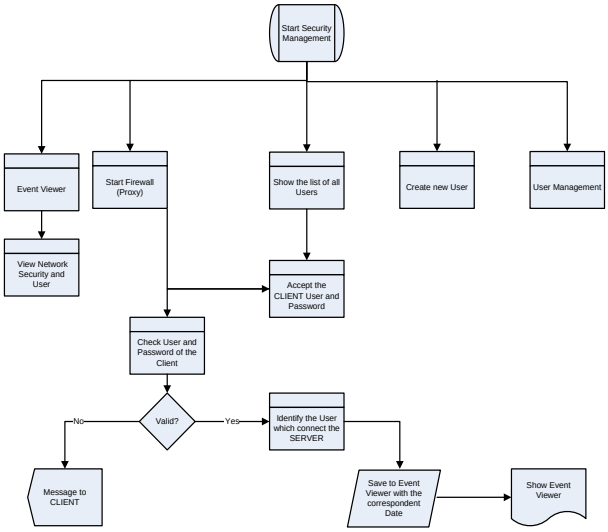

Figure 2.User Account Entry

4. TEST AND RESULTS OF THE SYSTEM

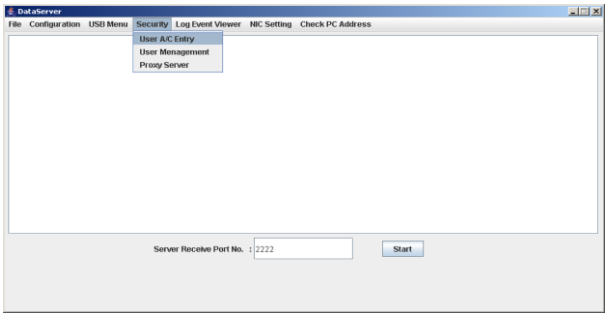

Figure 3.Security Menu

There are three sub menu of the security feature such as user Account Entry and user Management and proxy Server menu. In this menu, new users are added by this program and for the new user, user id and password and confirm password must be provided. And Password and Confirm password also must be the same in detail. And if the OK button is pressed, all of the user information will save in the Java Serializable object file. This file is to save all of the information of the user in the form of Ascii character. If the cancel button is pressed the user entry screen will clear and exit the program.

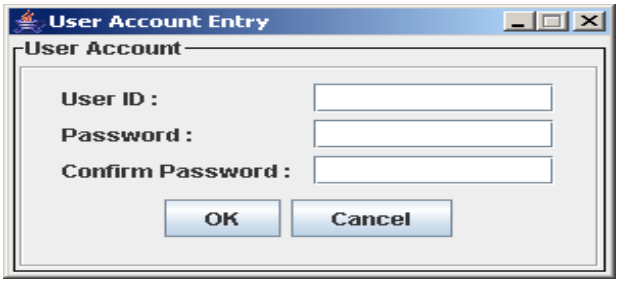

Figure 4.User Account Entry

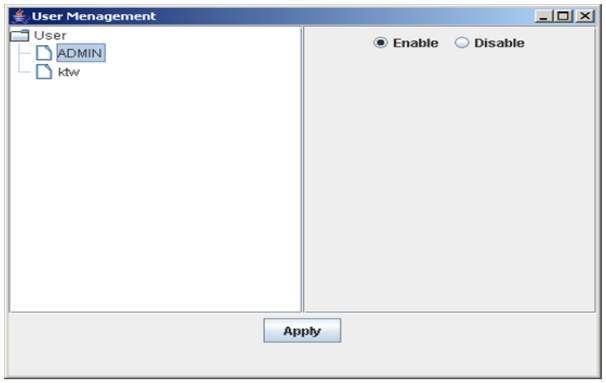

Figure 5. User Account Management Entry

User enable and disable feature can be updated by this program. When the user name node is pressed the user state is showed at the right side of the screen and the radio button will show the user is enable or disable. And when the user want to change the properties of the user id, click the radio button and then pressed the apply button. Then the user properties will save in the user profile file. This file is also java Serializable file.

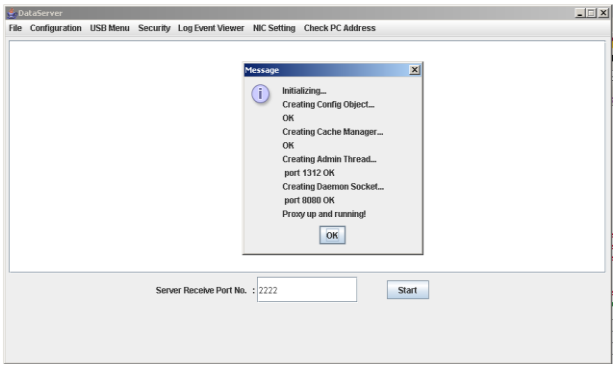

Figure 6. Proxy Server Menu

When the proxy server is on from the security sub menu, the proxy server will work. if the proxy server is actually work the message will show and Proxy up and running message will appear.

Figure 7. Log Event Viewer Menu

There are three type of the log event viewer such as Network, Security and User. When the network node of the Event Viewer program is clicked, all of the network history event which are concerned of the client program and which user is connected form which client at which time and which invalid user is connected at which time to server will show at the right side of the program. So the user can view the all of the network history of the client and server connected history and log in user history as shown in figure 7.

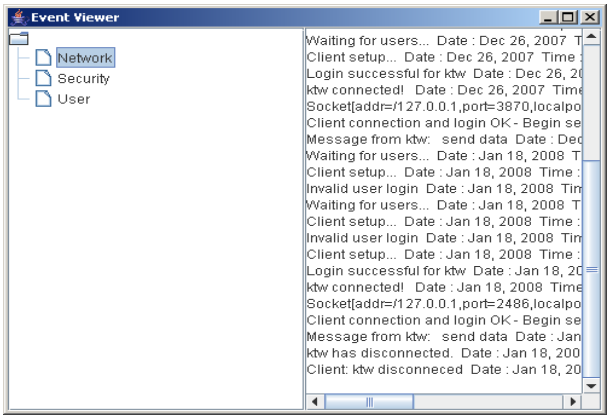

Figure 8. Network Event Viewer

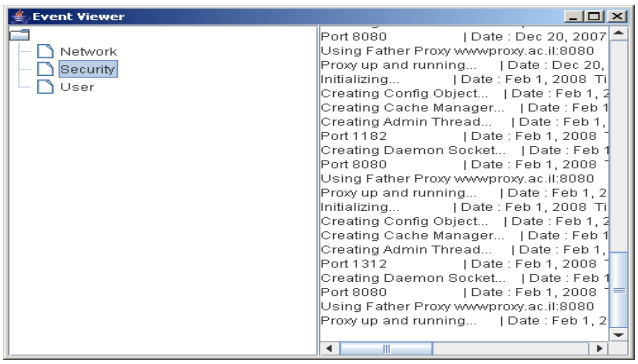

Figure 9. Network Security

When security node is pressed, the history of the network security history will show. In this message history, there are so many messages about the proxy server start up time and the message of the port using the server program.

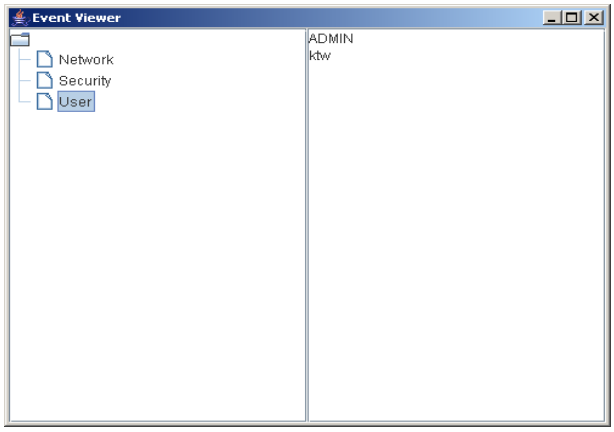

Figure 10. Users Control Menu

When user node is pressed, list all of the user who are create and accepted in the server program.

5. ACKNOWLEDGMENTS

Special thanks to my rector, Dr. Theingi from Technological University (Thanlyin), for her kindly support, encourage and valuable advice.

6. Conclusion

In this client server based network security system, the server can listen all of the requests of the clients and response to the clients. This system can provide the security feature for the user account setting and user management and proxy server feature and all of the history of the security such as user account and proxy server history are kept in the java standard serializable file. This system is used java programming language so all of the programs in the system are developed by java language and native dll file. But in this system, It is not implemented the function of which user has to invoke which service of the server and user level. So in the future, the user level function should include.

REFERENCES

[1] www.wikipedia.com, Local Area Network.

[2] Craig Hunt, 2002. TCP/IP Network Administration TCP/IP Guide, Third Edition.

[3] encyclopedia. thefreedictionary.com, Network

Management System

[4] Mr. Musa Odero , The Role of Network Management in the Emerging Infrastructure.

[5] Core Java (Students Guide), Java 2 Platform (StandardEdition) and the Java Developers Almanac

<http://www.javaabout.com/ad>and
<http://www.sun.com>

[6] Computer Network Study Guide with Microsoft NT 4.0

International Journal of Science and Engineering Applications
Volume 7–Issue 09,291-293, 2018, ISSN:-2319–7560

Analysis of Pb, AS and Zn Concentration in soil around Ririwai Tin Mine, Kano State, North Western Nigeria

Abdullahi M. A.
Department of Applied Physics
College of Science and Technology
Kaduna Polytechnic
Kaduna – Nigeria

Abigail E. Aye
Department of Applied Chemistry
College of Science and Technology
Kaduna Polytechnic
Kaduna – Nigeria

Okunola M. Rhoda
Department of Applied Chemistry
College of Science and Technology
Kaduna Polytechnic
Kaduna – Nigeria

ABSTRACT: Mining industry in Nigeria provides economic benefits of wealth creation and employment opportunities. However the industry is associated a number of negative challenges among which is the health impact of miners and surrounding communities arising from mining processes. In this study Xrf analytical techniques was used to determined the concentration of Pb, As and Zn in soil around Ririwai Tin mine Kano state Nigeria. The results shows that the mean concentrations of Pb, As and Zn were 113.54±3.92, 6.76±0.34 and 216.89±5.74mg/kg respectively. Zn have the highest concentration across all location followed by Pb while As have the lowest concentrations. The concentrations of Zn and As in the study area were within the worldwide range values in soil of 50-250mg/kg and 1-50mg/kg reported by USEPA for Zn and As respectively. Pb have very high concentration when compared with worldwide average value of 10mg/kg reported by USEPA. Suggesting that there is high deposits of Pb in the area. Therefore all means of ingesting of soil by human and animal around the area should be avoided because of the elevated concentration and the toxicity of Pb.

Keywords: Xrf, Concentration, Heavy Metals, Lead, Arsenic, Zinc, Tin Mine,

INTRODUCTION

Beside the socio-economic benefits of the mining industry in the developing countries such as Nigeria, the industry may be faced with three potential negative effects. The first one is the socio-economic dislocation all ill-prepared mining communities go through at mine closure, which arise from exploitation of a non-regenerative resources [1]). The second and third undesirable aspects arise when non-optimal management of mining operations results in environmental degradation and /or negative health impacts on miners and mining communities. Principal health problems among miners and mining communities from various countries that have been cited by the literature include respiratory disease, neoplasm/cancer, chronic hypertension, mental health and genetic impact [2] . The major cause of these diseases can be attributed to the heavy metal contamination and naturally occurring radioactive materials NORMs [3].

Mining and industrial processing are among the main sources of heavy metal contamination in the environment. Mining activities, through milling operations coupled with grinding, concentrating ores and disposal of tailings, along with mill wastewater provide obvious sources of heavy metal contamination of the environment. It is, therefore, not surprising that the degree and extent of heavy-metal pollution as a result of human activities has been one of the main topics studied in environmental geochemistry. Heavy metals can cause health problems at higher exposures and destroy aquatic organisms when leached into water bodies. Metals contamination in aquatic environmental has received huge concern due to their toxicity, abundance and persistence in the environment and subsequent accumulation in the aquatic habitats.[4].

Heavy metal residues in contaminated habitats may accumulate in microorganisms, aquatic flora and fauna, which in turn may enter the human food chain and result in health problems like the lead poisoning problems that killed more than 400 children in Zamfara State[5] .

Ions such as sodium, potassium, magnesium and calcium are essential to sustain life. Additional metals such as manganese, iron, cobalt, copper, Zinc, chromium, vanadium, selenium and molybdenum are also essential for optimal growth, development and reproduction. These metals function mostly as catalysts for enzymes activity in human bodies but become toxic when their concentration becomes excessive. In addition to the mercury, lead, cadmium, silver aluminum, arsenic and barium [6], Epidemiological studies in recent years have indicated a strong association between the occurrence of several diseases in humans, particularly cardiovascular disease, kidney related disorders, neurocognitive effects and various forms of cancer and the presence of toxic trace metals [7,8].

In this research, the concentrations of Pb, As and Zn in soil samples obtained from ten locations around Ririwai Tin mine in Kano state Nigeria were determined using energy Dispersive X-Ray Fluorescence (EDXRF) Spectrometer model FXL-83358 .

MATERIAL AND METHODS

Ten (10) soil samples were collected at ten different locations around the study area, at 10cm depth using a mechanical digger. The10cm depth was carefully chosen as the appropriate depth to obtain the samples in line with the facts established that these pollutants are highly absorbed to clayed materials and organic matters in the study areas [9]. Fig; 1 shows the map of the study area while Table; 1 shows the locations where samples were collected

The soil samples collected were pretreated by oven drying them at a regulated temperature of 55^0c for 48 hours. After drying, a series of mesh size 35µm was used to remove large undesirable particle sizes The dry test samples were analyzed using the energy dispersive X-ray florescence (EDXRF) FXL-83358 model to determine the concentration of the metals in the soil samples.

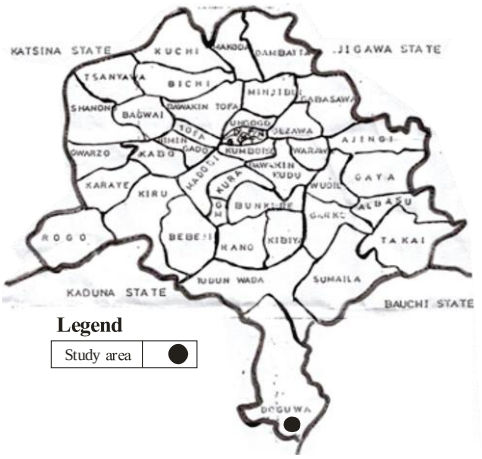

Fig. 1: Map of Kano State Showing the study area

Table 1: Sampling locations

S/No	North	East	Elevation
1	10^0 44′ 35.3″	008^0 45′ 16.4″	856m
2	10^0 44′ 36.7″	008^0 45′ 15.8″	856m
3	10^0 44′ 33.8″	008^0 45′ 17.8″	856m
4	10^0 44′ 32.3″	008^0 45′ 21.0″	858m
5	10^0 44′ 30.3″	008^0 45′ 27.0″	862m
6	10^0 43′ 48.2″	008^0 44′ 57.1″	896m
7	10^0 43′ 49.1″	008^0 44′ 53.4″	894m
8	10^0 43′ 48.5″	008^0 44′ 53.0″	895m
9	10^0 43′ 50.2″	008^0 44′ 58.7″	892m
10	10^0 43′ 49.5″	008^0 44′ 59.2″	894m

RESULTS AND DISCUSSION

Soils collected from the sampling locations were analyzed using Energy Dispersive X-Ray Fluorescence (EDXRF) method. It was found out that the concentrations of the elements varied from one sampling location to another. Inferential statistics and one-way ANOVA were used to compare the concentrations of Pb, As and Zn.

Table 2: Concentration of Pb, As and Zn

		Concentration in mg/kg		
S/No	Sample I.D	Pb	As	Zn
1	Rp1	189.40± 4.76	5.85 ± 0.35	420.55 ± 7.68
2	Rp2	100.24± 3.68	5.20± 0.28	161.78 ± 5.16
3	Rp3	47.75 ± 2.78	5.62± 0.40	57.58 ± 3.62
4	Rp4	65.22 ± 3.06	6.34 ± 0.24	75.04± 3.93
5	Rp5	62.64 ± 2.93	5.94±0.22	60.19± 3.56
6	Rp6	69.71 ± 3.31	7.22 ± 0.55	181.64 ± 5.39
7	Rp7	114.07±4.12	8.55 ± 0.31	188.18± 5.90
8	Rp8	118.10 ± 4.14	8.10 ± 0.31	178.29 ± 5.77
9	Rp9	218.00 ± 5.64	9.16± 0.42	581.34 ± 9.64
10	Rp10	150.30 ± 4.73	5.60 ± 0.35	264.31 ± 6.72
	Mean	**113.54 ± 3.39**	**6.76 ± 0.34**	**216.89 ± 5.74**

Concentration of Pb

The result from Table- 2 showed that the mean concentration of Pb is 113.54 ± 3.92 mg/kg in range between 47.75 to 218.00 mg/kg with standard deviation of 54’21.The concentration of Pb obtained in this study revealed very high values when compared with the world wide average of 10mg/kg reported by USEPA[10] thus suggesting high deposit of Pb in the area

Concentration of As

The concentration of As ranged between 5.20 to 9.16 mg/kg with a mean value of 5.20 ± 0.22 mg/kg with standard deviation of 1.33.The mean value is within 5.00mg/kg world average value and it fall within the world range of 1-50 mg/kg as reported by [10,11].

Concentration of Zn

The mean concentration of Zn is 216.89 ± 5.74 mg/kg between the range of 57.58 to 581.34 mg/kg with standard deviation of 159.12. The mean concentration of Zn in this study is higher than the world wide average value in soil of 1oomk/kg, however the concentration of Zn across all the locations fall within the world wide range of 100 – 500mg/kg reported by USEPA

In the sampling locations Zn was found out to have the highest concentration followed by Pb while As has the lowest concentration shown in Figure- 2.

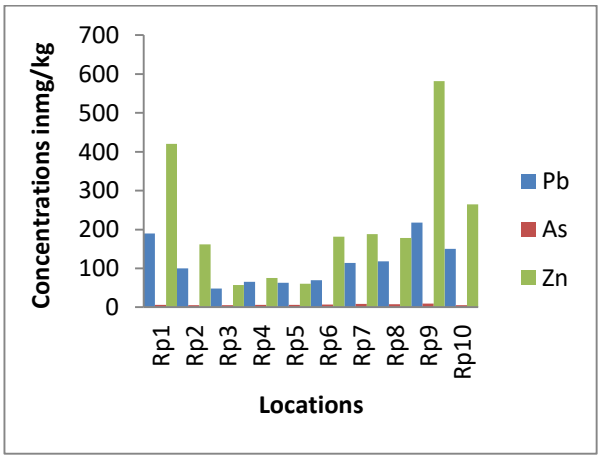

Figure 2: Plot of Concentrations against Locations

Similarly, the ANOVA (0.000> 0.05) showed that there is a significant difference in the relative abundance of the various metals. In other words some metals are more abundant than other in all the locations.

CONCLUSION

Xrf analytical technique was used to determined the concentrations of Pb, As and Zn in soil sample collected around Ririwai. Tin mine in Kano state Nigeria. The results indicated that Zn with mean concentration of 216.89±5.74mg/kg is the highest in all locations followed by Pb with mean concentration of 113.54±3.92mg/kg while As with mean concentration 5.20±0.22mg/kg has the lowest concentrations in all the locations. The concentrations of Zn and As obtained in this study falls within the values of the worldwide concentration ranges of these metals in soil. However, the concentration of Pb obtained in this study is very high when compared with the worldwide average value and range this therefore suggested that there is high deposits of Pb in the soil of the study area. All means of ingesting soil around the area by people and animals should be avoided because of the high toxicity of Pb.

REFERENCES

[1] Hayumbu, P. and *Mulenga, S. (2004: Status of Radon Dosemetry in Zambia under*ground mine, Proceedings of IAEA International Conference (NORM iv) S20Zyrk, Poland

[2] WHO 1999: Hazard prevention and control in the work environment. Air borne dust WHO/SDE/OEH/199.14,Geneva.

[3] ICRP 1994: Protection against Rado -222 at home and at work publication 6 5, Ann. ICRP 2 3, 2 Pergamon Press, Oxford and New York.

[4] Boamponsem, L. K., Adam, J. I., Dampane, S.B, Owusu-Ansah, E. and Addae, G. 2010. Heavy Matals, Lavel in Stream of Tarkwa gold mining areas of Ghana, *J. Chem. Pham res*, 2 (3): 504-527

[5] Galadima, A. and Garba, Z. N. 2012. Heavy metals pollution in Nigeria; Causes and consequences. Elixer pollution (45) 7917-7922.

[6] Chiroma T.M., Ebewele R.O. and Hymore F.K.,2012 Levels of heavy metals (Cu, Zn, Pb, Fe, and Cr) in Bushgreen and Roselle irrigated with treated and untreated urban sewage water, *I. Res. J. Environment Sci.,* **1(4),** 50-55

[7] Sharma R.K., Agrawal M. and Marshall F., 2000 Heavy metal Contamination of soil and vegetable in suburbam areas of Voranasi, India, *Ecotoxico. Environ. Safety*, **66**, 258–266

[8] Nwajei G.E., Okwagi P., Nwajei R. I and Obi-Iyeke G.E.,2012 Analytical Assessment of Trace Elements in Soils, Tomato Leaves and Fruit in the Vicinity of Paint industry, Nigeria, *Res. J. Recent Sci.,* **1(4),** 22-26

[9] Kabata–Pendias A 1993., Behavioral properties of trace metals in soils. Applied Geochemistry 2,3

[10] U.S Environmental Protection Agency 1992 Ground\ water issue. EPA/540/5-92/018.

[11] Udom B.E., Mbagwu J.S.C. Adosodium J.K. and Agbim N.N 2004., Distribution Zinc, copper cadmium and lead in a tropical ultisols after long-term disposal of sewage slude, *Eniron.Internat*, **30**, 467–470

International Journal of Science and Engineering Applications
Volume 7–Issue 09,294-297, 2018, ISSN:-2319–7560

Design and Implementation of Web Based Disease Diagnoses System

Dr. May Paing Paing Zaw
Lecturer
Technological University
(Thanlyin)
Yangon, Myanmar

Abstract: This paper is intended to implement the design and implementation of web-based diagnosis system. The major purposed is to diagnose or protect the health before going the feel the disease. In this system, people can detect the diabetes types for kids. And then people can detect which types of disease may cause when they are thirsty. This system is implemented by using HTML, CSS, JavaScript, Bootstrap. XAMPP software package is applied to test the results.

Keywords: diabetes; thirsty; php; diagnoses; artificial intelligence

1. INTRODUCTION

Globally, health care sector is the pivot and integral part of human lives. Thus, any error committed in the clinical services might leads to defect or termination of life. Recently, information and Communication has been used extensively to improve the various operations and services in the field of the health care service. Health care facility should be accessible by all at all times. But some of the people that should access these facilities are far removed from these facilities. Computer-based methods are increasingly used to improve the quality of medical services. Artificial Intelligence (AI) is the area of computer science focusing on creating expert machines that can engage on behaviors that humans consider intelligent [1]. An expert system is a system that employs human knowledge captured in a computer to solve problems that ordinarily require human expertise. Expert system seeks and utilizes relevant information from their human users and from available knowledge bases in order to make recommendations [2], [3], [4].

2. ARTIFICIAL INTELLIGENCE

2.1 Introduction to Artificial Intelligence

Artificial intelligence (AI) is an area of computer science that emphasizes the creation of intelligent machines that work and react like humans. Some of the activities computers with artificial intelligence are designed for include: Speech recognition, Learning, Planning, Problem solving [5].

2.2 Types of AI

Artificial intelligence is a branch of computer science that aims to create intelligent machines. It has become an essential part of the technology industry.Research associated with artificial intelligence is highly technical and specialized. The core problems of artificial intelligence include programming computers for certain traits such as: Knowledge, Reasoning, humans only if they have abundant information relating to the world. Artificial intelligence must have access to objects, categories, properties and relations between all of them to Classification determines the category an object belongs to and regression deals with obtaining a set of numerical input or output examples, thereby discovering functions enabling the generation of suitable outputs from respective inputs. Mathematical analysis of machine learning algorithms and their performance is a well-defined branch of theoretical computer science often referred to as computational learning theory. Machine perception deals with the capability to use sensory inputs to deduce the different aspects of the world, while computer vision is the power to analyze visual inputs with a few sub-problems such as facial, object and gesture recognition. Robotics is also a major field related to AI. Robots require intelligence to handle tasks such as object manipulation and navigation, along with sub-problems of localization, motion planning and mapping. Robots require intelligence to handle tasks such as object manipulation and navigation, along with sub-problems of localization, motion planning and mapping.

3. SYSTEM IMPLEMENTATION

3.1 System Overview

Web-based Disease Diagnose System is implemented to provide the customer for their good health by checking or detecting the symptoms by clicking the checkbox. In this system, users can detect the disease information, diabetes symptoms, dehydration symptoms, dry mouth symptoms. Symptoms are collected from the internet and write the code or algorithms to check the results. User can view about and can check the types of diabetes by choosing the symptoms. In addition, user can view or diagnose the disease such as dehydration or diabetes or dry mouth by choosing the symptoms checkbox. implement knowledge engineering. Initiating common sense, reasoning and problem-solving power in machines is a difficult and tedious task. Machine learning is also a core part of AI. Learning without any kind of supervision requires an ability to identify patterns in streams of inputs, whereas learning with adequate supervision involves classification and numerical regressions. Problem solving, Perception, Learning, Planning, Ability to manipulate and move objects, Knowledge engineering is a core part of AI research. Machines can often act and react like

3.2 Hardware and Software Requirements

This system is web-based disease diagnoses system and it can be used any devices such as personal computers, laptop, notebook, tablet, mobile which can access internet. Therefore, it is very convenient for user and no need to install any software. The following table is the description of hardware and software requirements to develop the web application program.

Table 1. Hardware Requirement

Hardware	Specification
Computers	At least one PCs
Memory	2 GB or more
Hard disk space	500 GB or more

Table 2. Software Requirement

Server	Client	Others	Server
XAMPP	HTML	Sublime Text	XAMPP
Apache Web Server	CSS	Photoshop	Apache Server
MySQL (Database)	JavaScript , AJAX	Browsers	MySQL
PHP	Bootstrap		PHP

4. TEST AND RESULTS

The web-based disease diagnose system starts from the home page of the system. In home page screen, there are three main menus. They are home, diabetes, thirsty, contact. Figure. 1 shows Home Page of the System.

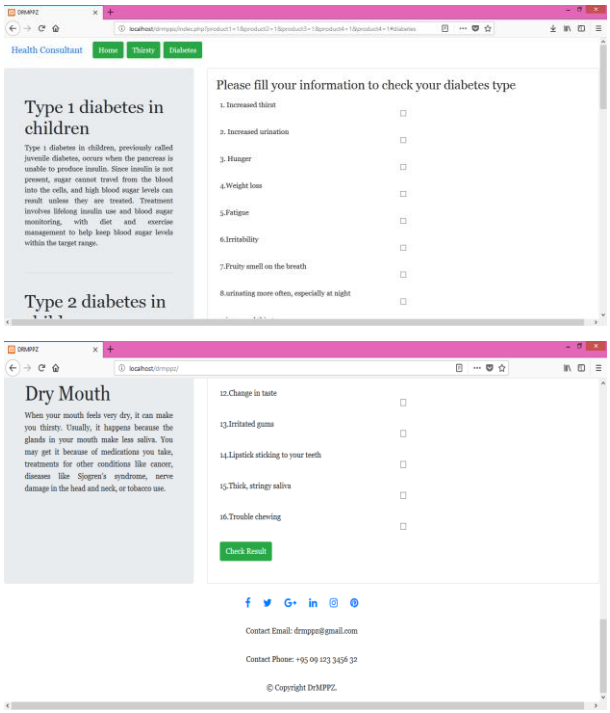

Figure 1. Home Page of the System

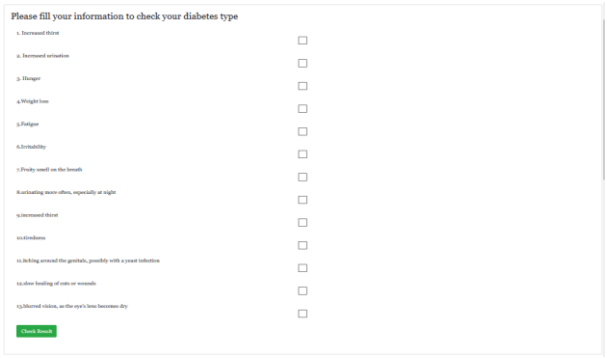

Figure. 2 Check Diabetes types form System

Figure 2 shows diagnose diabetes typed form. There are two types of diabetes: type 1 diabetes and type 2 diabetes. If the user chooses some symptoms and then click check result, the system will show the diabetes types results as shown in Figure 2, 3 and 4.

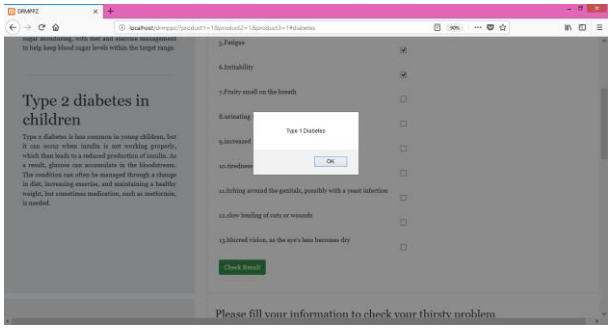

Figure. 3 Results for Diabetes types 1

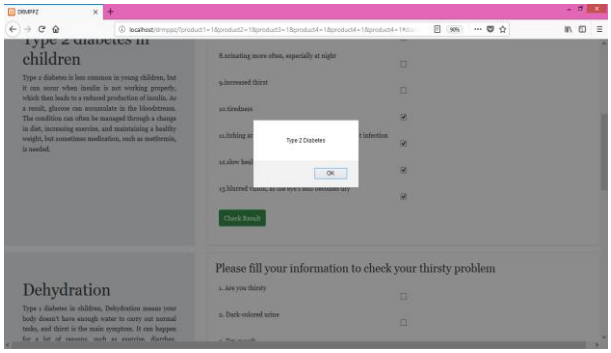

Figure. 4 Results for Diabetes types 2

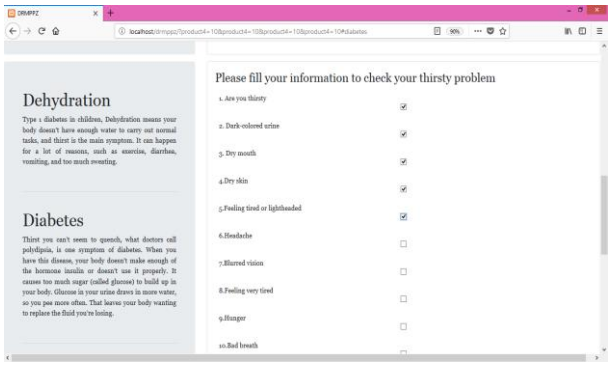

Figure. 5 Check Thirsty types form System

Figure 5 shows diagnose for thirsty form. There are three types of thirsty: dehydration, or diabetes, or dry mouth. If the user chooses some symptoms and then click check result, the system will show the diabetes types results as shown in Figure 6,7 and 8.

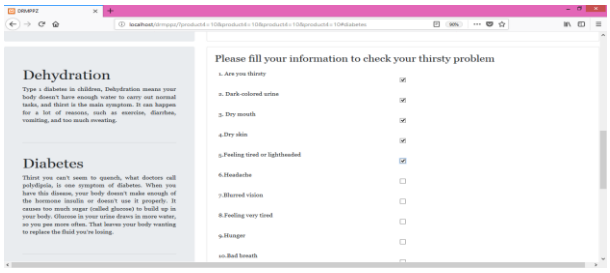

Figure. 6 Check Thirsty Form System

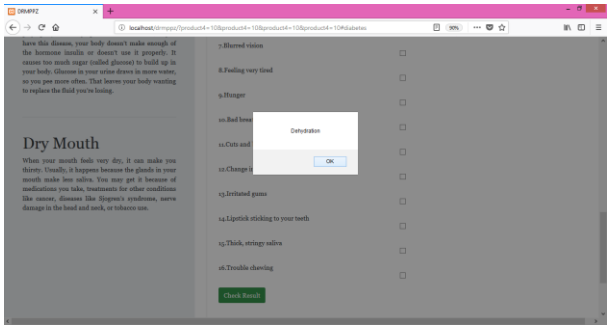

Figure. 7 Results for Dehydration

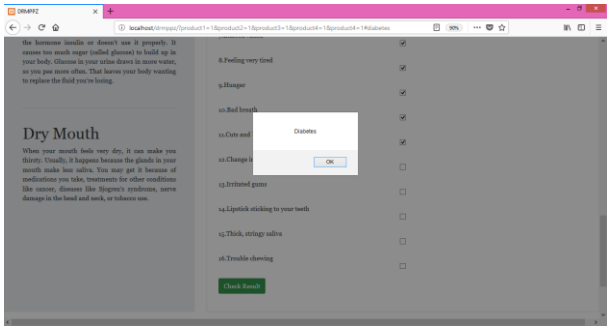

Figure. 8 Results for Diabetes

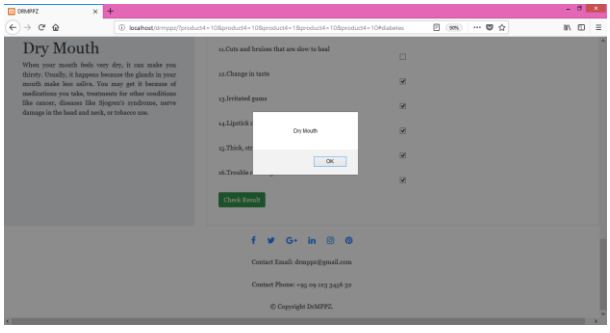

Figure. 9 Results for Dry Mouth

The following Figure 10 and 11 shows the information pages for web based diagnosis system and it shows the types of diabetes information and other thirsty symptoms.

Figure. 10 Information Page for Diabetes

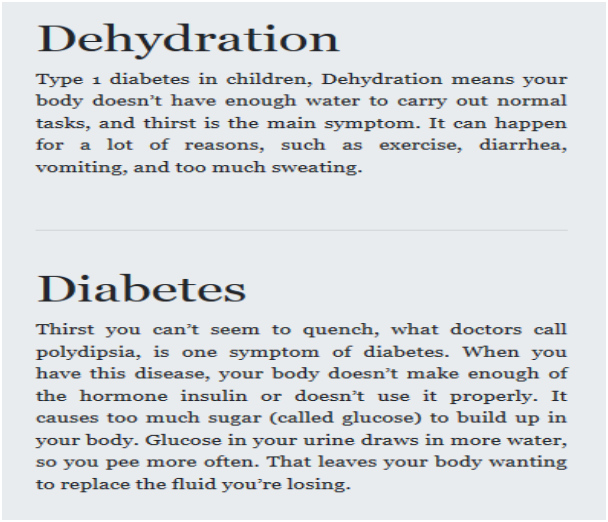

Figure. 11 Information Page for Thirsty

5. CONCLUSION

This system is intended to provide the people's health. The symptoms and disease are not very much. So, the more symptoms for headage or heart attack diagnoses function will be added in the future by discussing with the expert or doctors.

6. ACKNOWLEDGMENTS

The author would like to express her gratitude to Dr. Thein Gi, Rector, Thanlyin Technological University, for her kind encouragement, support, suggestions and guidance to complete the journal. Finally the author would like to thank her family and friends for their complete support.

7. REFERENCES

[1] Akinode, John Lekan, Oloruntoba S.A, "Design and Implementation of a Patient Appointment and Scheduling System", Department of Computer Science, Federal Polytechnic Ilaro Nigeria. December 2017.

[2]Mohd Ariff Bin Anuar. "Clinic Management System". Master of Science (Computer Science) in University MALAYSIA SARAWAK, 2006.

[3]Xin Dai. "Online Clinic Appointment Scheduling", Lehigh University,2013.

[4]S. Sri Gowthem, “Smart Appointment Reservation System”, Department of Computer Science Engineering, Bharath University, Chennai, India, June 2015.

[5]P.Santosh Kumar Patra, An Expert System for Diagnosis

of Human Diseases. SaIT, Bangalore, India

[6]Russell, S. and P. Norvig, 2002. Artificial Intelligence: A Modern Approach, Prentice Hall, Second Edition.

[7]Beverly G. Hope, Rosewary H. Wild, « AnExpert Support System for Service Quality Improvement», Proceedings of the Twenty-Seventh Annual Hawaii International Conference on System Science, 1994.

[8]Azaab S., Abu Naser S., and Sulisel O.,2000. A proposed expert system for selecting exploratory factor analysis procedures, Journal of the college of education, 4(2):9-26.

International Journal of Science and Engineering Applications
Volume 7–Issue 09,298-302, 2018, ISSN:-2319–7560

Kinematic Analysis of Crank Shaft for Diesel Engine

Maung Maung Yi
Department of Mechanical Engineering,
Technological University
Thanlyin, Myanmar

Su Yin Win
Department of Mechanical Engineering,
Technological University
Thanlyin, Myanmar

Thwe Thwe Htay
Department of Mechanical Engineering,
Technological University
Thanlyin, Myanmar

Abstract: As the crankshaft is subjected to complex bending shear and twisting loads, it needs to be well designed and manufactured in good quality material to withstand the stress. As these stresses may change in direction and magnitude as the crankshaft rotates. In the balancing of the crankshaft, it needs to consider both the static balancing and dynamic balancing. In design calculation of crankshaft kinematics of crank gear, indicator diagram, force acting on the crankshaft and torque acting to the major journal and crank pin are important. The influence of the forces due to inertia both the reciprocating and rotating masses must be taken into account as accurately as possible, especially for high speed. The engine is four cylinders, four-stroke engine, and compression ratio is 20. The maximum power output of the shaft is 70.4 kW at 3200 rpm. The crankpin diameter and length are 56 mm and 31 mm, the main journal diameter and length are 65 mm and 32 mm. The operating conditions of cranks gear elements characterized by the forces which appear in them at various engine duties.

Keywords: velocity, gas pressure, inertia force and net force

1. INTRODUCTION

The crankshaft serves as the main rotating members, or shaft of the engines. The main function of the crank shaft is charging reciprocating motion to rotary motion. The crankshaft has offset journals to which the connecting rods are attached; it converts their up and down motion into rotary motion. It withstands bending stresses and torsional stresses during the whole time of operation. The connecting rod is connected to the piston by piston pin and to the crankshaft by the crankpin the output end of the crankshaft has flywheel. The front end has the gear or sprocket that drives the crankshaft, the vibration damper and the drives-belt pulley.
Central crank gear is as shown Figure 1.

2. KINEMATIC of CRANK GEAR

The operation condition of the crank gear element are characterized by the forces which appear in them at various engine duties. The magnitude and the nature of the change of the mechanical loads taken by these elements are determined from kinematic and dynamic investigations of the crank gear. In many modern engine are piston pin axis is offset by 0.01 to 0.03 of its diameter from the cylinder axis in order to achieve continuous elimination of the clearance between the piston and the cylinder wall and the more favorable distribution of load on the piston wall. The ratio between the crank radius and the connecting rod length is assigned.

$$\lambda = \frac{R}{Load} \quad (1)$$

$$k = \frac{a}{R} \quad (2)$$

The piston travel can be calculated

$$s = R\left[(1-\cos\phi) + \frac{\lambda}{4}(1-\cos 2\phi) - k\lambda\sin\phi\right] \quad (3)$$

The piston velocity can be calculated

$$V_p = R\omega\left(\sin\phi + \frac{\lambda}{2}\sin 2\phi - k\lambda\cos\phi\right) \quad (4)$$

The acceleration of the piston is

$$A = R\,(\cos\Phi + \lambda\cos 2\Phi + k\lambda\sin\Phi) \quad (5)$$

where,
R = crank radius
λ = dimensionless parameters
k = the relative displacement
a = displacement of the plane of travel of the piston pin axis from crankshaft axis

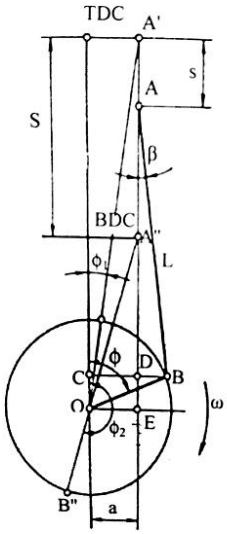

Figure 1.The offset engine crank gear

Φ = angle of crank travel counted from the cylinder axis in the direction of clockwise crankshaft rotation
β = angle between the connecting rod and cylinder axis
ω = angular velocity of crankshaft rotation
S = 2R = piston stroke
L_{Rod} = connecting rod length
V_p = piston velocity
A = acceleration of the piston

Take the rotational speed of engine N = 3200 rpm and the offset is 0.015D [2]. Piston-travel, velocity and acceleration with corresponding crank angle are shown in Table 1.

Table 1. Piston travel, velocity, acceleration with corresponding crank angle

Degree	Piston travel	Velocity	Acceleration
0	0	-0.130	6715.190
30	7.69	9.9597	5270.161
60	27.8379	15.287	1845.7815
90	52.511	15.415	-1505.959
120	73.837	11.413	-3319.750
150	87.367	5.818	-3676.801
180	92	0.130	-3615.872
210	87.756	-5.592	-3720.440
240	74.369	-11.2821	-3395.44
270	53.289	-15.415	-1593.359
300	28.512	-15.417	1770.090
330	8.082	-9.822	5226.460
360	0	-0.130	6715.190

2.1 Indicator Diagram

On the volume line, A piece of line AB corresponding to swept volume of cylinder. Then the volume which corresponding to the volume of combustion chamber is determine

$$V_c = \frac{AB}{r^{c-1}} \quad (6)$$

$$\tan \beta_1 = (1 + \tan\alpha)^{n1} - 1 \quad (7)$$

$$\tan \beta_1 = (1 + \tan\alpha)^{n2} - 1 \quad (8)$$

where,

n_1 and n_2 are polytropic exponents of compression and expansion respectively

where,

V_c = clearance volume

From Figure 2 ,construct a table ,which express the relationship of the crank angle and the gas pressure in the step up of 30 can be calculated.The developed indicated diagram is shown in followed.

2.2 Force acting on a crankshaft

The forces on the crank gear are divided into the force of gas pressure in the cylinder, the forces of inertia of the moving parts in the mechanism, and the inertia and centrifugal forces of the rotating parts. The gas pressure forces are the principal forces at low engine speeds, but the inertia force may be considerably larger at high speeds. The centrifugal force also increases rapidly with an increase in speed. The pressure of gas in the engine cylinder creates the force applied to the cylinder head. This force is directed along the cylinder axis and it is equal in magnitude and opposite in direction to the force acting on the piston.The force of gas pressure in the cylinder is determine by

$$P_G = (P_g - P_o).\ A_p \quad (9)$$

where ,

P_G = force of the gas pressure

A_p = area of the piston

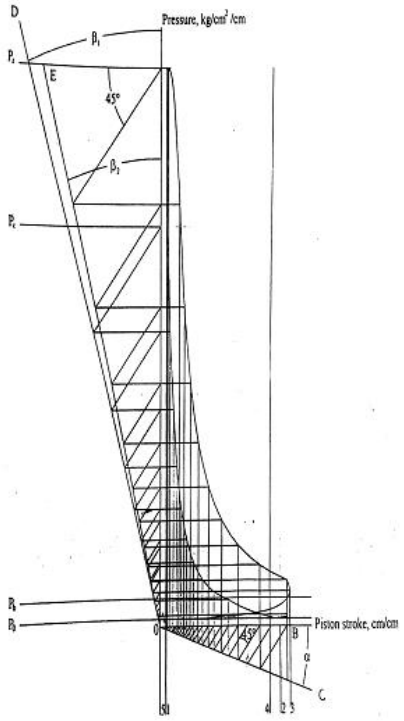

Figure 2. Indicator Diagram for vertical axis is pressure and horizontal axis is piston stroke.

Table 2. Gas pressure of various crank angles

Degree	Gas Pressure(kg/cm^2)
0	1.133
30	0.97275
60	0.86055
90	0.6908
120	0.7055
150	0.8819
180	0.9001
210	0.9259
240	1.204425
270	1.87517
300	3.35702
330	12.38406
360	65.7187

2.3 Inertia force

To determine the force of inertia, it is necessary to know the masses of crank gear elements. To simplify the calculations, the actual crank gear is replaced by a dynamically equivalent system of lumped masses. All the moving parts are divided into the groups with respect to the nature of their motion. They are,

(i) Parts reciprocating along the cylinder axis (piston group)

The mass of piston with piston rings assumed to be assumed to be lumped on the piston pin axis and is designated by, m_p.

(ii) Rotating parts of the crankshaft

Their mass are replaced by a mass reduced to the crank radius R and are designated by m_R. This reduction is so performed as to ensure quality between the centrifugal force of inertia of the actual masses and that of reduced mass.

The mass of the crank pin m_{cp} with adjacent parts of the webs(a is assumed to be lumped along the center of the crank pin axis and, since its center of the gravity is at a distance R from the shaft axis, this must need not be reduced.

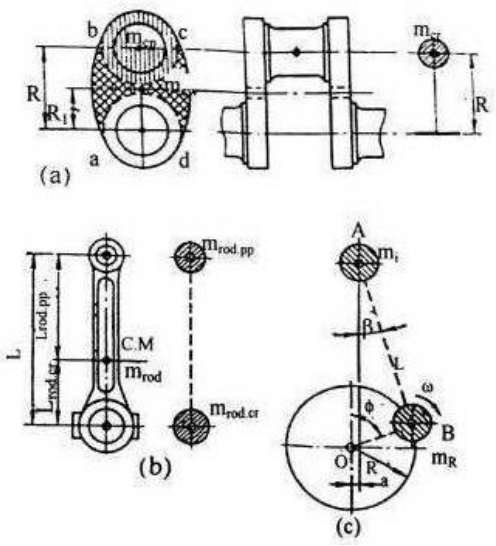

Figure 3. Reduction of the crank gear system to a two-mass one.[1]

The mass m_{cw} of the middle portion of the crank web over the countour "abcd" with its center of gravity on the radius is reduced to the radius R.

$$m_{cw}R_1\omega^2=(m_{cw})_R R\ \omega^2 \quad (10)$$

$$(m_{cw})_R= m_{cw}R_1/R \quad (11)$$

Therefore the reduced mass of the crank is,

$$m_{cr}=m_{cp}+2(m_{cw})R=m_{cp}+2\ m_{cw}R_1/R \quad (12)$$

(iii) Parts performing complex plane-parallel motion space (connecting rod group).The connecting rod is replaced with a certain approximation by a system of two masses statically equivalent to its mass-the mass $m_{rod.pp}$ lumped on the piston pin axis, and the mass $m_{rod.cr}$ the axis of the crankpin.For this purpose, the mass of the connecting rod m_{rod} is divided into two masses that referred to the piston pin axis.

$$m_{rod.pp} = m_{rod}\ L_{rodcr}/L_{rod} \quad (13)$$

and, that referred to the crank axis,

$$m_{rod.cr} = m_{rod}\ L_{rodpp}/L_{rod} \quad (14)$$

According to the statistical data, for most design of engine,

$m_{rod.pp}$ = (0.2 to 0.3) m_{rod}

$m_{rod.cr}$ = (0.7 to 0.8) m_{rod}

Thus, the entire crank gear is replaced by a system of two lumped masses connected by rigid weight less links-the reciprocating mass at point A,

$$m_1 = m_p + m_{rod.pp} \quad (15)$$

where, $m_{rod.pp}$ = mass of connecting rod referred to piston pin and the rotating mass at point B,

$$m_R = m_{cr} + m_{rod.cr} \quad (16)$$

where, $m_{rod.cr}$ = mass of connecting rod referred to crank pin.

The value of m_{pp} and m_{rod} are selected according to data of available designs. The design masses of crank gear elements referred to one unit area of piston A_p are given in Table.

Table 3.Design Masses of Crank Gear Elements(g/cm^2)

Type of Engine	Mass of Piston from aluminum alloy m_p''	Mass of connecting rod m_{rod}''
Carburetor engines(D= 60 to 100mm)	10-15	12-20
Diesel engines (D= 80 to 120mm)	20-30	25-35

The mass of piston group,

$$m_p = m_p'' \times A_p \quad (17)$$

The mass of connecting rod

$$m_{rod} = m_{rod} \times A_p \quad (18)$$

where , m_p = mass of piston

m_{rod} = mass of connecting rod

According to the statistical data, for most design of engine

$$m_{rod\ pp} = (0.2\sim0.3)\ m_{rod} \quad (19)$$

$$m_{rod\ cr} = (0.7\sim0.8)\ m_{rod} \quad (20)$$

The entire crank gear is replaced by a system of two lumped masses connected by rigid weightless links the reciprocating mass at point A,

$$m_1 = m_p + m_{rod\ pp} \quad (21)$$

Force of inertia (F_i) included by reciprocating mass is determined.

$$F_i = -m_i R\ \omega^2 (\cos\Phi + \lambda \cos 2\Phi + k\ \lambda \sin \Phi) \quad (22)$$

The rotating mass at pt B

$$m_R= m_{cr}+ m_{rod\ cr} \quad (23)$$

The gas pressure force and the inertia force may be combined algebraically to determine the net force acting along the cylinder axis.Force acting toward the crank shaft are plotted as positive values.Thus ,only the induction and the first part of the compression stroke will have negative value.The inertia forces are always negative at the top and positive at the bottom of the stroke.The net force acting along the cylinder axis can be determined by

$$F = P_G \pm F_i \quad (24)$$

At various crank angle Φ, the gas pressure force P_G, the inertia force F_i and the net force F are change or various with their corresponding crank angle and presented in Table 3.

Table 4.Gas pressure force of various crank angle

Degree,ϕ	Gas Pressure Force, P_G, kg	Inertia Force,F_I, kg	Net Force,F kg
0	7.591	-1056.098	-1048.506
30	-1.1829	-828.833	-830.017
60	-7.959	-290.643	-298.602
90	-17.648	236.842	219.194
120	-16.809	522.097	505.288
150	-6.741	578.251	571.51
180	-5.702	568.668	562.966
210	-4.229	585.159	580.93
240	11.668	533.736	545.404
270	49.953	250.539	300.492
300	134.536	-278.404	-143.868
330	649.790	-821.887	172.097
360	3694.078	-1356.098	2637.98

2.4 Piston side thrust and connecting rod force

The net force is exerted in the direction along the cylinder axis. The angularity of the connecting rod causes the net force to be divided into two components; one producing piston thrust against the cylinder wall, and the other acting along the axis of the connecting rod.

The piston side thrust against the cylinder wall determined by

$$Q = F \tan \beta = F \lambda (\sin \Phi - k) \quad (25)$$

The force along the connecting rod is determined by

$$K=\frac{F}{\cos\beta}=F\left[1+\frac{\lambda^2}{4}(1-\cos 2\phi)\right] \quad (26)$$

The tangential force at the crank pin is determined by the resolving the force along the connecting rod into two components, one acting tangentially to the crank circle at the crank pin and the other acting radially at the crank pin. The tangential force to the crank radius circle and normal force directed along the crank radius are

$$F_t=F\left(\sin\phi+\frac{\lambda}{2}\sin 2\phi-k\lambda\cos\phi\right) \quad (27)$$

$$N=F\left(\cos\phi-\frac{\lambda}{2}(1-\cos 2\phi)+k\lambda\sin\phi\right) \quad (28)$$

A couple of force appears with a moment, T called the torque and is determined

$$T=F_t\times R \quad (29)$$

Table 5. The relation of the force Q, k, F_t and N

Degree	Side Thrust Force	Force	Tangential Force	Normal Force
0	8.870	-1048.5	8.87	-1048.50
30	-117.48	-839.35	-516.75	-660.07
60	-75.05	-308.68	-296.12	-84.29
90	63.90	229.06	219.19	-63.9
120	127.00	522.34	373.91	-362.59
150	80.89	577.94	215.69	-535.39
180	-4.76	562.06	4.76	-562.96
210	-92.05	587.46	-210.70	-549.15
240	-146.31	563.81	-399.18	-399.40
270	-92.69	314.01	-300.49	-92.69
300	38.59	-148.72	143.89	-38.50
330	27.27	-174.03	109.66	-135.40
360	-22.32	2637.98	-22.32	2637.98

The relation of the force Q, k, F_t and N are shown in Table 3. The torque on the main journals V_s the torque of the crank pin for four cylinders four-stroke engine are shown following.

Table 6. Within the crank angle of Torque

Degree	Torque	Degree	Torque
0	0.40802	390	24.532
30	-23.770	420	2.699
60	-13.622	450	19.091
90	10.084	480	23.459
120	17.199	510	12.935
150	9.922	540	0.278
180	0.219	570	-10.105
210	-9.692	600	-18.164
240	-18.362	630	-11.589
270	-13.822	660	13.042
300	6.618	690	24.195
330	5.044	720	0.40802
360	-1.026		

Using the data of table 5,plotted the torque on the main journals and the torque on the crank pin for a four cylinder four stroke engine is plotted. Shown in followed.

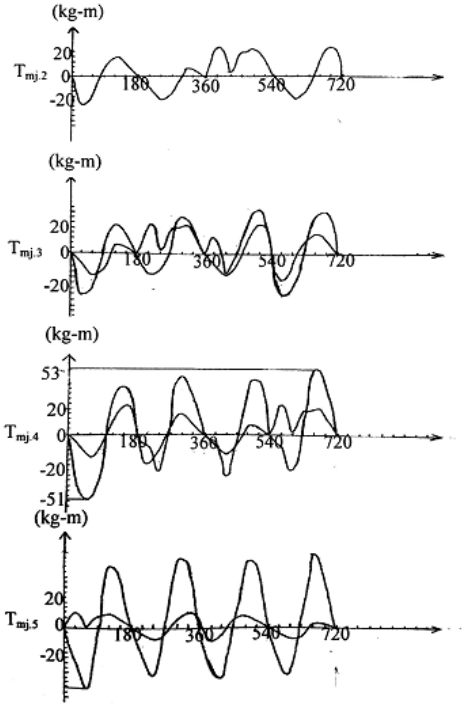

Figure 4. Accumulating torque diagram of main journal for diesel engine

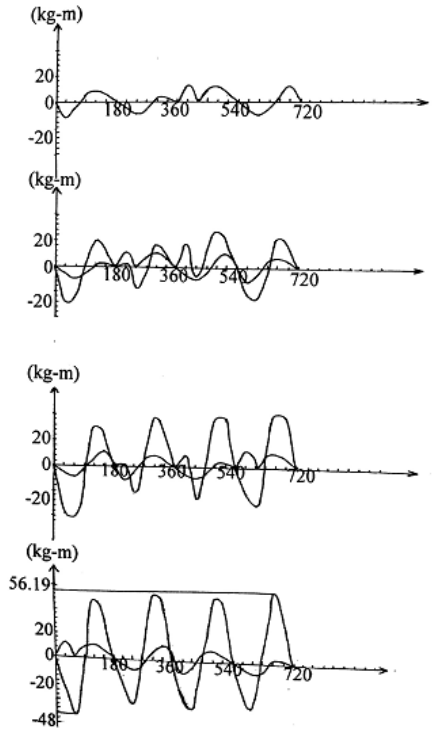

Figure 5. Accumulating torque diagram of crank pin for diesel engine.

3. CONCLUSION

In this paper, the author used the double span crankshaft. In the indicated diagram calculation taken the assumed valued i.e the polytropic exponent of compression n_1 is between the range of 1.32 to 1.4 and taken as 1.32 and polytropic exponent of expansion n_2 is 1.18 to 1.28 and taken as 1.18. The mean piston speed is within the range of 5 to 9 and taken as 7 m/s. This crankshaft design is specially design for high speed light vehicles. Not only this design is economy from commercial point of view but also it can be used for prolonged time.

4. ACKNOWLEDGMENTS

First of all, the author is grateful to Dr Thein Gi, Rector of Technological University(Thanlyin), for giving the permission to submit the paper.

The author wishes to express his heartfelt thanks to each and every one who assisted in completing this paper.

Finally, the author deep gratitude and appreciation go to his parents for his moral supports, patience, understanding and encouragement.

5. REFERENCES

[1] M.KHOVAKH, 1979: Motor Vehicle Engines, MIR Publisher-Moscow.

[2] Charles Fayette Taylor, 1960: The Internal-Combustion Engine in Theory and Partice. The Technology Press of The Massachusetts Institute of Technology and John Wiley and Sons,Inc.

[3] George H.Martin,1969: Kinematic and Dyanmics of Machines. McGraw- Hill Book Company,Inc

[4] Ray H.Bacom,1968: The car Engine and Structure Macmillan & Cleaver.

[5] Malee,v.L 1945: Internal Combustion Engine, Tokyo.

[6] H.F.P Purday, 1962: Diesel Engine Designing. Constable & Company Ltd.

[7] A.T.J.Kersey,1947: Internal-Combustion Engineering. Third Edition, Blackie and Son Limited

[8] RobertL.Streeter, 1915: Internal Combustion Engine (Theory and Design). First Edition, McFraw-Hill Book Company, Inc.

International Journal of Science and Engineering Applications
Volume 7–Issue 09,303-306, 2018, ISSN:-2319–7560

Apogee Measurement of a Polyvinyl Chloride Rocket Using a Sugar Composite Propellant and Open Source Computer Rocket Simulation Software

Iguniwei B.Paul
Post Graduate School
Nigeria Defence Academy
Kaduna, Nigeria

Mohammed Y'au
Department of Chemistry
Nigerian Defence Academy
Kaduna, Nigeria

S. O. Okeniyi
Department of Chemistry
Nigerian Defence Academy
Kaduna, Nigeria

Abstract: The Bokoharam insurgency against the Nigerian State and the Nigerian Military effort at Counter insurgency operation, is a catalyst for this research, in to the apogee flight measurement of a locally constructed polyvinyl rocket with a sugar composite propellant, using an open source computer simulation software. The weight and dimensions of the locally constructed rocket with the dimensions and weights of 3 BATES propellant grains was imputed in to the open rocket computer software, creating a 3 Dimension model of the rocket. A simulation for peak altitude was initiated and an apogee of 729 meters was obtained. The result shows a potential application in infantry rocketry for close quarter battles.

Keywords: Bokoharam, Military, Apogee, Open source, Sugar, Propellant, Rocket and Simulation

1. INTRODUCTION

Chemists have always played the very fundamental role in the synthesis of propellants, be it for propelling a cannon ball, 7.62 by 59 ammunition, an artillery round, a free flight infantry rocket or a research rocket. The Bokoharam Insurgency against the Nigerian state and their unconventional asymmetric battle methodology [1] has led to this research of the local construction of a pvc rocket and simulate its apogee in a computer environment using a sucrose composite propellant.

The dearth of specific response to the speed with which the insurgents produce their explosives, IEDs etc as compared to the Nigerian military conventional logistic chain of supply is also an indicator for a change of approach. One of which is to produce quickly and easily certain weapons like the short range infantry rockets which would impact a close quarter battle often engaged in my the insurgents. This research attempts to show that cheap materials like polyvinyl chloride (pvc) sucrose and potassium nitrate can be used to propel a rocket, which when equipped with a destructive warhead can, be deployed against the insurgent enemy.

According to [2] Infantry Rocket Systems are man-portable direct fire weapons usually smaller than field artillery rockets. Anti-tank rockets are the most common infantry rocket system. They are designed to be carried by the individual soldier and fired from the shoulder. Examples of Free Flight Infantry rockets are the Light Anti-Armour Weapon (LAW) and an improved version of the LAW code named FGR-17 VIPER.

Sugar propellants like the KNSU are moderate performance propellants in which the binder fuel is one of the common sugars (sucrose, dextrose & maltose etc). Technically KNSU is a composite propellant since it has a separate fuel and oxidizer component.

Potassium nitrate will not burn at all on its own, unless it is presented with a fuel source like sugar. When these two components are mixed together in a fuel-oxidizer matrix, the combustion is violent because of the rich source of oxygen from the KNO_3. This kind of combustion reaction according to [3] is represented stoichiometrically as:

$$C_{12}H_{22}O_{11(s)} + 6.3KNO_{3(s)} \longrightarrow 4CO_{2(g)} + 5CO_{(g)} + 8H_2O_{(g)} + 3H_{2(g)} + 3N_{2(g)} + 3K_2CO_{3(l)} + 0.3KOH_{(l)}$$

However the binder-fuel is not a polymer and is already partially oxidized. These two properties provide two useful characteristic of the propellant, first the binder decomposes more rapidly, than does the polymer, and so a lower-energy oxidizer such as KNO_3 will be employed with excellent results. Secondly, a lower proportion of oxidizer can be used with good results. Sugar propellants have been found to be intermediate in performance [4]. Typical delivered specific impulse is between 115 - 130 seconds, which is not dependent on the fuel.

2. LITERATURE REVIEW

The firepower of Rockets and Missiles, combined with sustaining the bombing Tempo significantly led to the weakness at home (in Germany) of the German war-fighting capabilities hence the ultimate defeat by the Allied combined Bombing offensive against Nazi Germany during the period of 1943-1945 [5].Few declassified literature on Military Rockets exists, not because of lack of research, but because of the classified nature of military research [6] Some of the most common rockets powered by solid propellant motors are (i) the Milan Infantry anti-Tank Missile (Ballistite) (ii) the soviet Anti Tank AT-4 Missile (cordite). However a recent contemporary effective deployment of rockets in warfare was found in the Hezbollah Israel war of 2006 [7]

Some Common Propllants	Isp
Potassium Nitrate /Sugar (KNSU)	115-130
Gunpowder	80-90
APCP–Ammonium perchlorate composite propellant	190-210

Table 1: Specific Impulse (Isp) of Some Common Propellants

[8] Reported the re-crystallization process of KN/Sucrose which resolves some limitations of the use KN/sucrose. He also reported the melting of KN/sorbitol in a boiling-water bath. The propellant mix was enclosed in a plastic bag and immersed in hot water. This is the safest method yet of melting sugar propellants. Further literature has shown that there are different types of sugar used for rocket propellant Apart from sucrose, dextrose and sorbitol-a sugar alcohol are commonly use too.

3. MATERIALS AND METHODS

3.1Materials

(i) Sucrose (ii) Potassium Nitrate (iii) cone (iv) Ziploc anti moisture bag (v) PVC tubes (vi) PVC sheet (vii) Acrylic Adhesive (viii) Heating Pan (ix) Heat resistant Thermometer (x) Hacksaw and cutting tool (xi) Measuring tape and Ruler (xii) Heat Resistant Hand gloves (xiii) Goggles (xiv) Digital Weighing Balance, Model Wuwangni 5kg+_ 1gm (xv) Thermostat controlled heat Source.

3.2 Sample Collection

Five hundred grams (500) of sugar (sucrose) manufactured by Dangote Company was obtained from the market, and was used without further purification. Industrial grade potassium nitrate was obtained from a chemical store. The sugar was kept in a polythene bags while the potassium nitrate was kept in its container as it was bought. PVC pipe was bought from the open market Method of Synthesis

3.3 Method of Synthesis

A modified Melt and Cast method of Richard Nakka [9] was used in the production of the varying composites of the propellants for this research work. This method involves grinding the sugar and potassium nitrate separately in to powdery form (to increase their surface area) and melting the sugar and mixed with potassium nitrate, making a batch of 200grams of the KNSU mix. This mixture was done slowly! (To avoid a deflagration). The mixture was further heated using a hot plate to a melting temperature of 180^0C forming a viscous paste, (figure 1) which was quickly poured into pvc BATES moulds (figure 2). It was allowed to cool, weighed and dimensions measured. It was stored in a desiccator to prevent contact with moisture. The composition ratio used was 65% Potassium Nitrate and 35% Sugar)

Figure 1 Melting of the Sucrose and Potassium Nitrate mixture

Figure 2 Cast BATES grains

3.4 Rocket Sketch and Construction

A workable design was sketched and constructed using Polyvinylchloride (PVC) tubing. All dimensions are in millimeters

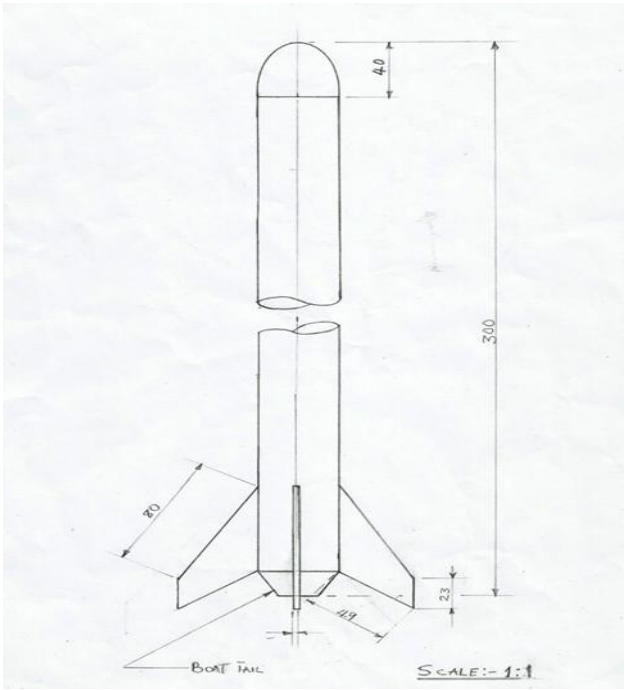

Figure 3 Design sketch with Dimensions of the PVC rocket

4.0 RESULTS AND DISCUSSION

4.1 Results

The Ballistic Tests and Evaluation System (BATES) grain for composition A (Potassium nitrate 65% and Sucrose 35%) measured dimensions.

Table 1 Composition A weight and dimensions of the synthesized BATES Propellant

S/No	Weight(g)	Length (mm)	Diameter (mm)	Inner Diameter (mm)
1	78	51	33	5
2	77.9	51	33	5
3	78	51	33	5

The BATES moulds for producing the BATES grains are uniform in dimensions, hence the uniform dimensions obtain from the grains measurement, except for the weight of the propellants.

Below is the life size of the constructed rocket, a product of the sketched rocket, of figure 3

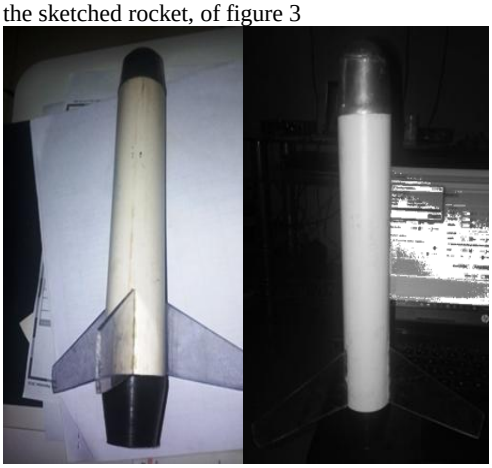

Figure 4: Constructed Rocket

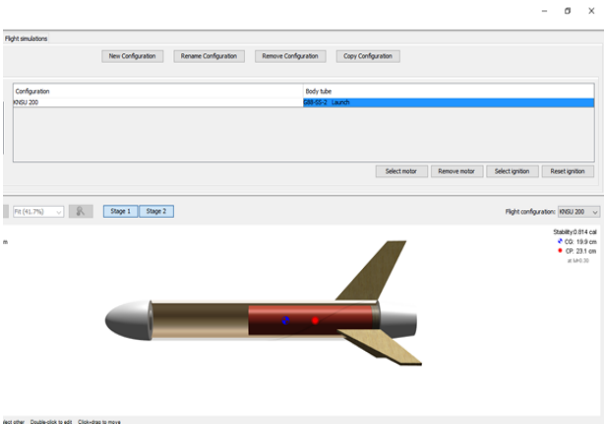

Figure 5: Screen shot of 3 Dimension designed rocket model

Table 2: Computer rocket flight performance analysis

Specific Impulse	**116**
BurnOut Altitude(z_1) m	**-**
BurnOut Velocity(v_1) ms^{-1}	**104**
Apogee(z_2) Peak Altitude m	**729**
Peak Altitude Time(t_2) secs	**10.1**

4.2 Discussion

Table 1 shows the dimensions and the weight of the BATES grains. Apart from the small variations in weights of the grains, other parameters like the internal diameter and the length of the BATES grains are the same. This is because these parameters are intrinsic for the grains to be qualified as a BATE grain. The small deviation in the weights of KNSU grains may be due to rapid cooling of the molten propellant becoming more viscous during pouring in to the pvc moulds creating pockets of tiny air bubbles [10].

Figure 4 is the completed life size of the test rocket. Which was built on the design parameters from figure 3. It was ensured that the rocket is stable by locating the Centre of gravity (CG) and the Centre of Pressure (CP) according to [11]. Figure 5 shows the 3 dimension screen shot of the designed rocket, using the open rocket software [12]. The design was based on the sketched dimensions of figure 3. It enabled the KNSU composite propellant and the rocket to be simulated for some of the performance parameters as listed in Table 2.

From the design of the rocket and the synthesis of the propellant, it can be deduced that the propellant and the PVC material has a production advantage because of its simplistic production process, eliminating error through the use of the computer simulation software. The apogee distance of 729m indicates a viable military application in short range infantry operations against the Bokoharam insurgents in the Northeastern region of Nigeria. The choice of selection of the materials: pvc, sucrose and potassium nitrate ensures a readily supply if and when the rocket is weaponised for military operations and confers huge economic advantage in terms of cost of procurement and the speed of field deployment.

5.0 CONCLUSION

A KNSU propellant was synthesized successfully using the Melt and Cast method. The BATES grain type of the KNSU propellant was used to propel a rocket in a computer simulated environment successfully to an apogee of 729m, a distance well over half a kilometer. This shows an important potential for military use of this propellant in infantry rocketry and close quarter battles (once the rocket is fitted with an explosive charge) as we are experiencing in Nigeria's Northeastern counter insurgency operations against the Bokoharam Insurgents.

6.0 ACKNOWLEDGEMENT

I am grateful to Dr Omale and Dr Mohammed Y'au both of the Department of Chemistry, the Nigerian Defence Academy, Kaduna. Nigeria, for their fundamental support and professional inputs.

7. REFERENCES

[1] Michael, E., Alan, R., & Russell, P. (Eds.). (2004) Future Armies Future Challenges –Land warfare in the information Age. Crow's Nest, Australia.

[2] MIL-HDBK-762, Design of Aerodynamically Stabilized free Rockets, Volume One (1990) US Army Missile Command, Military Handbook. Redstone Arsenal. pp 23-24

[3] Smiley, J. (2013) Easy PVC Rockets.pdf. Create space Independent Publishing. Retrieved from www.amazon.com

[4] Lesilie, S. & Yawn, J. (2002) Proposal for the inclusion of KNO_3/Sugar Propellants in the Tripoli Research Agency (TRA) Experimental Rocketry Program. A Technical Report Retrieved from www.4sightinc.com/stu/docs/sugar_Pro_Proposal.pdf

[5] Michael, E., Alan, R., & Russell, P. (Eds.). (2004) Future Armies Future Challenges –Land warfare in the information Age. Crow's Nest, Australia

[6] Krieger, F.J.(1960) The Russian Literature On Rocket Propellants, Physics Division. The Rand Corporation. Presented at the 137th National Meeting of the American Chemical Society in Cleaveland Ohio. April 8 1960. Retrieved March, 2016 from www.rand.org

[7] Rubin, U. (2007) The rocket Campaign Against Israel, 2006 Labanon War. MidEast Security and Policy Studies No 71. The Begin-Sadat Center of Strategic Studies, BAR-ILAN UNIVERSITY, Ramat Gan, Israel

[8] Lesilie, S. & Yawn, J. (2002) Proposal for the inclusion of KNO_3/Sugar Propellants in the Tripoli Research Agency (TRA) Experimental Rocketry Program. A Technical Report Retrieved from www.4sightinc.com/stu/docs/sugar_Pro_Proposal.pdf

[9] Nakka, R.A. (1984) Solid Propellant Rocket Motor Design and Testing. A Thesis Presented to the Department of Mechanical Engineering, University of Manitoba.

[10] Nakka, R.A. (2007) Sugar Motors (pdf) Retrieved April 2016 from www.nakka-rocketry.net

[11] Ponder, D.M. (2013) Designing Your Own Model Rocket (pdf) retrieved from www.ohio4h.org

[12] Sampo Niskanen, OpenRocket Simulation software. Downloaded September 2015 from http://openrocket.info/

International Journal of Science and Engineering Applications
Volume 7–Issue 09,307-312, 2018, ISSN:-2319–7560

Aerodynamic Analysis of Curved Blade for Water Pumping Windmill

Khaing Zaw Lin
Department of Mechanical Engineering,
Technological University
Thanlyin, Myanmar

Thwe Thwe Htay
Department of Mechanical Engineering,
Technological University
Thanlyin, Myanmar

Su Yin Win
Department of Mechanical Engineering,
Technological University
Thanlyin, Myanmar

Abstract: Design of a rotor of a windmill is very important to extract the energy from the wind. The design of rotor involves the calculation the rotor parameters and its components to produce maximum power. Although the design of a wind mill looks simple, it involves complex and detailed design of its components like rotor, transmission, load matching, yawing mechanism etc. In this paper, aerodynamic analysis of a curved blade for windmill is simulated by comparing NACA standard airfoils. Two-dimensional numerical modelling of the airfoil of the windmill is performed with COMSOL Multiphysics software. The velocity and pressure distribution around airfoil can be checked from the simulation results. The 2D airfoil geometry is realized in COMSOL's geometry tools. Two dimension and steady state model has been used and boundary conditions are considered within computations as the flow in wind tunnel.

Keywords: windmill, curved blade, CFD, velocity field, pressure distribution

1. INTRODUCTION

Today, wind pumps are used in many places all over the world because wind energy is a good alternative power source for water pumping. In this system horizontal axis multi-blade windmill is considered and pinions and gears will be used for power transmission. A reciprocating pump will be used to operate at low speed. This system consists of three main parts, which are a wind mill, a transmission system and a single acting reciprocating pump. Available wind energy can be received by wind blades from a windmill and then takes out the mechanical energy via the crank arm to the reciprocating pump.

2. WINDMILL

The use of mechanical equipment to convert wind energy to pump water goes back many years. Windmills are classified as vertical or horizontal axis machines depending on the axis of rotation of the rotor. Vertical axis windmills can obtain power from all wind directions whereas horizontal axis windmills must be able to rotate into the wind to extract power. Windmills are also classified as either electrical power generators or water pumpers. Power generators typically operate at high rotational speeds with low starting torques. Direct water pumping windmills are characterized by a multi-blade, horizontal axis design set over top of the well as shown in Fig.1. Water pumping requires a high torque to start the pump and it can get by using the multi-blade design. [1]

3. NUMERICAL SIMULATION

The rapid evolution of computational fluid dynamics (CFD) has been driven by the need for faster and more accurate methods for the calculations of flow fields around configurations of technical interest. In the past decade, CFD was the method of choice in the design of many aerospace, automotive and industrial components and processes in which fluid or gas flows play a major role. In the fluid dynamics, there are many commercial CFD packages available for modeling flow in or around objects. The computer simulations show features and details that are difficult, expensive or impossible to measure or visualize experimentally. For this reasons, the researchers and students are more concerned with the computer simulations. [2]

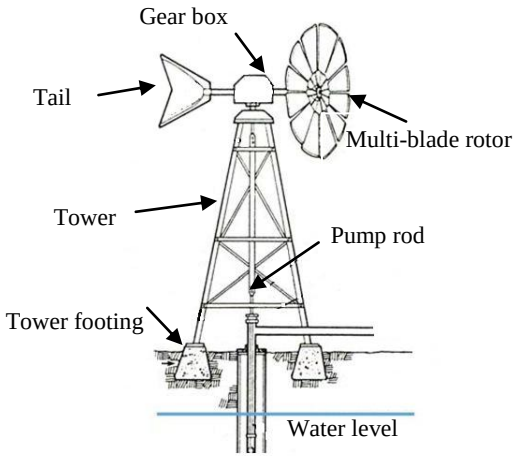

Figure. 1 Components of windmill for water pumping system [2]

Traditionally, drag and lift coefficients of an object can be measured with tests in a wind tunnel. Due to the decrease in the cost of computations compared to the increase in the cost of experiment, computational fluid dynamics is replacing the wind tunnel tests. With development of efficient and cost effective CFD software, CFD plays a pivotal role in academic and industrial research for preliminary result in design of new products. The numerical simulations are performed with COMSOL Multiphysics 4.3b, a finite element method based software. The COMSOL Multiphysics is a commercial partial differential equation solver that enables simultaneous computation of multiple physics. The advantage of COMSOL Multiphysics includes its user friendly modeling interface, versatility of physical models, and its accuracy.

The simulation process includes modeling of the geometry of the model, meshing the geometry created into elements to approximate the solution easily using simple functions,

defining material properties. Boundary, initial and loading conditions must also be specified which require experience, knowledge and engineering judgment. Finally, the solution is obtained by solving the simultaneous equations for the field variables at the nodes of the mesh. [3]

4. CFD MODULE

The CFD Module is an optional package that extends the COMSOL Multiphysics modeling environment with customized user interfaces and functionality optimized for the analysis of all types of fluid flow. The CFD Module is used by engineers and scientists to understand, predict, and design the flow in closed and open systems. At a given cost, these CFD simulations typically yield new and better products and operation of devices and processes compared to purely empirical studies involving fluid flow. As a part of an investigation, simulations give accurate estimates of flow patterns, pressure losses, forces on surfaces subjected to a flow, temperature distribution, and variations in fluid composition in a system.

The CFD Module's general capabilities include stationary and time-dependent flows in two-dimensional and three-dimensional spaces. Formulations of different types of flow are predefined in a number of fluid flow user interfaces to set up and solve fluid flow problems. The fluid flow user interfaces define a fluid flow problem using physical quantities, such as pressure and flow rate, and physical properties, such as viscosity. There are different fluid flow user interfaces that cover a wide range of flows such as laminar flow, turbulent flow, single-phase flow, and multiphase flow. In this thesis, single-phase flow at stationary in two-dimensional space is considered. [3]

The fluid flow user interfaces formulate conservation laws for the momentum, mass, and energy. These laws are expressed in partial differential equations, which are solved by the module together with the corresponding initial conditions and boundary conditions. The equations are solved using stabilized finite element formulations for fluid flow, in combination with damped Newton methods and, for time-dependent problems, different time-dependent solver algorithms. The results are presented in the graphic window and derived tabulated quantities obtained from a simulation. The work flow can be described by the following steps: define the geometry, select the fluid, select the type of flow, define boundary and initial conditions, define the finite element mesh, select a solver, and visualize the results. [4]

4.1. Single Phase Flow

The single-phase flow branch included with the CFD Module has a number of subbranches with physics interfaces that describe different types of single-phase fluid flow. They are laminar flow, turbulent flow, creeping flow and rotating machinery fluid flow. The Laminar Flow user interface is primarily applied flows of low to intermediate Reynolds numbers. The user interface solves the Navier-Stokes equations, for incompressible and weakly compressible flows (up to Mach 0.3). This fluid flow user interface also allows for simulation of non-Newtonian fluid flow.

The user interfaces under the turbulent flow branch model flow of high Reynolds numbers. These user interfaces solve the Reynolds-averaged Navier-Stokes (RANS) equations for the averaged velocity field and averaged pressure. The turbulent flow user interfaces have different models for the turbulent viscosity. There are several turbulence models such as a standard *k*-ε model, a *k*-ω model, an SST (Shear Stress Transport) model, a Low Reynolds number *k*-ε model and the Spalart-Allmaras model. The SST model combines the robustness of the *k*-ε model with the accuracy of the *k*-ω model, making it applicable to a wide variety of turbulent flows.

The creeping flow user interface approximates the Navier-Stokes equations for very low Reynolds numbers. This is often referred to as Stokes flow and is appropriate for use when viscous flow is dominant, such as in very small channels or micro fluidics applications. The physics user interfaces support compressibility (Mach < 0.3), laminar non-Newtonian flow, and turbulent flow using the standard *k*-ε model.

In this case, turbulent flow SST model is considered for the simulation of curved blade airfoil. The turbulent flow SST user interface has the equations, boundary conditions, and volume forces for modeling turbulent flow using the SST turbulence model. The main feature is fluid properties, which adds the Navier-Stokes equations and the transport equations for the turbulent kinetic energy (*k*) and the specific dissipation (ω), and provides an interface for defining the fluid material and its properties. Turbulence model parameters are optimized to fit as many flow types as possible, but better performance can be obtained by tuning the model parameters. The dependent variables such as velocity field, pressure, turbulent kinetic energy, specific dissipation rate and reciprocal wall distance must be defined for the simulation model. [5]

4.2. Theory of Lift and Drag in Turbulence Modeling

Turbulence is a property of the flow field and it is mainly characterized by a wide range of flow scales. The tendency for an isothermal flow to become turbulent is measured by the Reynolds number,

$$R_e = \frac{\rho U L}{\mu} \quad (1)$$

where μ is the dynamic viscosity, ρ is the density, and U and L are velocity and length scales of the flow, respectively. Flows with high Reynolds numbers tend to become turbulent and this is the case for most engineering applications. The Navier-Stokes equation can be used as a governing equation for turbulent flow simulations, although this would require a large number of elements to capture the wide range of scales in the flow. These equations are applicable for incompressible as well as compressible flows where the density varies.

$$\rho\frac{\partial u}{\partial t} + \rho(u.\nabla)u = \nabla\cdot\left[-pI + \mu\left(\nabla u + (\nabla u)^T\right)\right] + F \quad (2)$$

$$\rho\nabla\cdot u = 0 \quad (3)$$

- ρ - the density, kg/m^3
- u - the velocity vector, m/s
- p - pressure, Pa
- μ - dynamic viscosity, Pa.s
- T - the absolute temperature, K
- F - the volume force vector, N/m^3

Any solid object of any shape, when subjected to a fluid stream, will experience a force Ftot from the flow. The sources of this force are shear stresses (viscous effects) and normal stresses (pressure effects) on the surface of the object. For an airfoil, distribution of pressure and shear stress on its surface area, A is schematically shown in Figure 2. The negative pressures in the pressure distribution sketch means negative with respect to atmospheric pressure (negative gage pressure). The total force on the airfoil is the summation of pressure and viscous forces.

$$F_{tot} = \int_A p\,dA + \int_A \tau_W\,dA \quad (4)$$

This total force can be divided into two components: lift force which is normal to the free stream velocity, and drag force which is parallel to the free stream.

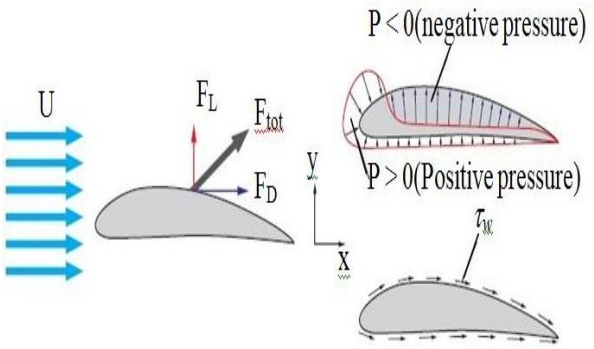

Figure 2. Pressure Distribution around an Airfoil [3]

Let's consider a small elemental area on an airfoil as shown in Figure 3. Components of the fluid forces in *x* and *y* directions can be determined.

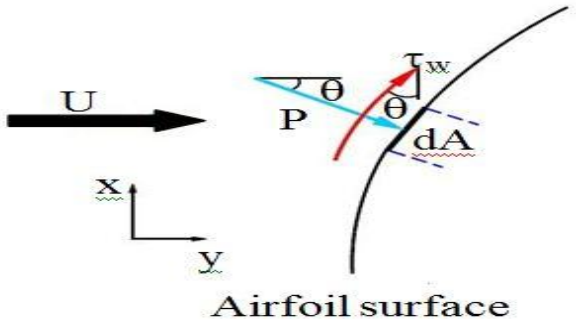

Figure 3. Normal Stress and Shear Stress on Elemental Surface Area [4]

Lift and drag coefficients are dimensionless quantities defined as,

$$C_D = \frac{\text{drag force}}{\text{dynamic pressure} \times \text{area}} = \frac{F_D}{\frac{1}{2}\rho U^2 A} \quad (5)$$

$$C_L = \frac{\text{lift force}}{\text{dynamic pressure} \times \text{area}} = \frac{F_L}{\frac{1}{2}\rho U^2 A} \quad (6)$$

where $\rho U^2/2$ is the dynamic pressure. The coefficients C_D and C_L strongly depend on the geometry of the object, and hence are usually determined by experiment or numerical simulation. The coefficient of pressure can be examined from the pressure distribution on upper and lower surface.

$$C_P = \frac{P - P_\infty}{\frac{1}{2}\rho U_\infty^2} \quad (7)$$

When the distribution of pressure is known, the net forces perpendicular and parallel to the air flow such as lift and drag forces. [6]

4.3. Curved Blade Airfoil Model

This model simulates the flow around an inclined curved airfoil using the SST turbulence model. The SST model combines the near-wall capabilities of the *k*-ε model with the superior free-stream behavior of the *k*-ω model to enable accurate simulations of a wide variety of internal and external flow problems. The model is considered with the flow relative to a reference frame fixed on a curved airfoil. The chord length of the blade is 0.32 m. The temperature of the ambient air is 20°C and the relative free stream velocity is 5 m/s resulting in a Mach number of 0.15. The Reynolds number based on the chord length is roughly 1.3×10^6, so the airfoil can be assumed that the boundary layers are turbulent over practically the entire airfoil. The airfoil is inclined at an angle α to the oncoming stream. The geometry is created by using COMSOL's geometry tools.

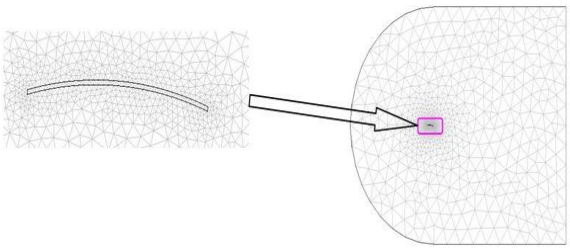

Figure 4. The Computational Mesh of the Circular Arc Airfoil [Simulation]

Meshing was performed in COMSOL Meshing by using free triangular mesh. The elements near the surfaces of airfoil were finer than that of the inlet and outlet boundaries. The computational mesh of the circular arc airfoil model is shown in Figure 4.Meshes were kept to maximum element size of 0.366 m and minimum element size of 0.0162 m. Inflation layers were implemented on all solid surfaces with a maximum growth rate of 1.15.

5. NUMERICAL SIMULATION RESULTS

Simulations for various angles of attack were done in order to compare the results of different airfoils and then the optimum airfoil was chosen. For these reasons, the models were solved with a range of different angles of attack from 0 to 8°. The pressure and velocity contours with the plots are shown for various angles of attack. The pressure coefficients of different airfoils are also shown as the curves. The lift and the drag coefficients of different airfoils and their ratios are plotted for various angles of attack. The simulation outcomes of pressure distribution of different airfoils at 4° angle of attack are shown in Figure 6. The pressure on the lower surface of the airfoil was greater than that of the incoming flow stream and as a result it effectively pushed the airfoil upward, normal to the incoming flow stream. At higher angle of attack, the pressure distribution is more obvious and the pressure difference is higher between the surfaces of the airfoils.

Velocity fields at angles of attack 4° are also shown in Figure 5. The trailing edge stagnation point moved slightly forward on the airfoil at low angles of attack. A stagnation point is a point in a flow field where the local velocity of the fluid is zero. The upper surface of the airfoil experienced a higher velocity compared to the lower surface. That was expected from the pressure distribution. As the angle of attack increased the upper surface velocity was much higher than the velocity of the lower surface.

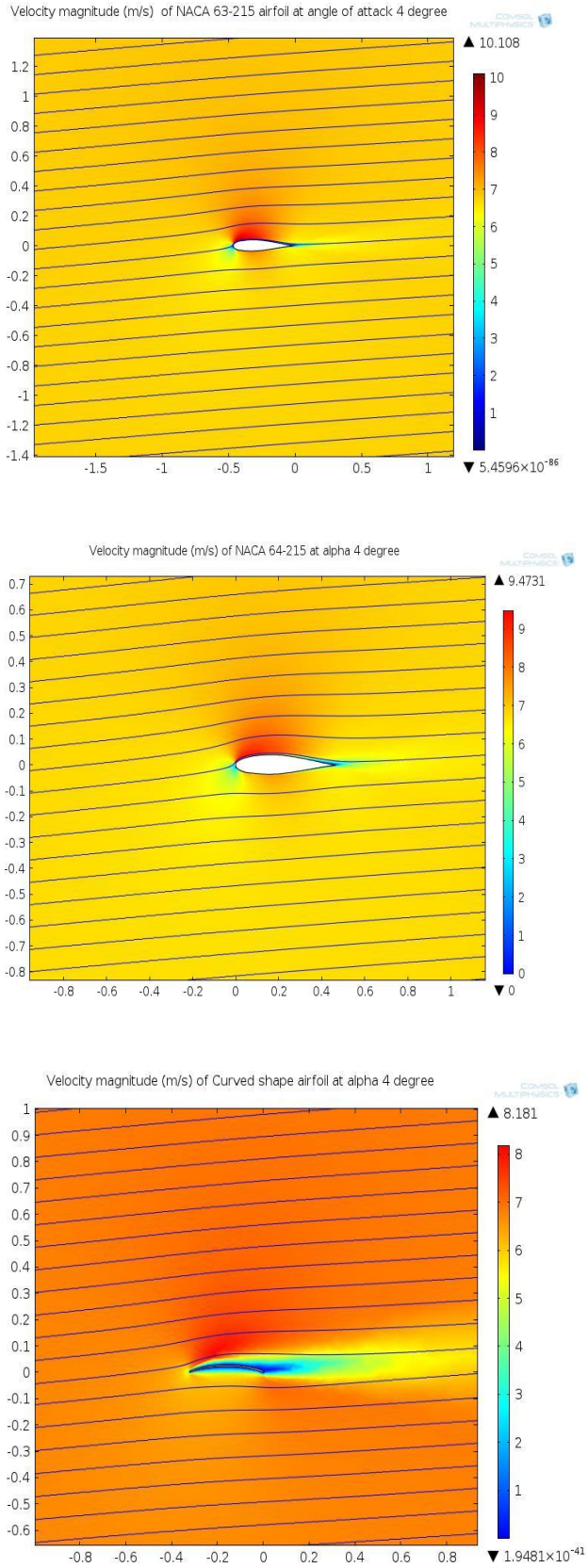

Figure 5. Velocity Magnitude of NACA 63-215, 64-215 and Curved blade at Angles of Attack 4°

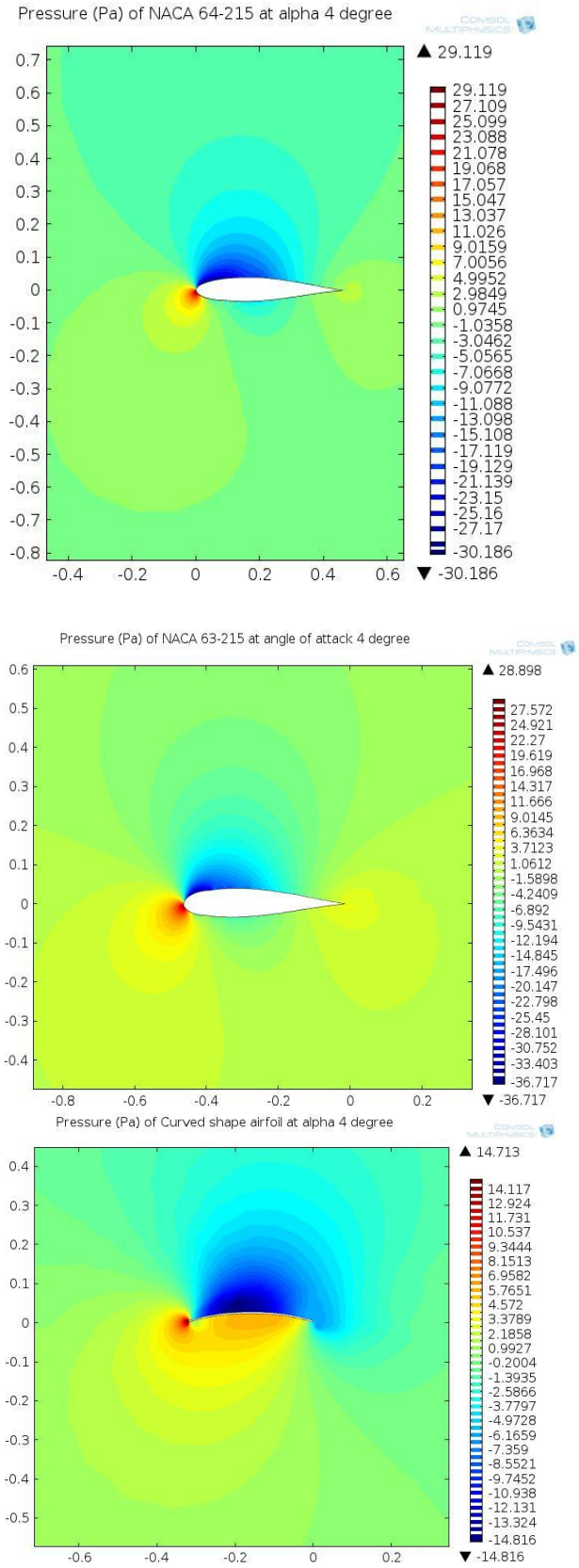

Figure 6. Pressure Distribution of NACA 63-215, 64-215 and curved blade at Angles of Attack 4°

The coefficient of pressure, C_P curves shows that the pressure on the lower surface was greater than that on the upper surface. The aerodynamics of circular arc airfoil is different from conventional profiles, where the pressure is positive on the lower surface except the trailing edge. Figure 7 shows the pressure coefficients of different airfoils at angle of attack from 4°. It is observed that the pressure coefficients mainly depend on angle of attack.

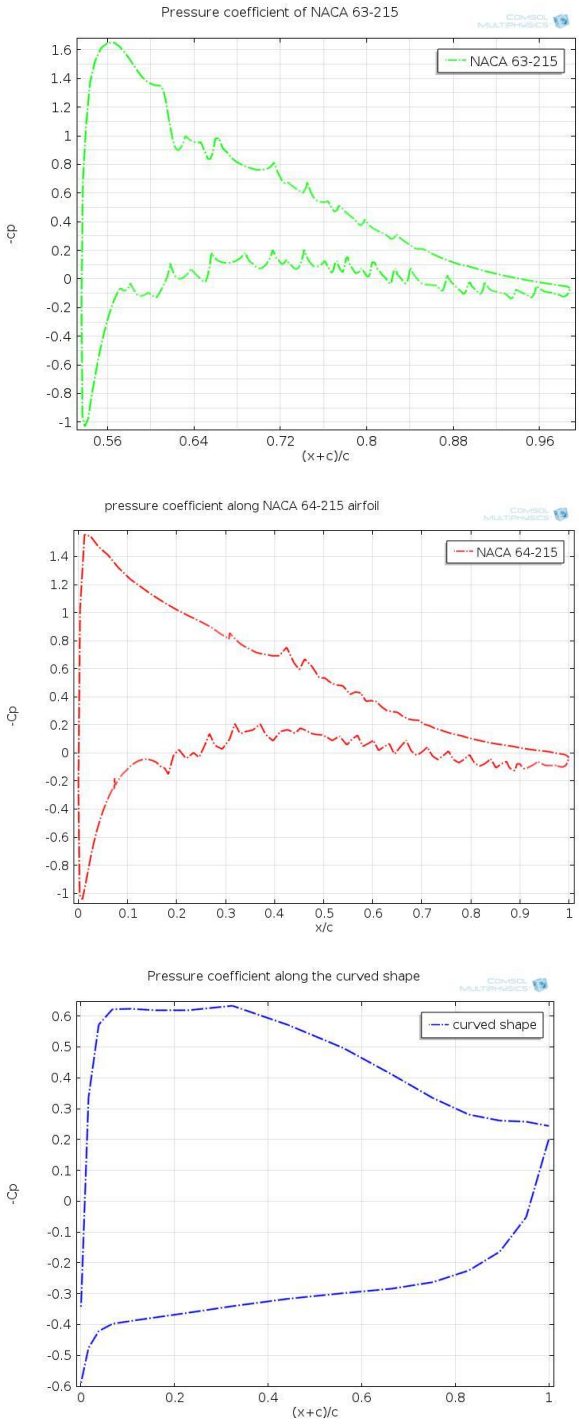

Figure 7. Pressure coefficients of Different Airfoils

The variation of lift coefficients with angle of attack in the range of 0 to 8° for different airfoils is shown in the Figure 8. In this paper, NACA 63-215 and NACA 64-215 are utilized to compare the performance of airfoil for windmill rotor. As the angle of attack increases, the lift coefficient increases linearly. Since the effect of flow separation becomes dominant at higher angle of attack, the slope of the curve begins to fall off. Eventually the lift coefficient reaches a maximum value and then begins to decrease. According to the figure, it can be seen that curved shape has higher lift coefficients than NACA airfoils with angle of attack in the range of 0 to 8°.

Figure 9 shows the drag coefficients of different airfoils at various angles of attack. When the angles of attack increase, the drag coefficients of NACA airfoils are also higher. The drag coefficients gradually increase with respect to the angle of attack. NACA 64-215 has higher drag coefficient than that of NACA 63-215. However, the curved shape has a different trend. The drag coefficients of curved shape decrease slightly between angles of attack 0° and 4° and then gradually increase after angle of attack 4°. According to the Figure 5.14, the curved shape has smaller drag coefficients after angle of attack 3°.

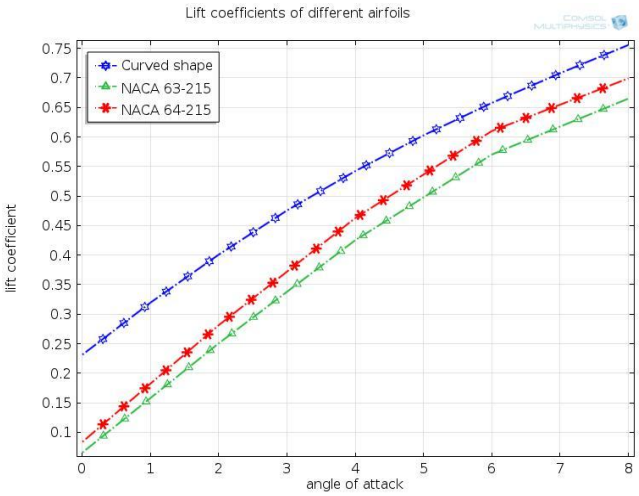

Figure 8. Lift coefficients of Different Airfoils

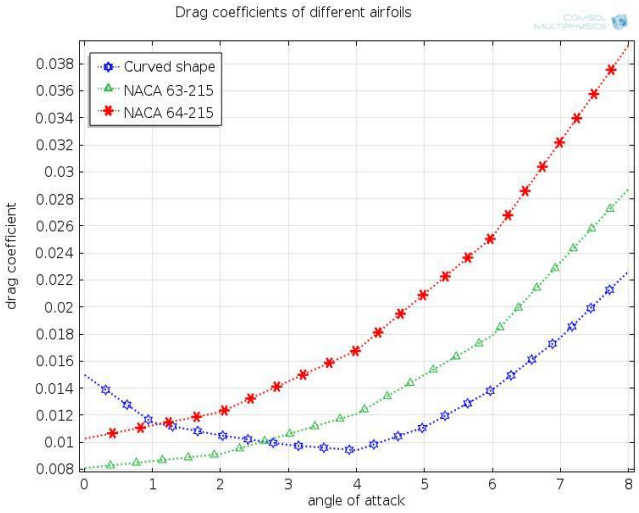

Figure 9. Drag coefficients of Different Airfoils

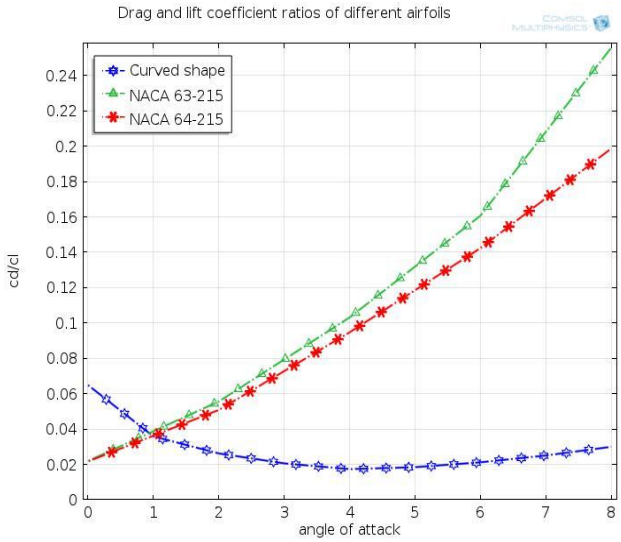

Figure 10. Drag and Lift coefficient ratios of Different Airfoils

The comparison of drag and lift coefficient ratios of different airfoils are illustrated in Figure 10. The slope of NACA 64-215 is linearly inclined with respect to higher angles of attack. NACA 63-215 has nearly the same trend of NACA 64-215 and it has higher drag and lift ratio than that of NACA 64-215. For the curved shape, the slope is gradually declined from 0 to 4° of angle of attack and then slightly inclined between 4° and 8° of angle of attack. By comparing the drag and lift coefficient ratios of three airfoils, the minimum ratio occurs at the curve shape with angle of attack 4°. This result is good agreement with the assumption data in theoretical design calculation. It can be proved that curved shape is the most suitable airfoil for water pumping windmill.

6. CONCLUSION

Wind energy conversion systems are an effective, environmentally friendly power source for household and other applications. With the increasing energy prices and growing energy consumption, many developing countries face the energy problems. In design consideration, the lift and drag coefficients of the blade has been one of the most careful works. For these results, wind tunnel experiments must be required. However, this method is very expensive and facilities are not yet possible for Myanmar to reach this step practically. So CFD software has to be used for this purpose. COMSOL Multiphysics has been selected because it is one of the most powerful tools for CFD problems. In this study, COMSOL Multiphysics 4.3b version has been used. In order to do research and select the most suitable airfoil shape for the rotor of windmill water pumping system, the different airfoils were simulated and the results are compared. The curved shape airfoil has the minimum ratio of drag and lift coefficients at angle of attack 4º. In order to get the maximum lift force, the maximum pressure difference from upper and lower section of blade airfoil must be chosen. As the results of simulations, the curved shape airfoil has maximum lift at the corresponding angle of attack.

7. ACKNOWLEDGMENTS

First of all, the author is grateful to Dr. Theingi, Rector of Technological University (Thanlyin), for giving the permission to submit the paper.
The author would like to thank his supervisor, Dr. Thwe Thwe Htay, Professor and Head of Mechanical Engineering Department, Technological University (Thanlyin), for her close supervisions and words of inspiration that have always been a motivation to me during the paper work.
The author wishes to express his heartfelt thanks to each and every one who assisted in completing this paper.
Finally, the author deep gratitude and appreciation go to his parents for his moral supports, patience, understanding and encouragement.

8. REFERENCES

[1] Lysen E. H, “Introduction to Wind Energy” 2nd Edition, Consultancy Sercices Wind Energy Developing Countries, 1983
[2] Peter Franenkel, “Water-pumping Devices” A handbook for users and choosers, 2nd Edition, Intermediate Technology Publications, 1997.
[3] IRA H. Abbott and Albert E. Van Doenhoff. 1959. “Theory of Wing Sections. Including a Summary of Airfoil Data” Dover Publications, Inc. New York, 1959.
[4] Mr. Vaibhav R. Pannase et al. “ Design and Analysis of Windmill” International Journal of Engineering Science and Technology (IJEST), 2013.
[5] Website:http://www.Windworkers.com.htm,Windpowr@netins.net
[6] Drummond Hislop. “Energy Options. An Introduction to Small-Scale Renewable Energy Technologies” Intermediate Technology Publications, 1992.
[7] Addison, H. The pump users handbook. London, UK, Pitman & Sons, 1958.
[8] Castro, W.E., Zielinski, P.B., Sandifer, P.B., Performance characteristics of wind pumps, World Mariculture Society Meeting, 6: 451-460, 1975.
[9] Ivens, E. M., (1984), Pumping by windmill, John Wiley and Sons, Inc., New York, 1984.
[10] Petel Frankel, Roy Barlow. Farnces Crick, Anthony Derrick and Various Bokalders. “Windpumps. A Guide for Development Workers” Intermediate Technology Publications in Association with the Stockholm Environment Institute, 1993.

International Journal of Science and Engineering Applications
Volume 7–Issue 09,313-317, 2018, ISSN:-2319–7560

Comparative Study on Analysis and Design between Flat Slab and Flat Plate System for RC Building

Phyoe Hnin Thu Htun
Department of Civil Engineering
Technological University
(Thanlyin),
Myanmar

Nyan Phone
Department of Civil Engineering
Technological University
(Thanlyin),
Myanmar

Kyaw Zeyar Win
Department of Civil Engineering
Technological University
(Thanlyin),
Myanmar

Abstract: During recent years, the flat slab and flat plate building construction have become popular in Myanmar. These slab systems have many benefits which enhance speeding up construction, low building height and economical. In this study, the 12½ storeyed RC building with flat slab system and flat plate system have been analysed by ETABS. Flat slab and flat plate are designed by SAFE software. Both structures are situated in seismic zone 2B. The purpose of the research is to compare the structural behaviour of both structure such as base shear, story drift and story displacement. Moreover, another purpose is to present the difference between slab stresses and slab design. Load considerations are based on UBC-97 and structural elements are designed according to ACI 318-08.For these 12½ storeyed RC building, the comparison results show that the flat plate building is more beneficial than flat slab building. As the structural behaviour of flat plate building is better stiffness than flat slab building, flat plate building is safer. Moreover, flat plate building is more economical so steel area of flat plate building is less than flat slab building.

Keywords: Flat Slab System, Flat Plate System, Base Shear, Story Drift, Story Displacement, Slab Stresses, Slab Design

1. INTRODUCTION

There are different kinds of reinforced concrete floor systems. Among many slab systems, flat slab and flat plate system are widely used in construction. A reinforced concrete slab supported directly by columns without the use of beams or girder, such a slab is called flat slab. Provision of thickened portion of slab around column is called drop panel that provides to reduce stresses due to shear and negative bending moment around the columns. It is a rectangular or square region centered on the column. Slabs of constant thickness which do not drop panels or column capitals is called flat plate. The slab directly rests on column and load from the slab is directly transferred to the columns and then to be foundation. The flat slab and flat plate are weak to resist the lateral loads. Since these slabs are carried directly by column, transferring from slab to column through shear increase and the slabs have to be failure due to punching shear. RCC flat slab structure is investigated the behavior of flat slab during the earthquakes and checked for increase of punching from gravity loads to earthquake loads and examined tendency of punching shear failure in flat slabs [1] .Many research studied the structural behavior of flat slab structures under seismic zones by using ETABS software and compared with other slab systems [2-4]. Flat slabs are being used chiefly in office buildings and residential buildings due to reduced formwork cost, fast excavation and easy establishment. The quantity of concrete and steel required and the structural behavior of flat slab are studied and compared with grid slab and conventional slab system [5]. The structural efficiency of the flat slab construction is poor under earthquake loadings because it has low stiffness. The shear walls are placed at suitable locations and it can be used to improve efficiency of flat slab with column structure in earthquake zones. The behavior of flat slab structure with shear wall is better than flat slab structure without shear wall [6]. In the analysis of a flat slab structure which subject to gravity loads, direct design method or equivalent frame method is generally used for the rectangular slabs while commercial software such as SAFE [7]. In this paper, the structural behavior of flat slab system and flat plate system are studied and compared by using ETABS software in linear static analysis. The slabs are designed and the differences of slab stresses are studied by applying SAFE software. The provision of this research is that the flat plate system for residential building is more suitable than the flat slab system depending upon the comparison of story drift, base shear, story displacement, slab stresses and slab reinforcement.

2. TYPE OF STRUCTURE

The 12½ storeyed RC building is considered with two slab system.

1. Flat slab structure with drop panels without parameter beam
2. Flat plate structure without drop panels with parameter beam

Both structures are designed with the same column, slab thickness and shear wall. Since these structures are low stiffness, shear walls are placed at suitable locations. Penthouse is located on the roof, so prop columns and roof beam system are used in this floor for both buildings. Rectangular columns are used depending on shape of structure.

Table 1. Material Specification

Concrete compressive strength (f_c')	4 ksi
Reinforcing yield strength (f_y)	50 ksi
Modulus of Elasticity	3605 ksi
Poisson's ratio	0.2

Table 2. Structural Plan Details

Number of stories	12½
Width of structure	63′-6″
Length of structure	96′
Total height of structure	139′-6″
Typical story height	10′-6″
GF and 1F height	12″
Number of bay's along X	4
Number of bay's along Y	4

Table 3. Structure Element Details

Column sizes	14″x20″,14″x24″,14″x28″,14″x30″ 16″x32″,18″x28″,18″x34″,
Beam sizes	16″x24″ , 14″x20″ , 12″x15″
Slab thickness	8″
Drop thickness	12″
Drop size	6′x8′
Shear wall thickness	12″

3. MODEL DESCRIPTION

The figure (1) shows 3D view of flat slab building and flat plate building. The figure (2) and (3) show the typical floor plan of both building.

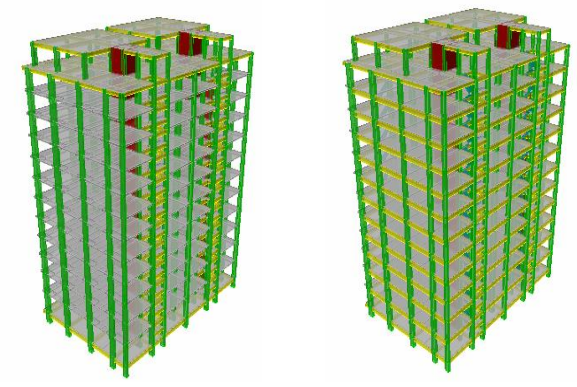

(i) Flat Slab System (ii) Flat Plate System

Figure 1. 3D View of Building

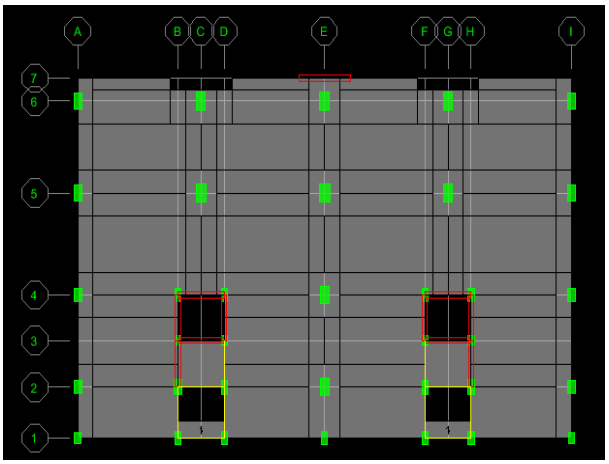

Figure 2. Typical Floor Plan of Flat Slab Building

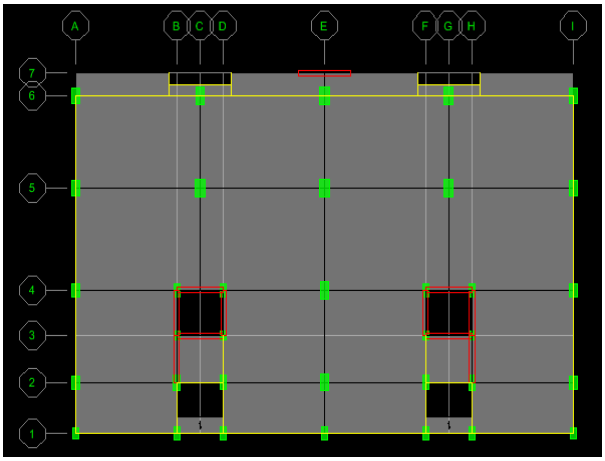

Figure 3. Typical Floor Plan of Flat Plate Building

4. RESULTS AND DISCUSSION

In this section the results obtained from the analysis of flat slab building and flat plate building using ETABS and SAFE software have been tabulated and compared. The performance and behavior of both structure on different criteria like story shear, story displacement, story drift, slab stresses, and slab reinforcement has been analyzed and discussed as follow.

4.1 Story Shear

The figure (4) and (5) show the comparison of story shear in X-direction and Y-direction.

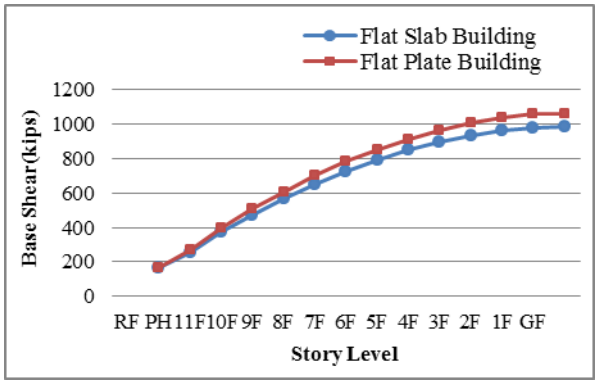

Figure 4. Comparison of Story Shear in X-Direction

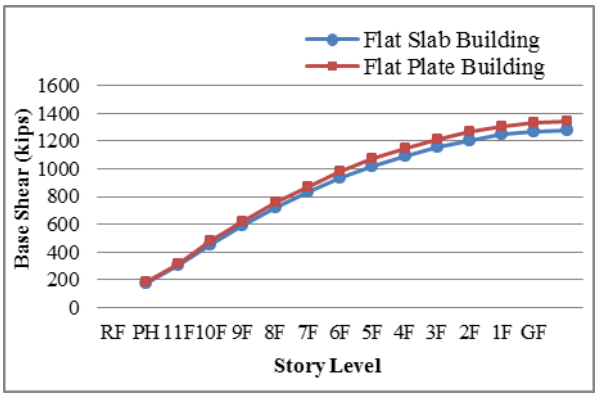

Figure 5. Comparison of Story Shear in Y-Direction

Above the figures show that the comparison of story shear values for flat slab and flat plate building. From the above results, it can be seen that the value of story shear of flat plate building is slightly more than that of flat slab building. Because the value of story shear depends upon the weight of the structure. The weight of flat plate building is more slightly than that of flat slab building. The story shear value is maximum at ground floor level and is gradually decreasing towards to the top story of structure. The difference of story shear in X-direction for both building is slightly more than Y-direction.

4.2 Story Drift

The figure(6) and (7) show the comparison of story displacement in X-direction and Y-direction.

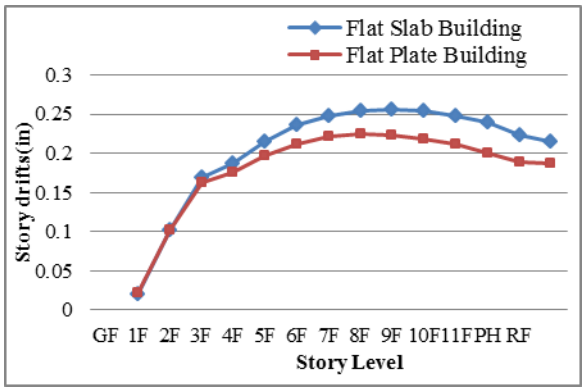

Figure 6. Comparison of Story Drift in X-Direction

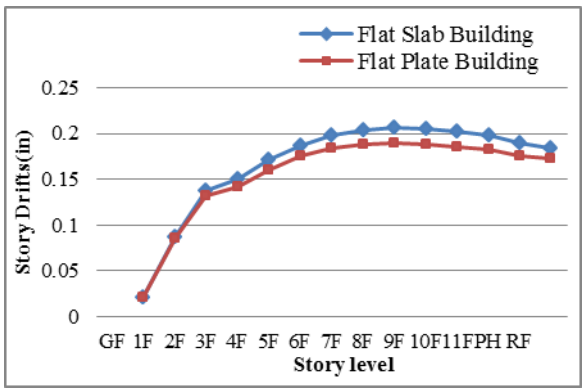

Figure 7. Comparison of Story Drift in Y-Direction

Story drift is the lateral displacement of one level relative to the level above or below. Story drift ratio is the story drift divided by the story height which is described in UBC-97(Chapter-16). Above the results have been tabulated and compared and it can be seen that the story drift of flat slab building is more than that of flat plate building. The story drift is minimum at ground floor level, increase at the middle stories and gradually decrease to the top stories of both structures.

4.3 Story Displacement

The figure(8) and (9) show the comparison of story displacement in X-direction and y- direction.

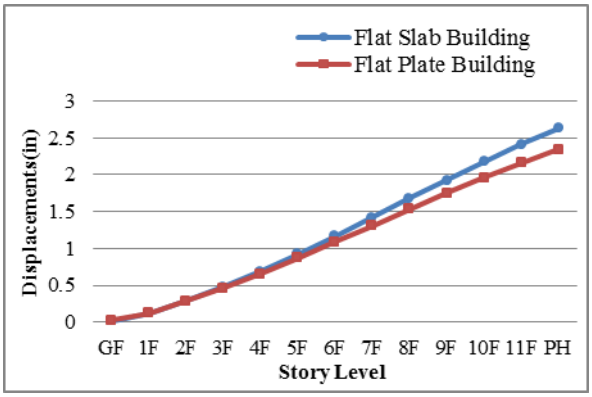

Figure 8. Comparison of Story Displacement in X-Direction

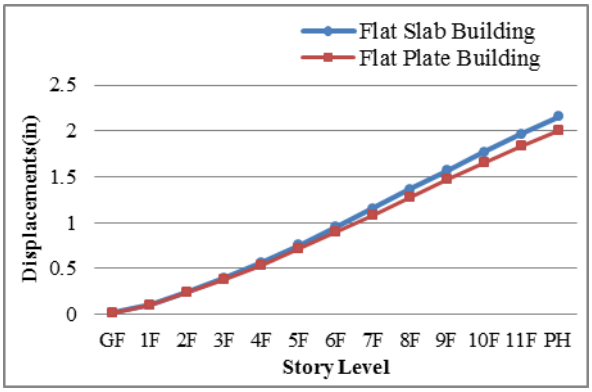

Figure 9. Comparison of Story Displacement in Y-Direction

From above figures, it can be seen that the story displacement of flat slab building is more than that of flat plate building. The displacement is dependent on the structure stiffness. The stiffness of flat plate building is better than that of flat slab building as the flat plate building is designed with perimeter beam and shear wall. Although the flat slab building is designed with drop panel and shear wall to have safe stiffness, it is less stiffness than flat plate building. Provision of drop panel to flat slab, story displacement reduces slightly. The thicker the drop panel, the more increase the stiffness. The story displacement is maximum at top story and minimum at ground floor.

4.4 Slab Deflection

From the figure.10 shows that the deflection of flat plate is a little more than that of flat slab. Slab deflection depends on slab thickness. As both buildings are the same slab thickness, the differences of deflection values are nearly equal. The

deflection is maximum at eleventh floor and all of the rest floors have nearly the same deflection values.

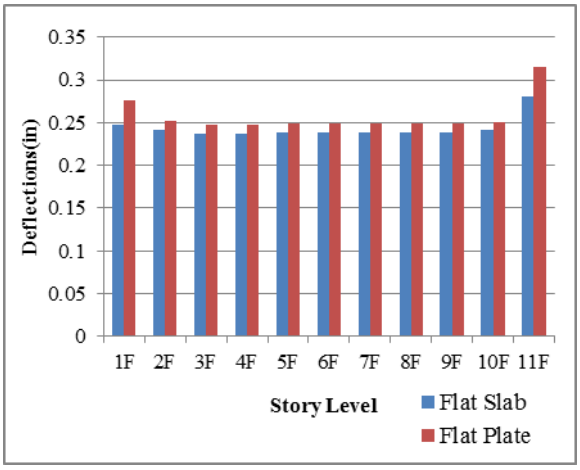

Figure 10. Comparison of Slab Deflection

4.5 Punching Shear Strength

Punching shear can occur around the column in flat plate and flat slab and failure can be occurred by it. The figure(11) shows that the comparison of punching shear strength of interior column in flat plate and flat slab building, it can be seen that the punching shear strength of flat slab is more than that of flat plate because the flat slab includes drop panel that increase shear strength. Punching shear strength depends on drop panel. However, the corner column in flat slab building is weak to resist punching shear as the perimeter of the reaction area is less. In flat plate building, as perimeter beams are provided, the corner columns don't suffer punching shear but it is affected by beam shear. The punching shear strength gradually increases towards the top floors.

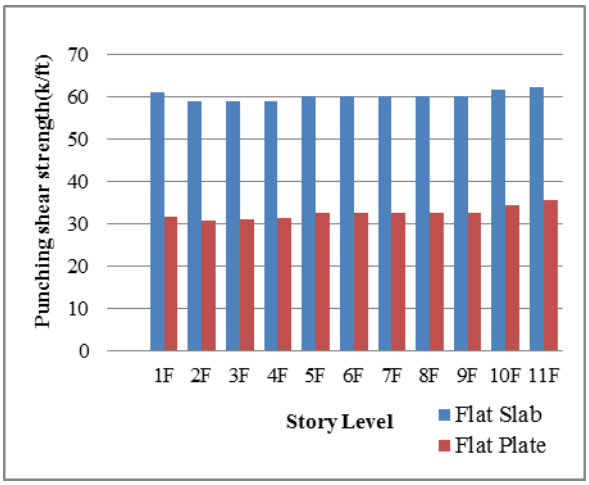

Figure 11. Comparison of Punching Shear Strength

4.6 Moment on Slab

The following figure(12) shows that moment of flat slab is more than that of flat plate. The moment at first floor and eleventh floor is large and all of the rest floors have not significantly difference.

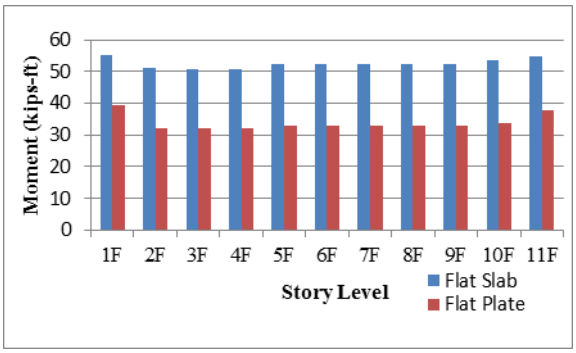

Figure 12. Comparison of Moment on Slab

4.7 Slab Reinforcement

Table 4. Comparison of Slab Reinforcement

Story	Layer		Flat Slab (in^2/ft)	Flat Plate (in^2/ft)
1F	Layer A	Top	0.5366	0.6259
		Bottom	0.269	0.2358
	Layer B	Top	0.7886	0.7736
		Bottom	0.3974	0.3844
2F	Layer A	Top	0.5104	0.5487
		Bottom	0.2586	0.1925
	Layer B	Top	0.766	0.7117
		Bottom	0.3886	0.3533
3F	Layer A	Top	0.5151	0.5469
		Bottom	0.2564	0.1915
	Layer B	Top	0.7869	0.6931
		Bottom	0.3849	0.3473
4F	Layer A	Top	0.5151	0.547
		Bottom	0.2564	0.1916
	Layer B	Top	0.7874	0.6933
		Bottom	0.3849	0.3473
5F	Layer A	Top	0.5252	0.5648
		Bottom	0.2537	0.1927
	Layer B	Top	0.7615	0.7103
		Bottom	0.387	0.3494
6F	Layer A	Top	0.5252	0.5648
		Bottom	0.2537	0.1927
	Layer B	Top	0.7615	0.7103
		Bottom	0.387	0.3494
7F	Layer A	Top	0.5252	0.5648
		Bottom	0.2537	0.1927
	Layer B	Top	0.7615	0.7103
		Bottom	0.387	0.3494
8F	Layer A	Top	0.5252	0.5648
		Bottom	0.2537	0.1927
	Layer B	Top	0.7615	0.7103
		Bottom	0.387	0.3494
9F	Layer A	Top	0.5252	0.5648
		Bottom	0.2537	0.1927
	Layer B	Top	0.7615	0.7103
		Bottom	0.387	0.3494
10F	Layer A	Top	0.5328	0.5831
		Bottom	0.2509	0.1946
	Layer B	Top	0.7671	0.7295
		Bottom	0.3902	0.3514
11F	Layer A	Top	0.5758	0.5473
		Bottom	0.2194	0.1919
	Layer B	Top	0.8187	0.6346
		Bottom	0.3651	0.3387

The slab design is considered ACI Code methods that a typical panel is divided, for purposes of design, into column strip and middle strip. Column strip is a design strip with a width on each side of a column centerline equal to $0.25l_2$ or $0.25l_1$, whichever is less. Middle strip is a design strip bounded by two column strips (ACI 318-08). The table shows that most of the steel area of flat slab is more than that of flat plate. The steel area of every floor in top steel of layer A in flat plate is larger than that of flat slab. The steel areas of almost all typical floors are equal. Variation of steel area depends upon the difference of moment.

5. CONCLUSION

1. Story shear in flat plate structure is more than flat slab structure and the shear value in X-direction is more than Y-direction.
2. Story drift and displacement in flat slab is more than flat plate because of difference use of perimeter beams and drop panels. Both values in Y-direction is less than X-direction as structure stiffness in Y-direction is stronger by providing rectangular column and shear wall.
3. The punching shear failure occurs more in flat plate. The difference of punching strength in interior column is nearly 50% between flat slab and flat plate. But corners column in flat slab, punching shear strength is weak and shear reinforcement and drop thickness will be considered. Provision of shear wall and column size may not effective in reducing punching shear stress.
4. The difference of moment values in flat slab and flat plate is nearly 40% and this may be effective the difference of steel area.

Considering all the above inference on analysis of flat slab and flat plate system, the flat plate system is safer than flat slab system according to comparison of structural behavior. And flat plate system is more economical than flat slab system for this residential RC building by comparing steel area of both slabs.

6. ACKNOWLEDGMENTS

The author wishes to express the deepest thanks and gratitude to her supervisor Dr. Nyan Phone, Professor and Head of Civil Engineering Department of Technological University (Thanlyin). The author special thanks go to her co-supervisor Dr. Kyaw Zeyar Win, Professor of Civil Engineering Department of Technological University (Thanlyin), for his invaluable advice and effective suggestion throughout the study. The author would like to express her thanks to her member Dr. Kyaw Lin Htat, Professor of Civil Engineering Department of Technological University (Thanlyin), for his valuable comments and indispensable guidance during this study. Finally, her special thanks to all who helped her towards the successful completion of this study.

7. REFERENCES

[1] M.Rajagopal Reddy 1. P.Rajesh 2. “Design of RCC Flat Slab Structure Under Earthquake Loading Using Etabs”.

[2] P. Srinivasulu, A. Dattatreya Kumar. (2015) “Behaviour of RCC Flat Slab Structure Under Earthquake Loading”, IJSER, Vol-5, Issue-7, 821-829.

[3] Mohana H.S, Kavan M.R. (2015) “Comparative Study of Flat Slab and Conventional Slab Structure Using ETABS for Different Earthquake Zones of India”. (IRJET), Vol-2, Issue-7.

[4] Sakshwari Guruprasad T N Raghu K S (2016) “Comparative Study on Conventional Beam Slab and Flat Slab under Various Seismic Zones and Soil Conditions”. (IRJET), Vol-3, Page: 1768-1774.

[5] Sudhir Singh Bhaduria, Nitin Chhugani. “Comparative Analysis and Design of Flat and Grid Slab System with Conventional Slab System”. (IRJET), Vol-4, Issue; 08, Aug-2017.

[6] Niharika .M. Keskar, Dr.S.P.Raut. “Comparative Study of Mult-Storey RC Building Having Flat Slab with and without Shear wall with Conventional Frame Structure Subjected to Earthquake”. International Journal of Advances in Scientific Research and Engineering (ijasre), Vol. 03, Issue 3, April-2017.

[7] Gaurav Ravindra Chavan, Dr. S. N. Tande. “Analysis and Design of Flat Slab”. International Journal of Latest Trends in Engineering and Technology (IJTET), Vol-7, Issue 1, May 2016.

[8] Arthur H.Nilson. Design of Concrete Structures”. Twelfth edition.

[9] M.Anitha B.Q.Rahman JJ.Vijay. “Analysis and Design of Flat Slabs Using Various Codes”. International Institude of Information Technology Hyderabad. April 2007.

[10] U Nyi Hla Nge, “Reinforced Concrete Design”.

International Journal of Science and Engineering Applications
Volume 7–Issue 09,318-323, 2018, ISSN:-2319–7560

Wiener Filter based Medical Image De-noising

Dr. Sana'a khudayer Jadwa
Assist. Prof.
Computers Unit
College of Medicine
Baghdad- Iraq

Abstract: Medical images such as , CT (Computed Tomography) scan imaging and MRI (magnetic resonance imaging) are considered as a collection of information that is used for visual diagnostics .Most of the medical images are affected by different types of noises during acquisition, storage and transmission, so the information associated with an image tends to loss or damage that can affect the quality of disease diagnosis or treatment. Image de-noising is the process to remove the noise from the image naturally corrupted by the noise. In this paper an effective noise reduction approach based on using Wiener filter is proposed to enhance the image qualities of various medical imaging modalities.

Keywords: Wiener filter; Image de-noising; Image processing; Medical Imaging; Noise.

1. INTRODUCTION

In medical science, the image processing techniques is playing an important role; these techniques are the reliable diagnosis tools in medical sciences. It is used for detecting cracks in bones and soft tissues like liver, kidney, spleen, uterus, heart, brain etc. These methods of diagnosis are widely acceptable because they are inexpensive, harmless to human body, portable and non–invasive. Another advantage of these techniques is that these are very fast [1].The advent of digital imaging technologies such as MRI has revolutionized modern medicine. Today, many patients no longer need to go through invasive and often dangerous procedures to diagnose a wide variety of illnesses. With the wide spread use of digital imaging in medicine today, the quality of digital medical images becomes an important issue. To achieve the best possible diagnoses it is important that medical images be sharp, clear, and free of noise and artifacts. While the technologies for acquiring digital medical images continue to improve, resulting in images of higher and higher resolution and quality, noise remains an issue for many medical images. Removing noise in these digital images remains one of the major challenges in the study of medical imaging[2]. Noise is introduced in the medical images due to various reasons. In medical imaging, noise degrades the quality of images. This degradation includes suppression of edges, blurring boundaries etc. [3]. Image de-noising has become an essential exercise in medical imaging especially the Magnetic Resonance Imaging (MRI). In recent years, technological development has significantly improved in analyzing medical images. Medical image enhancement has attracted much attention during the diagnosis process. Enhanced medical images are desired by a surgeon to help diagnosis and interpretation because medical image qualities are often deteriorated by artifacts. Nowadays Medical imaging is the best techniques for monitoring the person's diagnosis process. Most of the diseases are diagnosed by doctors using medical imaging methods. One problem that physician encounter because of the low quality of medical image, this low quality causes difficulty during the diagnosis. So it is necessary to improve the quality of the medical image [4]. In order to improve the quality of images, there are various filtering techniques used in image processing. There are various filters which can remove the noise from images and preserve image details [5]. This paper produce Wiener filter for medical images de-noising. The organization of the rest of this paper is as follows. Section 2 highlights the related works. Section 3 introduces image de-noising. Section 4 describes the Wiener Filter. The proposed method introduced in section 5. Section 6 presents the experimental results and section 7 concludes the paper.

2. RELATED WORKS

The image de-noising naturally corrupted by noise is a classical problem in the field of signal or image processing.[6] proposed de-noising method of medical images through thresholding and optimization using a randomized and stochastic technique of Particle Swarm Optimization(PSO) algorithm. PSO are population based optimization algorithm ,which is initialized with a group of random particles and then searches for optima by updating generations.[7] In this paper, an algorithm for image de-noising was designed to develop K-SVD by using Regularized Orthogonal Matching Pursuit (ROMP) over log Gabor wavelet adaptive dictionary.[8] In this paper Discrete Wavelet transform is used for image de-noising as it allows multiresolution decomposition. The wavelet coefficients are threshold using hard and soft thresholding techniques. This paper proposed a novel method of medical images de-noising through thresholding and optimization using Genetic Algorithm (GA). [9] In this paper, a novel global noise reduction approach based on the sparse representation and nonlocal means algorithm is proposed to enhance the image qualities of various medical

imaging modalities including ultrasound images and magnetic resonance images. By using an over complete dictionary, a medical image is decomposed into a sparsest coefficients matrix populated primarily with zeros. A nonlocal means algorithm is developed to deal with these sparse coefficients to exploit the repetitive characters of structures in the whole image, realizing a "truly" global de-noising.[10] A new signal-preserving technique for noise suppression in event-related magnetic resonance imaging (MRI) data is proposed based on spectral subtraction. Simple form, the new method does not change the statistical characteristics of the signal or cause correlated noise this suggests the new technique as a useful preprocessing step for MRI data analysis. .

3. IMAGE DE-NOISING

Image de-noising is an important image processing task both as a process itself, and as a component in other processes. many ways to de-noise an image or a set of data exists. Image de-noising still remains a challenge for researchers because noise removal introduces artifacts and causes blurring of the images [6].Image de-noising is a kind of processing of image which belongs to image restoration, and the ultimate goal of restoration techniques is to improve an image in some predefined sense. So de-noising is the key step of image processing and recognition [11].An image is often corrupted by noise in its acquition and transmission. Image de-noising is used to remove the additive noise while retaining as much as possible the important signal features. [12].There is many schemes for removing noise from images. The good de-noising scheme must able to retrieve as much of image details even though the image is highly affected by noise[13].In case of image denoising methods, the characteristics of the degrading system and the noises are assumed to be known beforehand. The image $s(x,y)$ is blurred by a linear operation and noise $n(x,y)$ is added to form the degraded image$w(x,y)$. This is convolved with the restoration procedure $g(x,y)$ to produce the restored image $z(x,y)$. The "Linear operation" shown in Figure 1, is the addition or multiplication of the noise $n(x,y)$ to the signal$s(x,y)$. Once the corrupted image $w(x,y)$ is obtained, it is subjected to the de-noising technique to get the de-noised image $z(x,y)$ [14].

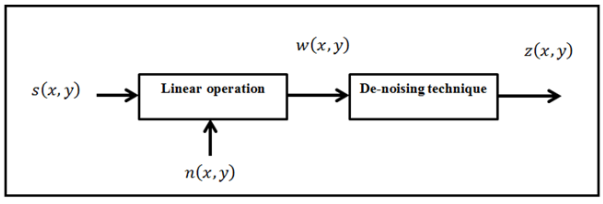

Figure 1. De-noising Concept.

3.1 Noise

Noise is basically a disturbance that distorts the information present in the image. It is usually an unwanted signal that can create a variation in image intensity levels of pixels which cause degradation of image quality .The noise is introduced in image automatically due to following reasons:

Digital Image Acquisition Process: In acquisition process, the optical image is converted into a series of electronic signals. During this process, unwanted signals may be added into original series of electronic signals there may be certain other unavoidable situations such as mechanical problem, out of focus blur, motion, in appropriate illumination.

Image Transmission Process: The most of time noise is added during transmission process such as scanning of image using scanner, converting one image format into another format, wireless network transmission of image etc. During transmission process, noisy channel and error due to measurement process may introduce unwanted signals into data stream which results in noised image.

Sensitivity of Image Sensors: The image sensors are sensitive to motion and cause noising during capturing process due to malfunctioning of pixel elements in the camera sensors, faulty memory locations, or timing errors in the digitization process [15]. .

3.2 Types of Noise

There are many types of noises occurs in medical images. Mostly occurred noise is: Gaussian noise, Speckle noise, Salt and pepper noise.

3.2.1 Gaussian Noise

Gaussian noise has a Gaussian distribution, with a bell shaped distribution and probability function given by:

$$f(g) = \frac{1}{\sqrt{2\pi\sigma^2}} e^{-(g-m)^2/2\sigma^2} \qquad (1)$$

where g represents the gray level, m is the mean or average of the function, and σ is the standard deviation of the noise[16].

3.2.2 Salt and Pepper Noise

Salt and pepper noise is an impulse type of noise, and caused due to errors in data transmission. It has only two possible values, low and high.. The corrupted pixels are set alternatively to the minimum or to the maximum value, giving the image a "salt and pepper" like appearance. Unaffected pixels remain unchanged. For an 8-bit image, the typical value for pepper noise is 0 and for salt noise is 255[16].

3.2.3 Speckle Noise

For Speckle noise is a repetitive type of noise and occurs in imaging systems such as laser and SAR (Synthetic Aperture Radar) . The source of this noise is attributed to random interference between the coherent returns. The

Mathematical expression for this noise is given by:

$$f(g) = \frac{g^{\alpha-1}}{(\alpha-1)!\,a^{\alpha}} e^{-\frac{g}{a}} \qquad (2)$$

Where a^{α} is variance and g is the gray level .

4. WIENER FILTER

Wiener filter is proposed by Norbert Wiener in 1940 and published in 1949. It is used to reduce noise in signal. When the image is blurred by a known low pass filter, it is possible to recover the image by inverse filtering. But inverse filtering is very sensitive to additive noise. The Wiener filtering executes an optimal trade-off between inverse filtering and noise smoothing. It removes the additive noise and inverts the blurring simultaneously. The Wiener filter minimizes the mean square error between the estimated process and the desired process. It minimizes the overall mean square error in the process of inverse filtering and noise smoothing. The Wiener filtering is a linear estimation of the original image [17].The important use of Wiener filter is to reduce the amount of noise present in an image by comparison with an estimation of the desired noiseless signal. It is based on a statistical approach. Wiener filters are characterized by three important factors.
1-**Assumption: stationary** linear stochastic processes of image and noise with known spectral characteristics or known autocorrelation and cross correlation.
2-**Requirement:** the filter must be physically realizable/ causal.
3-**Performance criterion** minimum mean-square error (MMSE). This filter is frequently used in the process of deconvolution[18].

The Wiener filter is commonly utilized because of its simplicity and its speed. It is deemed simple because it uses a system of linear equations to calculate a set of optimal filter weights that reduce the noise level of a received signal. It estimates cross-correlation and covariance matrices of noisy signals to calculate these weights and provide an accurate Estimate of the undistorted deterministic signal under Gaussian noise. The noise statistics are estimated and then used to determine a set of optimal filter weights. By then processing a new input signal, containing similar noise characteristics with the optimal filter weights, the signal deterministic component is estimated. This method is optimal when the noise distribution is Gaussian. Furthermore, its execution only requires a few computational steps that are very fast to process[19].

Wiener Filter in the Fourier Domain:

$$G(u,v) = \frac{H^*(u,v)P_s(u,v)}{|H(u,v)|^2 P_s(u,v) + P_n(u,v)} \qquad (3)$$

Dividing through by P_s makes its behavior easier to explain :

$$G(u,v) = \frac{H^*(u,v)}{|H(u,v)|^2 + \frac{P_n(u,v)}{P_s(u,v)}} \qquad (4)$$

Where :

$H(u,v)$ = Degradation function

$H^*(u,v) =$ Complex conjugate of degradation function

$P_n(u,v)$ = Power Spectral Density of Noise

$P_s(u,v)$ = Power Spectral Density of un-degraded image

The term $\frac{P_n}{P_s}$ can be interpreted as the reciprocal of the signal –to-noise ratio [20].

The Wiener filter is used to remove the noise from a corrupted found to image based on statistics estimated from a local neighborhood of each pixel . This filter depends on noise power (i.e. noise variance in a corrupted image). When the variance is large, the filter performs little smoothing and when the variance is small, the filter performs more smoothing[21].

5. PROPOSED METHOD

In this paper a de-noising approach for medical images based on applying a Wiener filter is proposed. At first the color image is read from a database that contain a collection of medical images, then these images are converted to grayscale images, later the Wiener filter is applied in order to remove the noise from the medical image. The Wiener filter de-noising process diagram is illustrated in Figure 2, as shown below:

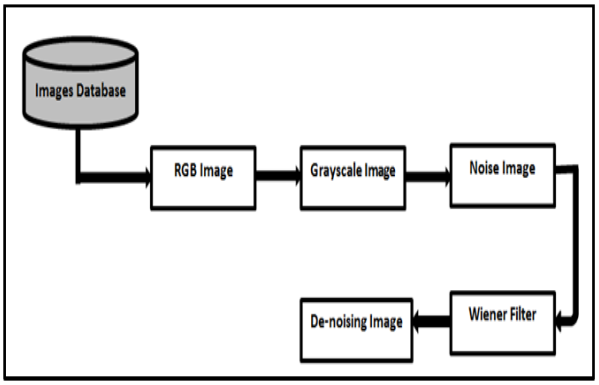

Figure 2 :Process of image De-noising based on Wiener filter

5.1 Images Database

A database for the proposed method containing six medical images (lung, Stomach, and liver) images, are collect from the web with different sizes . As shown in Figure 3:

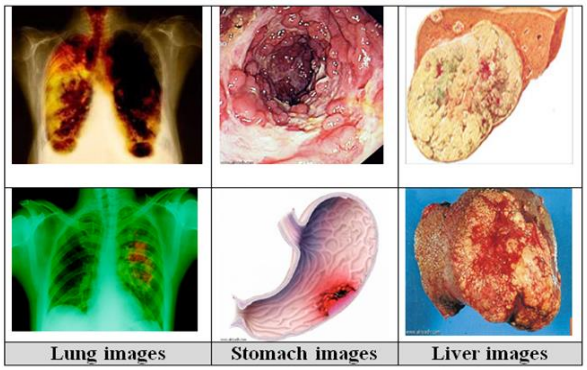

Figure 3 : Images Database

5.2 RGB Image Conversion

The input image is coloured medical image that is converted to grayscale image by converts RGB values to grayscale values by forming a weighted sum of the R, G, and B components using Eq.(5):

$$y = 0.2989R + 0.5870G + 0.1140B \quad (5)$$

5.3 Noise Image

The noisy image is produced by adding the Gaussian noise to the grayscale image, Gaussian noise is statistical noise having a probability density function (PDF) equal to that of the normal distribution, which is also known as the Gaussian distribution. In other words, the values that the noise can take on are Gaussian-distributed.

5.4 Wiener Filter

By using the wiener2 function to remove the noise from noisy image . The Wiener filter tailors itself to the local image variance. Where the variance is large, wiener2 performs little smoothing. Where the variance is small, wiener2 performs more smoothing.

6. EXPERIMENTAL RESULTS

The experiments of the proposed Wiener filter method is realized by Matlab software and are implemented on Intel Core i7-2330M CPU, 2.20 GHz with 2 GB RAM under Windows 8 platform. The coloured medical image first is reading from the database then the RGB image is converted to grayscale as shown in Figure 4:

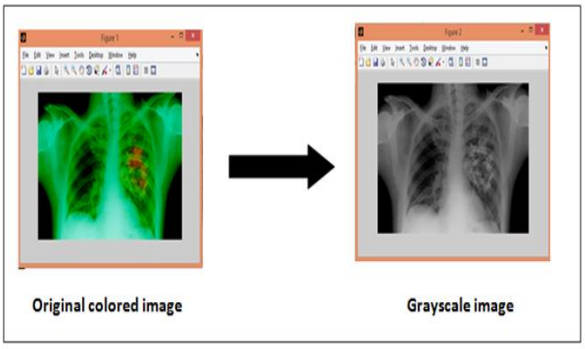

Figure 4: Colored Image Conversion.

Then, adding Gaussian noise with “0” as mean and “0.025” as standard variance to grayscale image, which is shown in Figure 5:

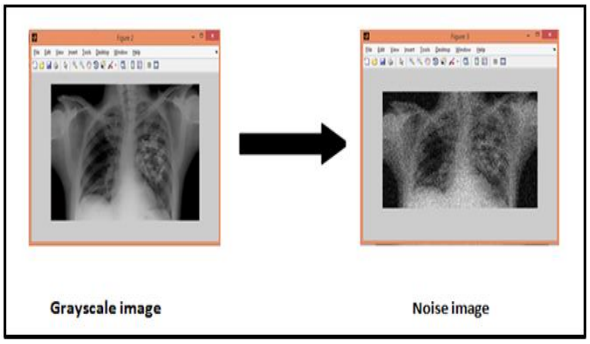

Figure 5: Noisy Image (σ =0.025)

Finally the de-noising image is produced by using the wiener2 function ,as shown in Figure 6:

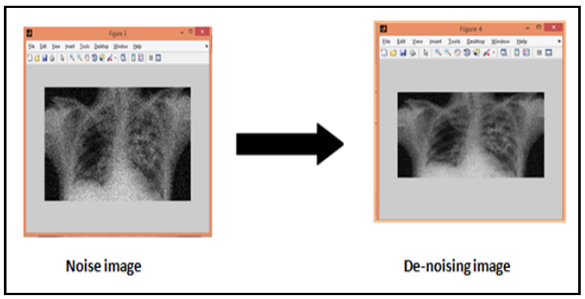

Figure 6: The De-noising Image

After processing, the de-noised experimental results of noised image can be obtained by simulation, which are shown in Figure 7, respectively:

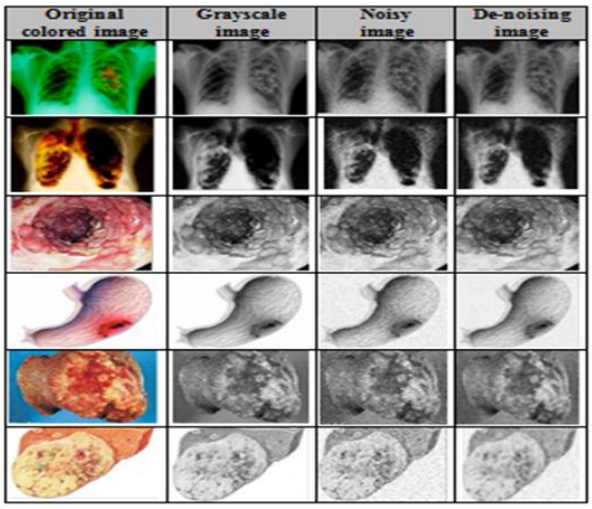

Figure 7: Results for the De-noising of Medical Images

7. CONCLUSION

Medical images are often affected by noise because of both image acquisition from the medical modalities and image transmission from modalities to workspace in the main computer system. This noisy usually affects the visual quality of the original images so image de-noising always has been issued in the medical image processing to make the diagnosing more efficient. In this work we have introduced a relatively simple and efficient method for removal of Gaussian noises from Medical Images using the Wiener filter. Wiener filter is an excellent filter when it comes to noise reduction or de-blurring of images. It considers both the degradation function and noise as part of analysis of an image. The experimental results reveals Wiener filter robustness and detail preservation. The Wiener filter is commonly utilized because of its simplicity and its speed. It is deemed simple because it uses a system of linear equations to calculate a set of optimal filter weights that reduce the noise level of a received signal. The resulting figure show the efficiency, simplicity and robustness of medical image de-noising. Wiener filtering has the advantages of small calculation and good noise effect, so it has been used widely. Many efficient de-noising algorithms are based on the principle of Wiener filtering, whose purpose is to restore the original image and reach the minimum mean error with the original image.

8. REFERENCES

[1] Jagdeep Kaur†* and Ruchika Manchanda, (Feb 2015)," Optimizing Wavelet based Medical Image De-Noising", International Journal of Current Engineering and Technology, Vol.5, No.1.

[2]Prakash B. L. , Vudimudi R. B.,2014," Performing Various Image Denoising Techniques for Medical Images" ,International Journal of Advance Research in Computer Science and Management Studies, Volume 2, Issue 1.

[3] Senthilraja S., Dr. Suresh P., Dr. Suganthi M., March-2014, " Noise Reduction in Computed Tomography Image Using WB – Filter", International Journal of Scientific & Engineering Research, Volume 5, Issue 3.

[4] Deepa B. and Sumithra M. G., 2015," MRI Medical Image Denoising by Combined Spectral Subtraction and Wavelet based Methods", ARPN Journal of Engineering and Applied Sciences, VOL. 10, NO. 4.

[5] Malothu Nagu, Shanker N.V.,2014 " Image De-Noising By Using Median Filter and Weiner Filter", International Journal of Innovative Research in Computer and Communication Engineering, Vol. 2, Issue 9.

[6] Ms. Dansena1P., Mr. Dewangan O., 2015, " Adaptive Thresholding for Wavelet Denoising on Medical Images through PSO Algorithm", International Journal of Advanced Research in Computer Engineering & Technology (IJARCET) Volume 4 Issue 5.

[7] Farouk R.M., Elsayed M. and Aly M., 2016," Medical Image De-noising based on Log-Gabor Wavelet Dictionary and K-SVD Algorithm", International Journal of Computer Applications (0975 – 8887 Volume 141 – No.1.

[8] Singh S., Wadhwani S. , 2015," Genetic Algorithm Based Medical Image Denoising Through Sub Band Adaptive thresholding", International Journal of Science, Engineering and Technology Research (IJSETR), Volume 4, Issue 5.

[9] Guo Yi, Hanchao C. , Yuanyuan W.,2014," A Global Approach for Medical Image Denoising via Sparse Representation", International Journal of Bioscience, Biochemistry and Bioinformatics.

[10] Priyadharsini.B, Vanitas, 2014,"Denoising MRI Images Using A Non-Linear Digital Filter", International Journal of Advanced Research in Electronics and Communication Engineering (IJARECE)Volume 3, Issue 4.

[11] Mr. Kethwas A., Dr. Jharia B. , 2014,"Comparison Study on Image Denoising Through Wiener Filter", International Journal of Engineering Research & Technology (IJERT)Vol. 3, Issue 8 .

[12] Mondal T., Dr. Maitra M. , 2014," Denoising and Compression of Medical Image in Wavelet 2D", International Journal on Recent and Innovation Trends in Computing and Communication Volume 2, Issue 2.

[13] Govindaraj V., Sengottaiyan G.,2013," Survey of Image Denoising using Different Filters", International Journal of Science, Engineering and Technology Research (IJSETR)Volume 2, Issue 2.

[14] Chandrika S., Prof. Deepak K. ,2014, " Noises and Image Denoising Techniques: A Brief Survey", International Journal of Emerging Technology and Advanced Engineering Volume 4, Issue 3.

[15] Pathak M. , 2014, " COMPARATIVE ANALYSIS OF IMAGE DENOISING TECHNIQUES", Monika Pathak et al. ,International Journal of Computer Science & Engineering Technology (IJCSET), Vol. 5 No. 02.

[16] Tamilselvan K.S. , Murugesan G., and Vinothsaravanan M, 2013, " A Histogram based Hybrid Approach for Medical Image Denoising using Wavelet and Curvelet Transforms", International Journal of Computer Applications (0975 – 8887) Volume 74– No. 21.

[17] Jaspreet k., Rajneet k. , 2013," Biomedical Images denoising using Symlet Wavelet with Wiener filter ", International Journal of Engineering Research and Applications,Vol.3,Issue 3.

[18] Umapathi V.J., Narayanan V.,2014," MEDICAL IMAGE DENOISING BASED ON GAUSSIAN FILTER AND DWT SWT BASED ENHANCEMENT TECHNIQUE", International Journal of Soft Computing and Artificial Intelligence,Volume-2, Issue-2.

[19] Anilet B., Chiranjeeb H. and Punith C.,2014," Image Denoising Method Using curvelet Transform and Wiener Filter", International Journal of Advanced Research in Electrical Electronics and Instrumentation Engineering ,Vol. 3, Issue 1.

[20]Suresh K., Papendra K., Manoj G., and Ashok K. N.,2010, " Performance Comparison of Median and Wiener Filter in Image De-noising", International Journal of Computer Applications, Volume 12– No.4.

[21] Sarungbam B. and Yambem J.,2015, "Denoising of Image by Wiener Filtering in Wavelet Domain", Advanced Research in Electrical and Electronic Engineering, Volume 2, Issue 11.

International Journal of Science and Engineering Applications
Volume 7–Issue 09,324-330, 2018, ISSN:-2319–7560

Modelling and Optimization of Corrosion Penetration Rate (Transportation Processes by Pipeline

Rania Ahmad Elrifai
Benghazi University, Industrial and Manufacturing System Engineering
Benghazi, Libya

Abstract: In the study presented the CO_2 corrosion penetration rate for crude oil transportation processes by pipeline, made of carbon steel, has be years. Many parameters have been known to be effective for corrosion control especially in the pipeline transportation process, these parameters are pH are used to determine the optimal parameters with obtaining the optimal value of CO_2 corrosion penetration rate. This study is aimed to review of some of pipeline corrosion penetration rate that are taking place when transporting the oil and gas, to investigate the effect of the oil and gas transportation pro rate, to develop a suitable mathematical modeling technique to model the effect of crude oil transportation processes variables and to determine the opt The response surface methodology (RSM) is utilized to mathematically model the corrosion penetration rate that takes place during crude oil transpor such as fuzzy logic (FL) was developed using Matlab (2016) Toolbox that is used to predict corrosion penetration rate that is affected by the operation the errors by 0.1482mm/y, which means, using fuzzy logic model to predict the material corrosion penetration rate is sufficiently accurate. The optim fuzzy logic model with the formula by using Root- Sum Square (RSS), were found that CPR value is2.16 mm/y, the temperature is 44.4 ^{o}C, pressure i

Keywords: CO_2 corrosion penetration rate (CPR), Norsok -506 software, Response Surface Methodology, ANOVA, Fuzzy logic mode

1. INTRODUCTION

Corrosion of carbon steel is a significant problem in the oil and gas production and also their transportation process, which causes significant economic loss [1]. As a result of corrosion, rupture of the pipe wall frequently causes failure of petroleum and gas pipelines. The breakdowns are followed by large losses of the products, environmental pollution and ecological disasters [2]. The majority of oil and gas pipelines failures result from CO_2 corrosion of carbon and low alloy steels [3]. It occurs at all stages of production from downhole to surface *equipment and processing* facilities [4]. The mechanism of carbon dioxide corrosion is a complicated process that is influenced by many factors and conditions temperature, pH, a partial pressure of CO_2, etc.)[5].

Oilfield corrosion manifests itself in se corrosion) and hydrogen sulfide (H_2S) and corrosion by dissolved carbon dio forms of attack found in oil and gas p selected as case study as to predict an will be review several steps for obta corrosion penetration rate (mm/y) ,throu temperature(^{o}C), CO_2 total pressure (ba is implemented to relate the corrosion transportation processes of the main lin measurements were used as true value novel analysis methods. The predictio

Response Surface Method (RSM) and fuzzy Logic(FL) method, for the prediction and analysis of the effect of some selected parameters, namely, temperature, pH, pressure, shear stress by the ANOVA. The defuzzification process in FL will select with two methods, the centroid and Root- Sum Square method. Root- Sum Square method will result in the corrosion penetration rate with explain the reason of selection this method. The developed fuzzy logic model will also test by comparing the results with the result using RSM technique. The comparison was carried out based on the mean absolute error between the predicted values and the actual values, Based on comparison between models that were developed by using fuzzy logic and RSM technique, it was concluded that, models based on fuzzy logic were better Mean Absolute Error (MAE) of 0.0412with in comparison 0.168for RSM.

2. MATERIALS AND METHODS

2.1. Material

The Work Material of Pipeline used in the present study is Grade API X52 refer as the following, API refers to American Petroleum Institute, the X symbol followed by a two or three digit number equal to the specified minimum yield strength in 1000 psi rounded down to the nearest integer, 52 refers to Minimum Yield at pipe body 360 MPa(52,200 psi). Basic pipeline data represent the following are pipeline length is 513 km, pipe diameter is(outside diameter) 34in (864mm) and wall thickness is 9.52 mm, pipe type is seam welded/ spiral welded. The mechanical properties specified minimum yield strength is 358 MPa, specified ultimate tensile strength is 455 MPa and coating by field applied tape wrap. Chemical properties of X52 pipeline with a composition of 0.16%C, 0.20% Cu and 0.45%Si, 1.10 – 1.60% Mn as shown in Table1.

Table1:Chemical composition of X52 with thickness (t) ≤ 25 mm

C	0.16	**Cu**	0.20	**Cr+ Mo+ Ni+ Cu**	0.5
Si	0.45	**N**	0.014	**Nb+V**	0.1
Mn	1.10 – 1.60	**Nb**	0.04	**Nb+ V+ Ti**	0.12
P	0.025	**Ti**	0.02	**CEV (IIW)**	0.34[2]
S	0.005	**V**	0.05	**PCM**	0.23[2]

Cr	0.20	**A**
Mo	0.08	Sl
Ni	0.20	Sn
Al	0.020– 0.060	Pb

CEV= C+ Mn /6 +(Cr+ Mo+ Cu)/15
PCM= C+ Si /30 + (Mn +Cu +Cr)/20 +Ni/60 + M

In this study, an attempt is made to corrosion penetration rate (CPR) of the It is important to note that selection important consideration.

Table 2: Factors an

No	*Factors*	*Un*
1	***pH***	**pH**
2	***Temperature***	**° C**
3	***Total pressure***	**ba**
4	***Shear stress***	**Pa**

2.2. Method

For the four variables the design requir points to form central composite desi estimate the experimental error. The MINITAB16 statistical package. The le coded form to have a central composite

Table 3: Matrix of order and d

Exp.	Temperature (°C)	Pressure (bar)	pH	Shear stress

1.	0	0	0	0.05	48.59	23.8	5.58	16.2	2.30
2.	0	0	0	0	48.59	23.8	5.58	15.5	2.30
3.	-1	1	-1	-1	44.40	34.2	5.51	1.00	3.07
4.	1	-1	1	-1	52.78	13.4	5.65	1.00	1.63
5.	0	0	0.05	0	48.59	23.8	5.58	15.5	2.29
6.	0	0	-0.05	0	48.59	23.8	5.57	15.5	2.31
7.	-1	-1	1	1	44.40	13.4	5.65	30.0	2.08
8.	-1	1	-1	1	44.40	34.2	5.51	30.0	3.12
9.	0	0.05	0	0	48.59	24.32	5.58	15.5	2.33
10.	-0.05	0	0	0	48.38	23.8	5.58	15.5	2.30
11.	0.05	0	0	0	48.79	23.8	5.58	15.5	2.30
12.	1	-1	-1	-1	52.78	13.4	5.51	1.00	1.86
13.	0	0	0	-0.05	48.59	23.8	5.58	14.8	2.30
14.	1	1	1	1	52.78	34.2	5.65	30.0	2.20
15.	-1	1	1	-1	44.40	34.2	5.65	1.00	2.72
16.	-1	-1	-1	1	44.40	13.4	5.51	30.0	2.30
17.	0	0	0	0	48.59	23.8	5.58	15.5	2.30
18.	1	-1	-1	1	52.78	13.4	5.51	30.0	1.81
19.	-1	-1	1	-1	44.40	13.4	5.65	1.00	1.38
20.	1	-1	1	1	52.78	13.4	5.65	30.0	1.58
21.	0	0	0	0	48.59	23.8	5.58	15.5	2.30
22.	1	1	-1	1	52.78	34.2	5.51	30.0	2.55
23.	0	0	0	0	48.59	23.8	5.58	15.5	2.30
24.	0	-0.05	0	0	48.59	23.28	5.58	15.5	2.27
25.	1	1	1	-1	52.78	34.2	5.65	1.00	2.90
26.	-1	1	1						
27.	0	0	0						
28.	1	1	-1						
29.	0	0	0						
30.	0	0	0						
31.	-1	-1	-1						

3. DEVELOPMENT OF THE

Fuzzy Logic (FL) is based on Fuzzy Set The industrial control application, the informati system is divided in two kinds: numerical i skilled human beings. These systems are closer to the original goal. Simulations a performance for the specific problem[12]. they both have a common characteristic; eac can be controlled successfully by a human transferring his or her experience onto a numerical data is not enough to predict fut fuzzy-logic finds applications in unclear a trends, fuzzy-logic-based multi-criteria deci doing optimization of different manufactu system's designer with more flexibility in t that the Mamdani FIS can be used directly f as well as for MIMO systems (multiple inpu used in MISO systems [8-9-10-11]. Fuzz found a number of applications in such c diagnosis, assessment of credit worthiness, fuzzy control system is based on Fuzzy Lo shown in Figure 1.

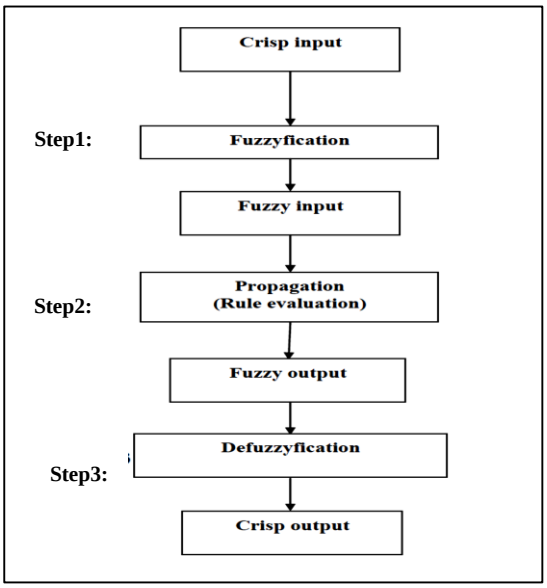

Figure 1: Steps of fuzzy control system

The structure of the four inputs and one outputs fuzzy logic controller developed for this study is shown in Figure 2.

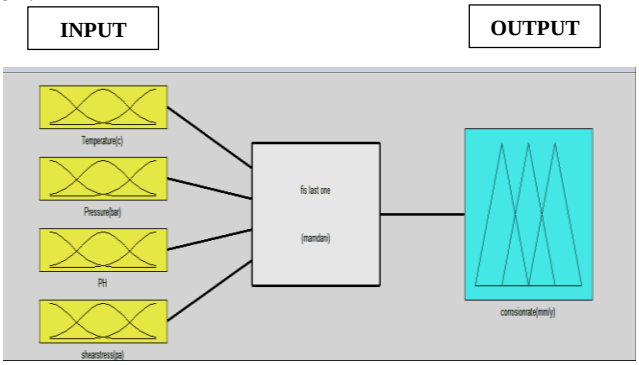

Figure 2: The four inputs-one output in "FIS Editor"

Four inputs and one output (CPR) fuzzy-logic system is used. The inference engine (Mamdani fuzzy inference system) performs fuzzy reasoning with fuzzy rules for generating a fuzzy value. These fuzzy rules are shown in the form of 'if–then' control rule. Temperature , pH, pressure, shear stress are inputs to the fuzzy logic system. The linguistic membership function for instance

Low, Medium, High and are used to repre
represented by the membership functions su
triangular and Gaussian shaped membe
fuzzification of the four inputs e.g. Tempe
membership function graph is shown to def
are mapped to a value between 0 and 1.
Medium And High are used to represent o
by the membership functions such as Very
shaped membership function used in this w
with 31 rules as shown in Table 4.

Table 4: Fuzzy rule for corrosion pe

Rule1. If (Temperature(° C) is Med) and
Stress(Pa) is Med) then (corrosion penetrati

Rule 2. If (Temperature(° C) is Med) and
Stress(Pa) is Med) then (corrosion penetrati

Rule 3. If (Temperature(° C) is Low) and
Stress(Pa) is Low) then (corrosion penetrati

Rule 29. If (Temperature(° C) is Med) and
Stress(Pa) is Med) then (corrosion penetrati

Rule 30. If (Temperature(° C) is Med) and
Stress(Pa) is Med) then (corrosion penetrati

Rule 31. If (Temperature(° C) is Low) and
Stress(Pa) is Low) then (corrosion penetrati

The fuzzy inputs are linguistically divided i
is shown in Figure 3.

Figure 4 shows the fuzzy output linguistica
and very high .

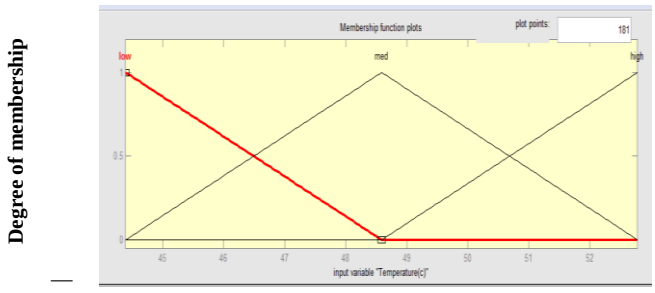

(a)Temperature(°C).

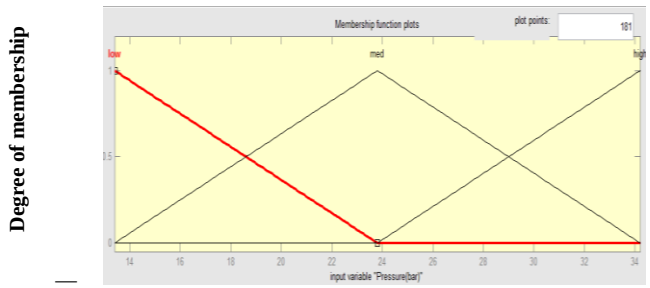

(b) pressure(bar) .

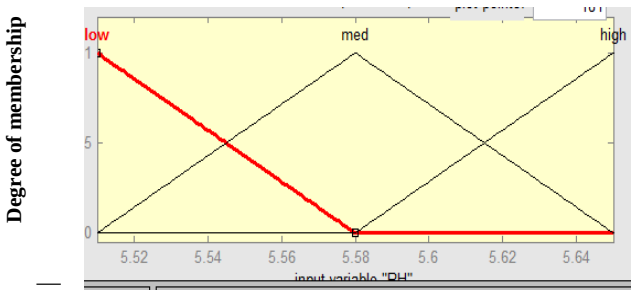

(c) pH

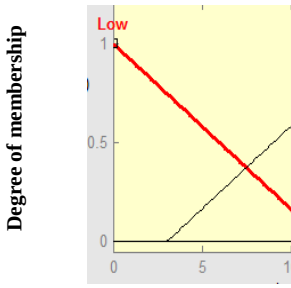

(d) Sl

Figure 3: Membershi

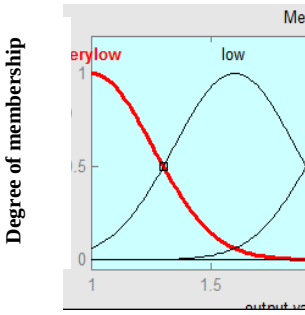

Figure 4: Membership functions

4. SIMULATION OF LOGIC

In this study, the fuzzy model has been
penetration rate of process parameters.
which has been done within the range o
for the three levels of each parameter.
the error of outputs for test case exp
developed to predict CPR. Moreover,
the predicted values of the corrosion ra
were compared with the predicted valu
comparison are shown in Table 4.8 with

the predicted of corrosion penetration rate by using the proposed fuzzy logic model is lower than the predicted of corrosion penetration rate by using RSM, the difference was observed to be 0.1269mm/y. The results from fuzzy logic simulation indicated that the predicted values and experimental values closely agreed. In some cases, the predicted values and experimental values are observed to be little deviated. That might be due to some experimental error.

Table 5 : The experimental, predicted and mean absolute error of the corrosion penetration rate

Exp. No	*Predicted CPR, Using RSM ,(mm/y)*	*FL predicted result*	*Experimental CPR, Using (Norsok)*	*Error Using RSM*	*Error Using Fuzzy*
1	2.32	2.3	2.3	0.02	0
2	2.30	2.3	2.3	0	0
3	2.30	2.1	2.1	0.2	0
4	1.52	1.2	1.0	0.52	0.2
5	2.29	2.3	2.3	0.01	0
6	2.31	2.3	2.3	0.01	0
7	2.19	1.61	1.7	0.49	0.09
8	3.88	3.2	3.4	0.48	0.2
9	2.33	2.3	2.3	0.03	0
10	2.30	2.3	2.3	0	0
11	2.30	2.3	2.3	0	0
12	1.68	1.2	1.2	0.48	0
13	2.28	2.3	2.3	0.02	0
14	2.90	2.71	2.7	0.2	0.01
15	2.02	1.9	1.9	0.12	0
16	2.48	1.9	2.0	0.48	0.1
17	2.30	2.3	2.3	0	0
18	1.98	1.8	1.8	0.18	0
19	1.26	1.2	1.1	0.16	0.1
20	1.70	1.61	1.6	0.1	0.01
21	2.30	2.3	2.3	0	0
22	3.31	3.19	3.2	0.11	0.01
23	2.30	2.3	2.3	0	0
24	2.27	2.3	2.3	0.03	0
25	2.19	1.69	1.7	0.49	0.01
26	3.47	3	3.0	0.47	0
27	2.30	2.3	2.3	0	0
28	2.48	2.2	2.0	0.48	0.2
29	2.30	2.3	2.3	0.02	0
30	2.30	2.3	2.3	0	0
31	1.43	1.3	1.3	0.2	0
			MAE	**0.1814**	**0.0332**

5. CONCLUSION

During this study, attempts were done
pipelines that are used for transporting
The corrosion values were measured by
and principles of corrosion were also
follow:

1. Based on ANOVA analysis, the te
significant effect on corrosion rate,
However, the interaction between (ter
(pressure and shear stress) and (pH and
corrosion penetration rate.

2. Based on comparison between mode
RSM technique, it was concluded that
mean absolute error of 0.0412mm/y wi

3. The optimal values for the numerica
with the formula using Root- Sum
temperature= 44.4◦C, pressure= 34.28

4. The study proved that there was oth
instead of Norsok software which spen

6. ACKNOWLEDGMENTS

First of all, I would like to express my s
for such an opportunity in my life and t
department at Arabian Gulf Oil Compa
help me for support to complete the stu

7. REFERENCES

[1] . Song, F.M., Kirk, D.W., Graydo
carbon dioxide corrosion of bare steel u
pp. 736- 743.

★★★

[2]. Mikhailovskii, Y.N., Marshakov, A.I., and Petrov, N.A (1997) Monitoring of underground pipeline corrosion condition with sensory instruments. Prot. Met., 33, pp. 293-295.
[3]. Lopez, D.A., Schreiner, W.H., de Sanchez, S.R., and Simison, S.N. (2003) " The influence of carbon steel microstructure on corrosion layers: an XPS and SEM characterization". Appl. Surf. Sci., 207, pp. 69-85.
[4]. Fu, S.L., Garcia, J.G., and Griffin, A.M. (1996) " Corrosion Resistance of Some Downhole Tubing Materials and Inhibitor Effectiveness in Sweet Environments". Proceedings of CORROSION / 1996, NACE International, Houston, Taxes, Paper no. 21.
[5]. Kermani, M.B., and Morshed, A. (2003) "Carbon dioxide corrosion in oil and gas roduction – A compendium". Corrosion, 59, pp. 659-683.
[6]. Villamizar, W., Casales, M., Gonzalez-Rodriguez, J.G., and Martinez, L. (2007) "CO_2 corrosion inhibition by hydroxyethyl, aminoethyl, and amidoethyl imidazolines in water–oil mixtures". J. Solid State Electrochem., 11, pp. 619-629.
[7] luis alfonso," LEANRNING FUZZY LOGIC FROM EXAMPLES" ". [Thesis]. Ohio University; March 1994.
[8] E. H. Mamdani and S. Assilian, “An experiment in linguistic synthesis with a fuzzy logic controller”, International Journal of Man-Machine Studies, Vol. 7, No.1,pp. 1-13, 1975.
[9] T. Takagi and M. Sugeno, “Fuzzy identification of systems and its applications to modeling and control”, IEEE Trans, on Systems, Man and Cybernetics, 15, pp. 116-132, 1985.
[10] Jassbi, J.J.; Serra, P.J.A.; Ribeiro, R.A.; Donati, A.; "A Comparison of Mamdani and Sugeno Inference Systems for a space Fault Detection Application" Automation Congress, 2006. WAC '06. World. Issue Date: 24-26 July ,On page(s): 1 – 8,2006.
[11] J. Mendel, "Uncertain rule-based fuzzy inference systems: Introduction and new directions", Prentice-Hall, 2001.
[12] Mamdani, E.H. and S. Assilian, "An experiment in linguistic synthesis with a fuzzy logic controller," International Journal of Man-Machine Studies, Vol. 7, No. 1, pp. 1-13, 1975.